CD95L derived si- and shRNAs and the CD95L mRNA kill cancer cells through an RNAi mechanism by targeting survival genes

William Putzbach[1,6], Quan Q. Gao[1,6], Monal Patel[1,6], Aishe A. Sarshad[5], Abbas Hadji[1,7], Stijn van Dongen[4], Ashley Haluck-Kangas[1], Elizabeth Bartom[2], Austin Stults[1], Abdul S. Qadir[1], Kwang-Youn A. Kim[3], Markus Hafner[5], Jonathan C. Zhao[1], Andrea E. Murmann[1] and Marcus E. Peter[1,2,*]

[1] Division Hematology/Oncology and [2] Department of Biochemistry and Molecular Genetics, [3] Department of Preventive Medicine, Feinberg School of Medicine, Northwestern University, Chicago, IL 60611, USA; [4] European Bioinformatics Institute (EMBL-EBI), Hinxton, Cambridge CB10 1SD, UK; [5] Laboratory of Muscle Stem Cells and Gene Regulation, NIAMS, NIH, Bethesda, MD 20892, USA.

Corresponding author: Marcus Peter, E-mail: m-peter@northwestern.edu, phone: 312-503-1291; FAX: 312-503-0189.

[6] Shared first authorship

[7] Current address: Department of Pediatrics, Section of Hematology/Oncology/Stem Cell Transplantation, University of Chicago, Chicago, IL 60637

Keywords:
RNAi, Fas, cancer, CRISPR, cell death, DISE

Abstract

>80% of a large number of siRNAs and shRNAs targeting CD95 or CD95 ligand (CD95L) induce a form of cell death that is characterized by the simultaneous activation of multiple death pathways and preferentially affects transformed and cancer stem cells. We now show that these si/shRNAs kill cancer cells through canonical RNAi by targeting the 3'UTR of critical survival genes in a unique form of off-target effect. By testing 4666 shRNAs derived from the CD95 and CD95L mRNAs and an unrelated control gene, Venus, we have located the most toxic sequences in the open reading frame of CD95L. Consistently, CD95L mRNA is highly toxic to cancer cells after complete deletion of CD95. Our data provide the first evidence for mRNAs to affect cell fate through RNAi in mammalian cells. In addition, they suggest that cancer cells can be targeted with specific toxic RNAi active sequences present in the genome.

Introduction

CD95 (Fas/APO-1) is a death receptor that when bound by its ligand, CD95L, mediates induction of apoptosis, most prominently in the context of the immune system (Krammer, 2000). However, in recent years it has become apparent that the CD95/CD95L system has multiple tumor-promoting activities (Peter et al., 2007). CD95 signaling promotes cell growth (Chen et al., 2010), increases motility and invasiveness of cancer cells (Barnhart et al., 2004; Kleber et al., 2008), and promotes cancer stemness (Ceppi et al., 2014; Drachsler et al., 2016; Qadir et al., 2017). In fact, we reported that tumors after deleting the CD95 gene barely grew in vivo (Chen et al., 2010; Hadji et al., 2014). Therefore, it appeared consistent when we discovered that multiple shRNAs and siRNAs targeting either CD95 or CD95L slowed down cancer cell growth (Chen et al., 2010) and engaged a form of cell death that was found to be a combination of multiple cell death pathways (Hadji et al., 2014); it could not be inhibited by conventional cell death or signaling pathway inhibitors or by knockdown of any single gene in the human genome (Hadji et al., 2014); it preferentially affected transformed cells (Hadji et al., 2014) and among them cancer stem cells (Ceppi et al., 2014).

One of the popular methods to reduce expression of genes in cells is RNA interference (RNAi) which has been used to identify genes that are critical for the survival of human cancer cell lines (Hadji et al., 2014; Hart et al., 2014; Morgens et al., 2016; Wang et al., 2015). During RNAi, small interfering (si)RNAs, small hairpin (sh)RNAs or micro (mi)RNAs inhibit gene expression. miRNAs are generated as primary transcripts in the nucleus, undergo processing to pre-miRNAs by the Drosha-DGCR8 complex before being exported to the cytosol by exportin 5 (Ha and Kim, 2014; Krol et al., 2010). siRNAs are produced from both shRNAs and miRNAs when the RNase III, Dicer in complex with TRBP, cleaves double-stranded (ds)RNA into 21-23 nucleotide long fragments that have a two nucleotide 3' overhang (Zamore et al., 2000). DsRNA fragments or chemically synthesized siRNAs are loaded into the RNA-induced silencing complex (RISC) (Siomi and Siomi, 2009). A near-perfect complementary between the guide strand of the si/miRNA and the target mRNA sequence results in cleavage of the mRNA (Pratt and MacRae, 2009). Incomplete complementarity results in inhibition of protein translation, and contributes to mRNA degradation (Guo et al., 2010). mRNA targeting is mostly determined by the seed sequence, positions 2-7/8 of the guide strand, which is fully complementary to the seed match in the 3'UTR of targeted mRNAs. Similar to miRNAs, although not fully explored, siRNAs and shRNAs also target multiple other mRNAs besides the mRNAs they were designed to silence, a phenomenon commonly referred to as off-target effect (OTE) that is generally sought to be avoided (Birmingham et al., 2006; Jackson et al., 2006; Lin et al., 2005).

Results

si/shRNAs kill cells in the absence of the targeted site.

More than 80% of a large number of tested shRNAs or siRNAs designed to target either CD95 or CD95L were toxic to multiple cancer cells (Hadji et al., 2014). We have now extended this analysis to DICER substrate 27mer DsiRNAs (***Figure S1A*** and (Kim et al., 2005)). All five DsiRNAs designed to target CD95L displayed toxicity when introduced into HeyA8 cells at 5 nM (***Figure S1B***) reinforcing our previous observation that the majority of CD95 and CD95L targeting sh- and siRNAs are toxic to cancer cells. From our own experience and from multiple published genome-wide RNAi screens (Hadji et al., 2014; Hart et al., 2014; Morgens et al., 2016; Wang et al., 2015) it appears that only a small fraction (between 2% and 5%) of si/shRNAs are usually toxic. This toxicity could in part be due to an OTE. However, the high percentage of

toxic si/shRNAs derived from CD95 and CD95L seemed to exclude an OTE and pointed at a survival activity of CD95 and CD95L.

We wondered whether exogenously added recombinant CD95L protein could protect cells from the toxicity of CD95L derived shRNAs. When NB7 cells were incubated with different concentrations of a soluble form of CD95L (S2), toxicity exerted by shL1 was not affected (***Figure S2A***). NB7 neuroblastoma cells were chosen for these experiments because they lack expression of caspase-8 (Teitz et al., 2000) and hence are completely resistant to the apoptosis inducing effects of CD95L.

To test whether human CD95L or CD95 proteins could protect human cancer cells from death, we introduced silent mutations into the targeted sites of three very toxic shRNAs, shL1 and shL3 (both targeting CD95L), and shR6 (targeting CD95). We first introduced eight silent mutations into the sites targeted by either shL1 or shL3 (***Figure S2B***) and expressed these proteins in NB7 (***Figure S2C***). Both mutant constructs were highly resistant to knockdown by their cognate shRNA but still sensitive to the knockdown by the other shRNA (***Figure S2C***). Over-expression of these shRNA-resistant versions of the CD95L ORF did not protect the cells from shL1 or shL3, respectively (***Figure S2D***). We then mutated the CD95 mRNA in the targeted site of shR6 (***Figure S2E***). Expression of neither wt nor mutated CD95 in MCF-7 cells (***Figure S2F***) reduced the toxicity when cells were infected with the pLKO-shR6 or another toxic virus, pLKO-shR7 (***Figure S2G***). These data suggested that neither exogenously expressed or added CD95L or exogenously expressed CD95 protein can protect cells from toxic shRNA derived from these genes.

To determine whether the targeted sites in CD95 and CD95L were actually required for the shRNAs to kill we used CRISPR/Cas9 gene editing to excise sites targeted by different shRNAs and siRNAs in both alleles of the CD95 and CD95L genes. We first deleted a 41 nt piece of the CD95L gene in 293T cells, that contained the target site for shL3 (***Figure 1A, 1C***). While internal primers could not detect CD95L mRNA in three tested clones, primers outside of the deleted area did detect CD95L mRNA (***Figure 1D***, and data not shown). Three clones with this shL3 Δ41 deletion were pooled and tested for toxicity by shL3 expressed from a Tet-inducible plasmid (pTIP-shL3). Compared to a pool of control cells transfected only with the Cas9 plasmid, the 293T shL3 Δ41 cells were equally sensitive to the toxic shRNA (***Figure 1G***). This was also observed when the clones were tested individually (data not shown).

To exclude the possibility that shL3 was inducing cell death due to an activity unique to shL3 and/or 293T cells, we deleted the same 41 nt in CD95L in the ovarian cancer cell line HeyA8; We also removed 64 nt containing the target site for the siRNA siL3 in the CD95L coding sequence, and a 227 nt region containing the target site for shR6 in CD95 in HeyA8 cells (***Figure 1A, 1B*** and ***Figure S3***). In all cases homozygous deletions were generated (***Figure 1E***). To confirm the deletion of the shR6 target site, we infected HeyA8 cells treated with the Cas9 plasmid only and HeyA8 with the deleted shR6 site with shR6, shR2 (both targeting the CD95 ORF) and shR6' (targeting the CD95 3'UTR). Five days after infection, CD95 mRNA was quantified by real time PCR (***Figure 1F***). Using a primer located outside the 227bp deletion, the mutated CD95 mRNA was still detectable in the cells. While shR2 and shR6' caused knockdown of CD95 mRNA in both the Cas9 expressing control and the R6 Δ227 k.o. cells, shR6 could only reduce mRNA expression in the parental cells. These data document that HeyA8 CD95 shR6 Δ227 cells no longer harbor the sequence targeted by shR6.

Now having HeyA8 cells lacking one of three RNAi targeted sites in either CD95 or CD95L, we could test the role of the CD95 and CD95L genes in protecting HeyA8 cells from the death induced by either shRNAs (shL3 and shR6, two different vectors: pLKO or the Tet inducible pTIP) or the siRNA siL3. In all cases, the shRNA or siRNA that targeted the deleted region was

still fully toxic to the target-site deleted cells (***Figure 1H*** and ***1I***). Strikingly, We saw efficient growth reduction and cell death in siL3 site deleted cells transfected with as little as 1 nM siL3, well below the commonly used and recommended concentration of siRNAs (5-50 nM) (***Figure 1I***, and data not shown). These data firmly establish that cells were not dying due to targeting either CD95 or CD95L.

Involvement of canonical RNAi.

shRNAs and early generation naked siRNAs showed general toxicity when introduced in large amounts, presumably by eliciting an interferon (IFN) response (Marques and Williams, 2005) or by saturating the RISC (Grimm et al., 2006). However, both chemically modified siRNAs at very low concentrations and lentiviral shRNAs at an MOI<1 cells were still toxic (data not shown). We therefore decided to test whether the observed toxicity involved canonical RNAi and activity of the RISC. To be able to test all possible shRNAs or siRNAs targeting CD95L, we generated a sensor plasmid, comprised of Venus followed by the ORF of CD95L (inset in ***Figure 2A***). To minimize production of functional CD95L protein we deleted the first A in the ATG start codon of the CD95L cDNA in the sensor. Likely due to a small amount of CD95L still produced from the CD95L sensor, HeyA8 cells infected with this sensor virus slowed down in growth and some cells died by apoptosis (data not shown). We therefore used the CD95 protein k.o. cells we had generated in the process of deleting the shR6 site (***Figure S3*****,** clone # 2 was used for the following studies, see figure legend for strategy and characterization of the clones). While ds-siL3 effectively silenced Venus expression and induced toxicity, neither the sense nor the antisense single stranded (ss)RNAs significantly affected Venus expression or toxicity (***Figure 2A***). In addition, no activity was found when ds-siL3 was transfected into the cells synthesized as deoxyribo-oligonucleotides (***Figure 2B***). Using this type of analysis, we tested a number of modified siRNAs. For siRNAs to be fully active they require 3' overhangs in both strands. Converting siL3 to a blunt-end duplex resulted in a substantial loss of RNAi activity and toxicity (***Figure 2C***). Due to the topology of the RISC siRNA activity is decreased by modification of the 5' end of the antisense/guide strand. To test whether cell death induced by siL3 was affected by a bulky modification, we placed a Cy5 moiety at either of the four possible ends of the siL3 duplex. Only when the siL3 duplex carried a 5' modification in the guide strand did it prevent RNAi activity and toxicity, modifications in the three other positions had no effect (***Figure 2C***). This was confirmed for another siRNA, siL2. To test whether the toxicity of siL3 required association with a macromolecular complex consistent with RISC involvement, we performed a competition experiment. HeyA8 cells were transfected with 10 nM of siL3, and a mutated nontoxic oligonucleotide, siL3MUT, was titered in (***Figure 2D***). siL3MUT reduced the growth inhibitory activity of siL3 in a dose-dependent fashion suggesting that both siL3 and siL3MUT compete for the same binding site in the cells, pointing at involvement of the RISC.

To determine the involvement of components of the RNAi pathway in the toxicity of shRNAs we tested HCT116 cells deficient for either Drosha or Dicer (Kim et al., 2016). Growth of parental HCT116 cells was impaired after infection with shL3 or shR6 viruses (**Figure 2E**, left panel). Consistent with the requirement of Dicer to process shRNAs Dicer k.o. cells were completely resistant to the toxic shRNAs (***Figure 2E***, center panel). This was also supported by the inability of shR6 to silence CD95 protein expression (***Figure 2F***). Dicer$^{-/-}$ cells were not resistant to toxic siRNAs as these cells died when transfected with siL3, which does not depend on Dicer for processing (***Figure 2G***). Interestingly, Drosha$^{-/-}$ cells were hypersensitive to the two toxic shRNAs (***Figure 2E***, right panel) and shR6 efficiently knocked down CD95 expression in Drosha$^{-/-}$ cells (***Figure 2F***). Both Drosha$^{-/-}$ and Dicer$^{-/-}$ cells were much more susceptible to the toxicity induced by siL3 than parental cells (***Figure 2G***). The hypersensitivity of the Drosha$^{-/-}$

cells to toxic si/shRNAs and of Dicer$^{-/-}$ cells to toxic siRNAs is consistent with a model in which toxic shRNAs require RISC to kill cells and Drosha$^{-/-}$ and Dicer$^{-/-}$ cells which are almost completely devoid of miRNAs (Kim et al., 2016) allow much more efficient uptake of the toxic si/shRNAs into the RISC.

To test what the contribution of the seed sequence in the siRNAs was to their toxicity we generated a set of chimeric siRNAs in which we replaced nucleotides of the toxic siL3 siRNA with nucleotides of a nontoxic scrambled RNA. We did this starting either from the seed end or from the opposite end (***Figure 2H***). HeyA8 cells expressing both the Venus-CD95L sensor (to monitor level of knockdown) and a Nuc-Red plasmid to fluorescently label nuclei (to monitor the effects on cell growth) were transfected with 5 nM of the chimeric siRNAs; total green fluorescence and the number red fluorescent nuclei were quantified over time. The siL3 control transfected cells showed an almost complete suppression of the green fluorescence and high toxicity. In the top panel of ***Figure 2H*** the data are summarized in which siL3 nucleotides were stepwise replaced with siScr nucleotides from the seed match end. Both RNAi and toxicity were profoundly reduced when three of the terminal siL3 nucleotides were replaced with the siScr nucleotides in those positions suggesting that the seed region (6mer highlighted in blue) is critical for both activities (top panel in ***Figure 2H***). Consistently, when siL3 nucleotides were replaced with siScr nucleotides from the non-seed end, neither RNAi nor the toxicity was diminished until replacements affected residues in the seed region (bottom panel in ***Figure 2H***). These data suggest that the 6mer seed sequence of siL3 was critical for its CD95L specific RNAi activity and also its toxicity. These data provide strong evidence that the toxicity observed was a sequence specific event, and not the result of general toxicity resulting from a toxic sequence motif in the siRNA, or from poisoning the RISC. Rather, this toxicity followed the rules of canonical RNAi.

Toxic CD95L and CD95 derived sh- and siRNAs cause downregulation of survival genes.
A general OTE by RNAi has been reported (Birmingham et al., 2006; Jackson et al., 2006; Lin et al., 2005). However, this has not been found to cause toxicity in most cases and the targeted mRNAs were difficult to predict (Birmingham et al., 2006). The fact that 22 of the tested CD95 and CD95L targeting sh- and si/DsiRNAs were toxic to many cancer cells evoking similar morphological and biological responses (Hadji et al., 2014) generated a conundrum: Could an OTE trigger a specific biology? In order to test this we expressed two toxic shRNAs - one targeting CD95L (shL3) and one targeting CD95 (shR6) - in cells lacking their respective target sequences and subjected the RNA isolated from these cells to an RNA-Seq analysis. In order to detect effects that were independent of cell type, delivery of the shRNA, or targeted gene, we expressed shL3 in 293T (ΔshL3) cells using the Tet inducible vector pTIP and shR6 in HeyA8 (ΔshR6) cells using the pLKO vector. In each case, changes in RNA abundance were compared to cells in which we expressed a non-targeting shRNA in matching vectors. Total RNA was harvested in all cases at either the 50 hour time point (before the onset of cell death) or at the 100 hour time point (during cell death) (***Figure 3A***). In order to achieve high stringency, the data were then analyzed in two ways: first, using a conventional alignment-based analysis to identify genes for which the mRNA changed more than 1.5 fold (and an adjusted p-value of less than 0.05) and second, by a read-based method, in which we first identified all reads that changed >1.5 fold and then subjected each read to a BLAST search to identify the gene it was derived from. Only RNAs that were detected by both methods were considered (***Table S1***). The combination of the analyses resulted in one RNA that was upregulated and 11 mRNAs that were downregulated (***Figure 3B***). Using an arrayed qPCR approach, most of these detected mRNA changes were validated for both cell lines (***Figure S4A***). Interestingly, for nine of the eleven

genes, published data suggested that they are either highly upregulated in cancer and/or critical for the survival of cancer cells as their inhibition or knockdown resulted in either growth reduction or induction of various forms of cell death (see legend of ***Figure S4*** for details). Significantly, six of these eleven downregulated genes were recently identified in two genome-wide RNAi independent lethality screens to be critical for the survival of cancer cell lines (Blomen et al., 2015; Wang et al., 2015) (***Figure 3B*** and ***Figure S4B***) (***Table S2***). Considering that these two screens only identified 6.6% of human genes to be critical for cell survival, we found a significant enrichment (54.5%, $p<0.0001$) of these survival genes among the genes downregulated during the cell death induced by either shL3 or shR6. All six survival genes are either highly amplified or mutated in human cancers (***Figure S5A***). In addition to these six genes, GNB1 and HIST1H1C were reported to be required fitness genes in recent high-resolution CRISPR-based screen (Hart et al., 2015). A kinetic analysis showed that most of the deregulated mRNAs were downregulated early with a strong effect at around 26 hours, two days before the onset of cell death (***Figure S4C***). This suggested that the cells were dying because of the silencing of multiple critical survival genes providing an explanation for why multiple cell death pathways were activated. We are therefore calling this type of cell death DISE (for death induced by survival gene elimination).

To confirm that some of the downregulated genes were survival genes for HeyA8 cells, we transfected the cells with siRNA SmartPools targeting each of the eleven genes. Individual knockdown of seven of the targeted genes resulted in reduced cell growth when compared to cells transfected with a pool of scrambled siRNAs (***Figure 3C***). To mimic the effect of the CD95 and CD95L-derived shRNAs, we treated HeyA8 cells with a combination of siRNA pools targeting these seven genes. Remarkably, 1 nM of this siRNA mixture (35.7 pM of each individual siRNA) was sufficient to effectively reduce cell growth of the cells (***Figure S5B***) and to cause substantial cell death (***Figure S5C***), suggesting it is possible to kill cancer cells with very small amounts of siRNAs targeting a network of these survival genes.

To test the generality of this phenomenon we inducibly expressed another CD95L derived shRNA, shL1 in 293T cells using the pTIP vector, transfected HeyA8 cells with 25 nM siL3 and subjected the cells to RNA-Seq analysis 100 hours and 48 hours after addition of Dox or after transfection, respectively. In order to determine whether survival genes were downregulated in all cases of sh/siRNAs induced cell death, we used a list of 1883 survival genes and 423 genes not required for survival (nonsurvival genes) recently identified in a CRIPSR lethality screen (***Table S2***). We subjected the four ranked RNA Seq data sets to a gene set enrichment analysis using the two gene sets (***Figure 3D***). In all cases survival genes were significantly enriched towards the top of the ranked lists. In contrast, nonsurvival genes were not enriched. One interesting feature of DISE that emerged was the substantial loss of histones. Of the 16 genes that were significantly downregulated in cells treated with four sh/siRNAs, 12 were histones (***Figure 3E***). While it might be expected that dying cells would downregulate highly expressed genes such as histones, we believe that losing histones is a specific aspect of DISE because a detailed analyses revealed that the downregulated histones were not the most highly expressed genes in cancer cells (***Figure S6***). In addition, almost as many genes with similar high expression were found to be upregulated in cells after DISE induction.

Toxic CD95L and CD95 derived sh- and siRNAs target survival genes in their 3'UTR.

To test whether the introduced CD95 and CD95L-derived shRNAs directly targeted genes through canonical RNAi, we subjected the two gene lists obtained from the RNA-Seq analysis (the cell lines treated with either shL3 or shR6 at the 50 hour time point) to a Sylamer analysis (van Dongen et al., 2008) designed to find an enrichment of miRNA/shRNA targeted sites in the

3'UTR of a ranked list of genes (***Figure 4A***). This analysis identified a strong enrichment of the cognate seed match for shL3 and shR6 in cells treated with one of these two shRNAs. The analyses with cells treated with shRNAs for 100 hours looked similar but less significant, suggesting early targeting by the shRNAs followed by secondary events (data not shown). Enrichment in 6mers and 8mers were both detected (only 8mers shown) in the 3'UTRs but not the ORF of the ranked genes (data not shown).

Interestingly, the detected seed matches were shifted by one nucleotide from the expected seed match based on the 21mer coded by the lentivirus. RNA-Seq analysis performed for the small RNA fraction confirmed that in all cases (shScr and shL3 in pTIP, and shScr and shR6 in the pLKO vector) the shRNAs in the cells were being cleaved in a way that resulted in the predominant formation of an siRNA that was shifted one nucleotide away from the shRNA loop region (black arrow heads in ***Figure S7A***). This allowed us to design toxic siRNAs based on the sequences of shL3 and shL6. These shRNA-to siRNA converts were toxic to HeyA8 cells (***Figure S7B***) confirming that the observed toxicity was not limited to the TRC shRNA platform but based on a sequence specific activity of the sh/siRNAs.

This Sylamer results for shL3 and shR6 were confirmed with cells treated with either shL1 or siL3. In both cases when the ranked RNA Seq data were subjected to a Sylamer analysis again the seed matches of the sh/siRNA introduced was significantly enriched in the 3'UTR of downregulated RNAs (***Figure S7C***). In none of the Sylamer analyses of the four data sets did we see enrichment of seed matched in the 3'UTR of downregulated RNAs that matched the passenger strand. In all cases the only significantly enriched sequences matched the seed sequences in the guide RNA of the sh- and siRNAs. This suggests that the observed toxicity was not the result of passenger strand loading, one of the mechanisms that has been implicated in OTE of RNAi (Gu et al., 2012).

Our data suggested that DISE inducing sh- and siRNAs caused a early loss of survival genes and at the same time downregulated RNAs through canonical RNAi targeting their 3'UTR. However, it was not clear whether the most highly downregulated survival genes were targeted in their 3'UTR by RNAi active sequences. We had found that as little as 6 nucleotides determined whether an siRNA killed cancer cells (see *Figure 2H*). We found in 10 of the 11 targeted genes identified in the screen described in *Figure 3A* multiple 6mer seed matches for either shL3 and/or shR6 (***Figure 4B***). It is therefore likely that the two shRNAs, shL3 and shR6, killed cells by targeting a network of genes enriched in critical survival genes through RNAi. The only gene without an shL3 or shR6 seed match was HIST1HC1. Interestingly, only four of the histones downregulated in cells after treatment with any of the four tested sh/siRNAs had a 3'UTR (underlined in ***Figure 3E***) suggesting that most histones were not directly targeted by the sh/siRNAs.

To determine whether survival genes beyond these 11 genes were downregulated due to a direct targeting by the toxic sh/siRNAs we determined for each treatment whether there was a connection between the presence or absence of a predicted seed match of the sh/siRNA introduced and the significance of downregulation (>1.5 fold downregulated, $p<0.05$) among survival genes using the Fisher's Exact test (***Figure 4C***). In almost all cases this analysis revealed that survival genes containing a predicted seed match in their 3'UTR were statistically more likely to be selectively downregulated than survival genes without such a motif. The analysis with shL1 treated cells did not reach statistical significance, likely due to the fact that this shRNA was found to be very toxic and the 100 hour time point may have been too late to observe evidence of significant targeting. This interpretation is supported by the observation that the significance for both shL3 and shR6 to target survival genes was higher at 50 hours when compared to the 100 hour times points (***Figure 4C***) and that the Sylamer analysis of the shL1

treated cells was less significant after 100 hours of treatment than any of the other Sylamer analyses (***Figure S7C***). Overall the analyses suggested that cells die by DISE due to an early silencing of survival genes through targeting seed matches in their 3'UTR followed by the downregulation of histones.

Identification of toxic shRNAs in the CD95L and CD95 mRNAs.

The majority of commercially available si- Dsi-, and shRNAs derived from either CD95 or CD95L were highly toxic to cancer cells. We therefore asked whether these two genes contained other sequences with a similar activity. In order to test all shRNAs derived from either CD95L or CD95, we synthesized all possible shRNAs, 21 nucleotides long, present in the ORF or the 3'UTR of either CD95L or CD95 starting with the first 21 nucleotides after the start codon, and then shifting the sequence by one nucleotide along the entire ORF and 3'UTR (***Figure 5A***). We also included shRNAs from a gene not expressed in mammalian cells and not expected to contain toxic sequences, Venus. All 4666 oligonucleotides (700 Venus, 825 CD95L ORF, 837 CD95L 3'UTR, 987 CD95 ORF, and 1317 CD95 3'UTR shRNAs) were cloned into the Tet inducible pTIP vector (***Figure 5B***) as five individual pools. We first tested the activity of each pool to be toxic and to target the Venus sensor protein (fused to either the ORF of CD95 or CD95L). NB7 neuroblastoma cells were again used because of their resistance to CD95L induced apoptosis. NB7-Venus-CD95L cells infected with the Venus-targeting shRNA pool showed some reduction in fluorescence when Dox was added, however, the shRNA pool derived from the CD95L ORF was much more active in knocking down Venus (***Figure S8A***). No significant green fluorescence reduction was detected in cells after infection with the shRNA pool derived from the CD95L 3'UTR since the targeted sequences were not part of the sensor. Similar results were obtained when NB7-Venus-CD95 cells were infected with the Venus, CD95 ORF, and CD95 3'UTR targeting shRNA pools. To determine the ability to reduce cell growth (as a surrogate marker for toxicity), we infected NB7 parental cells with each of the five pools (parental cells were used to avoid a possible sponge effect by expressing either CD95L or CD95 sequences that were part of the Venus sensors). Interestingly, the pool of 700 shRNAs derived from Venus did not cause any toxicity (***Figure S8B***). In contrast, the pool of the shRNAs derived from CD95L significantly slowed down growth, while no toxicity was observed when cells were infected with the pool of shRNAs derived from the CD95L 3'UTR. In the case of CD95, both the shRNAs derived from the ORF and the 3'UTR showed some toxicity. However, the shRNAs derived from the 3'UTR caused greater toxicity compared to those derived from the ORF. The data suggests that overall the shRNAs derived from the CD95L ORF and the CD95 3'UTR contain the most toxic shRNAs.

To determine the toxicity of each of the shRNAs in the pools, NB7 cells were infected with the libraries of shRNA viruses (MOI<1), and after puromycin selection cells were pooled 1:1:1 (Venus ORF/CD95L ORF/CD95L 3'UTR pools or Venus ORF/CD95 ORF/CD95 3'UTR pools) to allow for competition between shRNAs when Dox was added (***Figure 5B***). Cells were cultured for 9 days with and without Dox to allow for cell death to occur. Next generation sequencing was performed on a PCR fragment containing the shRNA barcode (isolated from genomic DNA) to determine the relative abundance of each shRNA in three pools: 1) the cloned plasmid libraries, 2) cells after infection and culture for 9 days without Dox, and 3) cells infected and cultured with Dox for 9 days. A total of 71,168,032 reads were detected that contained a complete sequence of one of the cloned shRNAs. Almost all shRNAs were represented in the cloned plasmids (***Table S3***). The shRNAs in the CD95L pool (comprised of the Venus, CD95L ORF, and CD95L 3’UTR subpools) and the CD95 pool (comprised of the Venus, CD95 ORF, and CD95 3’UTR subpools) were ranked from highest (most toxic) to lowest

underrepresentation. During this and subsequent analyses we noticed that in many cases Dox addition did cause a reduction of shRNAs, indicating an increase in toxicity; However, in other cases infection alone without the addition of Dox was toxic. This effect was likely due to the well-described leakiness of the Tet-on system (Pham et al., 2008) which we confirmed for the shR6 shRNA (***Figure S9A***). To capture all toxic shRNAs, we therefore decided to split the analyses into two halves: 1) the changes in abundance after infection (infection -Dox) and 2) the changes in abundance after Dox addition (infection +Dox). The results for all shRNAs are shown in ***Figure S9B***. Grey dots represent all shRNAs and red dots represent only the ones that were significantly underrepresented at least 5 fold. Interestingly, the highest abundance of downregulated shRNAs was found in the CD95L ORF and the CD95 3'UTR pools of shRNAs, which is consistent with the increased toxicity that was observed when NB7 cells were infected with either of these two pools (see ***Figure S8B***). The shRNAs of these two toxic pools were highly enriched in the underrepresented shRNAs in the two pooled experiments (CD95L and CD95). Their toxicity was also evident when all shRNAs in each pool (2362 shRNAs in the CD95L and 3004 shRNAs in the CD95 pool) were ranked according to the highest fold downregulation (***Figure 5C***). The three subpools in each experiment are shown separately; Again this analysis identified the subpools with the highest enrichment of underrepresented shRNAs as the ORF of CD95L and the 3'UTR of CD95 (***Figure 5C***). In both analyses, the one with shRNAs underrepresented after infection is boxed in blue and the ones after Dox addition is boxed in orange.

This analysis allowed us to describe the toxicity landscape of CD95L and CD95 ORFs and their 3'UTRs (***Figure 5D***). All shRNAs that were significantly underrepresented at least five fold (red dots in ***Figure S9B***) are shown along the CD95L pool (***Figure 5D***, left) and the CD95 pool (***Figure 5D***, right) sequences. Blue marks show underrepresented shRNAs after infection, and orange marks show underrepresented shRNAs after culture with Dox. For both CD95L and CD95, toxic shRNAs were located in distinct clusters. The highest density of toxic sequences was found in the stretch of RNA that codes for the intracellular domain of CD95L (underlined in green in ***Figure 5D***).

Predicting shRNA toxicity - The toxicity index (TI).

Our data suggest that toxic shRNAs derived from either CD95L or CD95 kill cancer cells by targeting a network of genes critical for survival through canonical RNAi. Therefore, we wondered how many 8mer seed sequences derived from these toxic shRNAs would have corresponding seed matches in the 3'UTR of critical survival genes in the human genome. shRNAs containing these sequences could potentially be toxic to cells. To calculate such a hypothetical toxicity index, we used the ranked CRISPR data set (Wang et al., 2015) with 1883 SGs and 423 nonSGs. Based on our RNA Seq analyses, we hypothesized that the survival genes contained more putative seed matches of the shRNA in their 3'UTRs than the nonsurvival genes. We found 3'UTR information of 1846 of the survival genes and 416 of the nonsurvival genes.

In order to establish a Toxicity Index (TI) for each shRNA, we first generated a list containing a normalized ratio of occurrences of any possible 8mer seed match in the 3'UTRs of the survival and non-survival gene groups. This resulted in a ratio for each of the 65,536 possible 8mer combinations (***Table S4***), the TI. We then assigned to each of the 4666 shRNAs in our screen its TI and ranked each pool within the two experiments of our screen according to the highest TI and again separated the two groups of shRNAs, that were toxic just after infection and after addition of Dox (***Figure 5E***, ***Table S5***). In each ranked list, we could now assess whether the experimentally determined toxicity of shRNAs correlated with the *in silico* predicted TI. Remarkably, the highest enrichment of toxic shRNAs was found amongst those with higher TI

for the subpool of shRNAs targeting the CD95L ORF followed by shRNAs in the subpool targeting the CD95 3'UTR. To confirm the significance of this finding, we repeated the analysis 10,000 times by randomly assigning 8mers and their associated TIs to the two shRNA pools and again sorted the data from highest to lowest TI. The reported p-values were calculated based on these permutated datasets using Mann-Whitney U tests.

We noticed that survival genes tended to be more highly expressed than nonsurvival genes (data not shown). To address the question whether toxic si/shRNAs only targeted survival genes or all genes that are highly expressed, we recalculated the TI based on a set of 850 highly expressed and expression matched survival and nonsurvival genes (***Figure S10A***). This alternative TI tracked slightly less well with the toxic shRNAs we identified but the enrichment of toxic shRNAs towards the top of the list ranked according to the new TI was still statistically significant (***Figure S10B***). This analysis demonstrates that survival genes contain more seed matches for toxic shRNAs in their 3'UTR than nonsurvival genes regardless of the expression level. Our data suggests that to a certain extent it is possible to predict the experimental toxicity of shRNAs based on the *in silico* calculated TI.

CD95L mRNA is toxic to cancer cells.

Expression of CD95L in most cancer cells is known to kill them through induction of apoptosis. Consequently, expressing CD95L in HeyA8 cells, which are highly sensitive to CD95 mediated apoptosis, resulted in induction of apoptosis within a few hours of infecting the cells with lentiviral CD95L (***Figure 6A***, left panel). Severe growth reduction was seen without any signs of apoptosis (not shown) when a CD95L mutant was expressed carrying a Y218R point mutation (expressed at similar levels as wt CD95L, ***Figure 6B***) which prevents the CD95L protein to bind to CD95 ($CD95L^{MUT}$ in ***Figure 6A***) (Schneider et al., 1997). To prevent full length CD95L protein to be produced by the CD95L mRNA we also introduced a premature stop codon right after the start codon in the $CD95L^{MUT}$ vector ($CD95L^{MUT}NP$). This construct (confirmed to produce mRNA with no detectable full length CD95L protein, ***Figure 6B***) was equally active in reducing the growth of HeyA8 cells when compared to the $CD95L^{MUT}$ vector (***Figure 6A***, left panel). This result suggested that the CD95L mRNA could be toxic to HeyA8 cells without the CD95L protein inducing apoptosis. This was confirmed by expressing the three CD95L constructs in the presence of the caspase inhibitor zVAD-fmk (***Figure 6A***, center panel). Even with suppressed apoptosis all three constructs were equally toxic to HeyA8 cells. Finally, we tested three HeyA8 CD95 protein k.o. clones (***Figure S3***). In these cells without the addition of zVAD-fmk, wt CD95L and $CD95L^{MUT}NP$ were equally active in severely reducing the growth of the cells (***Figure 6A***, right panel and data not shown). These data suggested that it is the CD95L mRNA that killed the cells. Massive cell death could be seen in the $CD95^{-/-}$ cells treated with CD95L mRNA. This cell death resembled DISE induced by shRNAs (Hadji et al., 2014) and cells showed the same inability to pass through mitosis without dying (***Movies S1-S4***). Cell death was confirmed by quantifying nuclear fragmentation (***Figure 6C***) and we also detected a significant increase in ROS in CD95L expressing cells (***Figure 6D***), one of the main features of ongoing DISE (Hadji et al., 2014). To exclude the possibility that truncated CD95 protein or any part of the CD95 mRNA would play a role in this toxicity, we deleted the entire CD95 gene in MCF-7 cells (***Figure S11***). Wt CD95L killed these complete CD95 knock-out cells as well as CD95 shR6 deletion cells (***Figure S11F***). To determine the cause of cell death induced by CD95L mRNA in HeyA8 $CD95^{-/-}$ cells, we performed an RNA Seq analysis. Similar to cells treated with CD95L derived si/shRNAs, we observed that downregulated genes were enriched in survival genes versus the nonsurvival control genes (***Figure 6E***). In addition, cell death induced by CD95L mRNA resulted in a substantial loss of 11 of the 12 histones already detected to be

downregulated in cells treated with sh/siRNAs (***Figure 6F***). A Metascape analysis confirmed that nucleosome assembly, regulation of mitosis and genes that are consistent with the involvement of histones were among the most significantly downregulated RNAs across all cells in which DISE was induced by any of the four sh/siRNAs or by CD95L (***Figure 6G***). These GO clusters are consistent with DISE being a form a mitotic catastrophe with cells unable to survive cell division (Hadji et al., 2014).

CD95L mRNA kills cancer cells through RNAi

Very similar to the death induced by CD95L derived shRNAs, Drosha$^{-/-}$ cells were hypersensitive to the expression of CD95L^{MUT}NP (***Figure 7A***) and now virtually all cells died (***Figure 7B***). To test the hypothesis that Drosha$^{-/-}$ cells were more sensitive to DISE induction because their RISC was not occupied by large amounts of miRNAs and to determine whether CD95L derived toxic siRNAs were incorporated into the RISC, we pulled down AGO1-4-associated RNAs and analyzed their composition in wt and Drosha$^{-/-}$ cells after expressing the DISE inducing mutant CD95L mRNA. For the pull down we used a peptide recently described to bind to all four AGO proteins (Hauptmann et al., 2015). As expected in wt HCT116 cells large amounts of small RNAs (19-23nt in length) were detected bound to the AGO proteins (***Figure 7C***). Both AGO1 and AGO2 were efficiently pulled down. In contrast, in the Drosha$^{-/-}$ cells which cannot process canonical miRNAs, only very small amounts of small RNAs were detected confirming the absence of miRNAs in the RISC. Surprisingly, the amount of pulled down AGO proteins was severely reduced despite that fact that the Drosha$^{-/-}$ cells express normal levels of AGO2 (see ***Figure 2E***). This suggests that the peptide did not have access to the AGO proteins in Drosha$^{-/-}$ cells, either because it only binds to AGO proteins that are complexed with RNA or alternatively because AGO proteins without bound RNAs are no longer in the detergent extract used for peptide pull down.

The analysis of all AGO-bound RNAs showed that in the wt cells >98.4% of bound RNAs were miRNAs. In contrast in Drosha$^{-/-}$ cells only 34% of bound RNAs were miRNA derived (***Figure 7D***, data not shown). These include miRNAs that are processed independently of Drosha such as miR-320a (Kim et al., 2016) which in the Drosha$^{-/-}$ cells was found to be a major RNA species bound to AGO proteins (***Figure 7D***). In both wt and Drosha$^{-/-}$ cells a significant increase in CD95L derived short RNAs was detected that were bound to the AGO proteins. In wt cells they corresponded to 0.0006% of the bound RNAs and in the Drosha$^{-/-}$ cells to 0.043% of all AGO bound RNAs, a relative increase of >70 fold. Toxicity of CD95L was therefore not due to overloading the RISC. In the absence of most miRNAs the total amount of RNAs bound to AGO proteins in the Drosha$^{-/-}$ cells was roughly 10% of the amount bound to AGOs in wt cells (***Figure 7D***). The reduction of AGO-bound miRNAs in Drosha$^{-/-}$ cells was paralleled by a substantial increase in binding of other small RNAs to the AGO proteins (***Figure 7E***). Interestingly, the amount of AGO-bound CD95L derived small RNAs was >100 times higher in the Drosha$^{-/-}$ cells when compared to the wt cells (red columns in ***Figure 7E***).

These data support our hypothesis that Drosha$^{-/-}$ cells are more sensitive to DISE due to their ability to take up more toxic small RNAs into the RISC in the absence of most miRNAs. Interestingly, not only did AGO proteins in Drosha$^{-/-}$ cells bound more CD95L derived small RNAs but the length of the most abundant bound RNA species increased from 20 to 23 nt in the Drosha$^{-/-}$ cells (***Figure 7F***). To determine the sites within the CD95L mRNA that gave rise to small AGO bound RNAs we blasted all small AGO bound RNAs detected in all conditions against the CD95L ORF. This allowed us to align all CD95L derived reads to the CD95L sequence (***Figure S12***). Many regions in CD95L mRNA gave rise to small RNAs. As expected many of the same small RNAs detected in wt cells were also detected in Drosha$^{-/-}$ but at much

higher counts (green peaks in ***Figure 7G***, top panel). By comparing the AGO bound CD95L derived RNAs that had the same start site as the shRNAs in our toxicity screen we noticed that a large number of the AGO bound RNAs were derived from regions in the CD95L ORF that gave rise to toxic shRNAs (red peaks in ***Figure 7G***, center panel). We also found a number of reads that were located at positions in CD95L that did not contain toxic shRNAs (green peaks in ***Figure 7G***, center panel). This could be due to the fact that the toxicity screen was performed in NB7 cell whereas the AGO pull down experiments was performed in HCT116 cells. Our data suggest that the CD95L mRNA when overexpressed is toxic to cancer cells due to formation of small RNAs that are bound to AGO proteins presumably incorporated into the RISC and killing cells through RNAi. This process is independent of Drosha. To determine whether Dicer is required for either processing of CD95L or loading the small RNAs into the RISC we expressed the mutant CD95L mRNA in Dicer$^{-/-}$ HCT116 clones. Dicer$^{-/-}$ cells were susceptible to CD95L mRNA induced DISE suggesting that the processing of CD95L into small RNAs is independent of both Drosha and Dicer. In summary, our data suggest that CD95 and CD95L derived si- and/or shRNAs and the entire CD95L ORF are toxic to cancer cells by targeting critical survival genes through an RNAi mechanism that involves AGO proteins but is independent of both Drosha and Dicer. Furthermore, the data suggest that a high miRNA content by "filling up" the RISC might render cells less sensitive to DISE.

Discussion

Most of the current use of RNAi is aimed at achieving a highly specific silencing with little OTE. In fact, OTE represents one of the largest impediments to the use of RNAi in phenotypic screening applications. We now demonstrate that DISE is a unique form of OTE that results in the simultaneous activation of multiple cell death pathways in cancer cells. The discovery that DISE involves loss of multiple survival genes now provides an explanation for the unique properties we described for this form of cell death, especially the observation that cancer cells have a hard time developing resistance to this cell death mechanism (Hadji et al., 2014; Murmann et al.).

There are a number of rules that have been elucidated for designing sh/siRNAs (Bramsen et al., 2009) to avoid undesired effects such as OTE (Petri and Meister, 2013), general toxicity due to the presence of toxic sequence motifs (Fedorov et al., 2006; Petri and Meister, 2013), poisoning/saturating of the RISC (Grimm et al., 2006), or evocation of an IFN response (Marques and Williams, 2005). The following arguments and evidence support our conclusion that DISE is a manifestation of a novel, functionally important, conserved mechanism of genome regulation, and not the result of one of the above mentioned effects:

1) The sheer number of toxic shRNAs embedded in CD95L or CD95. A number of genome-wide shRNA and siRNA lethality screens have revealed that 2-5% of shRNAs targeting human genes are toxic to cells. We recently reported the identification of 651 genes out of about 18,000 targeted genes that are critical for the survival of eight different cancer cell lines (Hadji et al., 2014). Hence, targeting 97% of the genes using the shRNAs of the TRC library was not toxic. Many of the genes targeted by these shRNAs were actually established survival genes (as discussed in (Hadji et al., 2014)). That means that the number of shRNAs that are toxic due to a possible OTE or general toxicity would be expected to be very small. In contrast, we found that >80% of the shRNAs and siRNAs that were designed to target either CD95 or CD95L exhibited toxicity in multiple cell lines.
2) High concentrations of siRNAs can saturate the RISC, preventing access of crucial endogenous miRNAs (Khan et al., 2009). We have demonstrated that in general 5 nM of CD95L derived siRNAs are sufficient to kill cancer cells, and we have seen very efficient cell death with as little as 1 nM of siRNA (see *Figure 1I*). It is therefore unlikely that we are poisoning the RISC. It has been reported that in siRNA overexpression experiments, changes in mRNA expression can be caused by blocked access of endogenous miRNAs to the RISC, such as the highly expressed miRNA family, let-7 (Khan et al., 2009). However, we can exclude such an effect in our analysis, as there was no significant enrichment (or depletion) of the let-7 seed match motif (or that of any other miRNA) in our analyses (black lines in ***Figure 4A***).
3) No IFN response was observed. We have performed multiple RNA-Seq and gene array analyses of cells in which DISE was induced by multiple sh- and siRNAs targeting CD95 or CD95L. In none of these analyses did we detect an increase in any of the known IFN response genes (Schoggins et al., 2011) (data not shown). In addition, we demonstrated that the latest generation of Dicer optimized 27mer DsiRNAs that do not elicit an IFN response (Kim et al., 2005) and the shRNAs expressed from within the cells shown to have low IFN triggering activity (Robbins et al., 2006) have the same toxic activities as the standard 21mer siRNAs (see *Figure S1B*).
4) Mutation of just one position destroys activity. A major argument against DISE toxicity being caused by overloading the RISC, an IFN response or the presence of known toxic sequences,

lies in the analysis of the chimeras we generated between siL3 and a non-toxic scrambled oligonucleotide (see *Figure 2H*). This analysis demonstrated that the seed match positions of siL3 are critical for its toxicity. In fact, just replacing one nucleotide in a critical position in the center of the seed match almost completely abolished toxicity of the siRNA.

Part of our data was generated using a widely used first generation stem loop shRNA platform, the TRC library. The TRC shRNAs have recently been found to be prone to cause OTE. Gu et al. showed that the loop design of this system results in imprecise Dicer cleavage and, consequently, the production of different mature small-RNA species that increase passenger loading, one major source of OTE (Gu et al., 2012). More recently it was reported that most guide RNAs derived from the TRC hairpin were shifted by 4 nt 3' of the expected 5' start site (Watanabe et al., 2016). While we did see a shift in processing of these stem loop shRNAs we did not see such a high level of imprecision of cleavage of our toxic shRNAs. In fact, 99.4% of the shR6 guide RNA started at the same nucleotide position (***Figure S7A***). We did observe that the majority of processing of our pTIP and pLKO based shRNAs was shifted by one nucleotide (***Figure S7A***). This shift was consistent with the defined seed matches that were found by the Sylamer analyses. In general, one major seed match was detected with one other minor species (this was less obvious only for shL1, ***Figure S7C***). Furthermore, all four Sylamer analyses only detected enrichments in the 3'UTR of downregulated mRNAs that were consistent with the guide strand targeting the mRNA and not the passenger strand. In all cases including in cells transfected with the siRNA siL3, the mainly enriched sequence motifs were either 7, or 8mers present in the 3'UTR of the targeted mRNA.

Interestingly however, while the majority of tested siRNAs, DsiRNAs and shRNAs were toxic to many cancer cells a more recent RNAi screen did not report shRNAs against CD95 or CD95L as being toxic (Morgens et al., 2016). The authors of this study used a second generation shRNA platform based on a miR-30 backbone. Indeed we recently generated miR-30 based shRNA versions of some of our most toxic shRNAs (shL1, shL3, shL4, shR5, shR5, and shR7) and found none of them to be toxic to HeyA8 cells (data not shown). However, they also had very low activity to silence the Venus based CD95L and CD95 sensors (data not shown) suggesting that the amount of shRNAs produced by cells may not be sufficient to induce DISE.

Our data on DISE are consistent with a number of properties of RNAi OTE previously reported. Similar to DISE, OTE mediated silencing requires a 6/7nt seed sequence of complementarity (Birmingham et al., 2006; Jackson et al., 2006; Lin et al., 2005) and it targets mRNAs in the 3'UTR (Birmingham et al., 2006). Our data on shRNAs, siRNAs, and DsiRNAs suggest that DISE is not limited to one platform and requires sequence specific targeting. This conclusion is also consistent with a previous report that suggested that sequence-dependent off-target transcript regulation is independent of the delivery method (Jackson et al., 2006). The authors found the same enrichment of 6mers and 7mers in 3'UTRs of targeted mRNAs for siRNAs and shRNAs (Jackson et al., 2006).

The most compelling argument against an effect limited to si/shRNAs, however, is the discovery that the mRNA of CD95L, which we showed to be enriched in RNAi active toxic sequences, itself is toxic to cancer cells. Overexpression of CD95L ORF in most cells will induce massive apoptosis and when it was discovered previously that CD95L delivered using viruses very efficiently killed multiple cancer cells that were completely resistant to CD95 mediated apoptosis, this was interpreted as a form of CD95L induced apoptosis that occurred from within the cells (ElOjeimy et al., 2006; Hyer et al., 2000; Sudarshan et al., 2005; Sun et al., 2012). We now conclude that the mRNA of CD95L kills cells in the same way as CD95L-derived si/shRNAs based on the following observations: 1) The morphology of the cells undergoing DISE induced by shRNAs and by overexpressing CD95L is virtually identical (see

supplementary movies). 2) Both treatments result in generation of ROS. 3) The kinetics of these two forms of cell death are similar (days rather than hours). 4) We detect large numbers of cells that die just after the first attempt to divide (data not shown). 5) Drosha$^{-/-}$ cells are hypersensitive to si- and or shRNAs and CD95L RNA mediated toxicity. 6) Both forms of cell death result in a preferential loss of critical survival genes followed by loss of histones. 7) We have identified multiple CD95L derived small RNAs (mostly 19-23 nt) that are bound to AGO proteins in cells undergoing DISE. Many of them colocalize with CD95L sequences we have identified as toxic to cancer cells. Most importantly, we found a substantially increased loading of such small CD95L derived RNAs into the RISC in the absence of Drosha consistent with the increase susceptibility of these cells to DISE.

We previously reported that Dicer$^{Exo5-/-}$ HCT116 cells (with deleted Exon 5) were at least as sensitive to induction of DISE (by either shL3 or shR6) than wt cells suggesting that Dicer deficient cells could be killed by DISE (Hadji et al., 2014). It is has been reported that these Dicer deficient cells are hypomorphs (Ting et al., 2008) and indeed we had detected a small residual Dicer expression by Western blotting (Hadji et al., 2014). We have now revisited this issue with HCT116 cells rendered completely deficient for Dicer using CRISPR/Cas9 gene editing (Kim et al., 2016). The fact that these Dicer$^{-/-}$ cells were now completely resistant to the toxic effects of shL3 or shR6 demonstrates complete absence of Dicer protein. The comparison of the results with the two Dicer deficient cells now allows us to conclude that very small amounts of Dicer which resulted in a severe reduction of cellular miRNA levels (Hadji et al., 2014) are sufficient to allow DISE to occur. Similar to the Drosha k.o. cells in the absence of mature miRNAs which seem to inhibit DISE, Dicer$^{-/-}$ cells are hypersensitive to DISE induced by si/shRNAs.

Examining the actual length and location of all CD95L-derived sequences (see *Figure S12*) it appears that there are multiple defined areas that can give rise to small RNAs that are bound to AGO proteins. At present the mechanism of this specific degradation and/or RISC uptake is unknown. We can exclude the involvement of the components of the canonical miRNA biogenesis pathway as both Drosha and Dicer k.o. cells are fully sensitive to the toxic effects of CD95L mRNA.

We are proposing an entirely new concept of killing cancer cells that is based on the toxicity of CD95 and CD95L derived small RNAs. Naturally, there are many open questions such as:

1) Is DISE part of an anti cancer mechanism? We are proposing that DISE kills cancer cells in a way they usually cannot escape from. We have not found a way to block cancer cells from dying by DISE. We provide strong evidence to suggest that this is due to the simultaneous targeting of multiple survival genes that result in the activation of multiple cell death pathways. It will be difficult to prove that the cells are dying due to the preferential targeting of survival genes. It may never be possible to express multiple survival genes at the same time at physiological levels to render cancer cells resistant to the action of countless small RNAs. This prediction alone makes DISE a promising new strategy to kill cancer cells.

2) Does CD95L induce DISE in vivo? We and others have noticed upregulation of CD95L in multiple stress related conditions such as treatment with chemotherapy ((Friesen et al., 1999) and data not shown). While the amount of CD95L RNA and the level of upregulation alone may not be enough to induce DISE, it could be the combination of multiple RNAs that are generated that kills cells by DISE. We view CD95L as just one of many RNAs that have this activity.

3) Are there other genes in the human genome with activities such as CD95L? We recently identified other genes in the genome that contain DISE inducing shRNAs (Patel and Peter). It is therefore possible that when cells are subjected to genotoxic or oncogenic stress that they generate numerous small RNAs that can be taken up by the RISC and in combination execute

DISE.

At a minimum our data provide the first evidence of an overexpressed cDNA to be toxic to all tested cancer cells through an RNAi dependent mechanism. It was first shown in plants that overexpressed transgenes can be converted into RNAi active short RNA sequences (Hamilton and Baulcombe, 1999). Our data on the effects of overexpressed CD95L RNA maybe the first example of transgene determining cell fate through the RNAi mechanism in mammalian cells.

We interpret the hypersensitivity of both Drosha$^{-/-}$ and Dicer$^{-/-}$ cells to DISE in the following way: Most of the small RNAs in the cells that are loaded into the RISC are miRNAs. Using Ago pull-down experiments we determined 98.4% of AGO associated RNAs in HCT116 cells to be miRNAs (99.3% in HeyA8 cells, data not shown). It was recently reported that Drosha$^{-/-}$ cells showed a reduction of miRNA content from roughly 70-80% to 5-6% and Dicer$^{-/-}$ cells had a reduction down to 14-21% (Kim et al., 2016). Since neither Drosha$^{-/-}$ nor Dicer$^{-/-}$ cells express reduced AGO2 protein levels (see *Figure 2E*), it is reasonable to assume that their RISC can take up many more of the toxic DISE inducing RNAs than the RISC in wt cells explaining the super toxicity of both DISE inducing si/shRNAs and CD95L mRNAs in these cells.

We previously showed that expression of either shL3 and shR6 induced DISE in immortalized normal ovarian fibroblasts much more efficiently than in matching nonimmortalized cells (Hadji et al., 2014), suggesting that this form of cell death preferentially affects transformed cells. Our data now provide an interesting model to explain the higher sensitivity of cancer cells to DISE when compared to normal cells. It is well documented that cancer cells in general have global downregulation of miRNAs when compared to normal tissues (Lu et al., 2005). This might free up the RISC for DISE inducing RNAs and would imply that miRNAs may protect normal cells from DISE.

Overall our data allow us to predict that any small RNA with DISE inducing RNAi activity that does not require Dicer processing can kill cancer cells regardless of its Dicer or Drosha status. In fact, in an accompanying manuscript we demonstrate that DISE can be triggered in vivo to treat ovarian cancer in xenografted mice by delivering CD95L-derived siRNAs using nanoparticles (Murmann et al.). No toxicity was observed in the treated mice. These data suggest that it might be possible to develop a novel form of cancer therapy based on the DISE OTE mechanism.

Materials and methods

Reagents and antibodies. Primary antibodies for Western blot: anti-β-actin antibody (Santa Cruz #sc-47778), anti-human CD95L (BD Biosciences #556387), and anti-human CD95 (Santa Cruz #sc-715), anti-human AGO2 (Abcam #AB186733), anti-human Drosha (Cell Signaling #3364), and anti-Dicer (Cell Signaling #3363). Secondary antibodies for Western blot: Goat anti-rabbit; IgG-HRP (Southern Biotech #SB-4030-05 and Cell Signaling #7074), and Goat anti-mouse; IgG1-HRP; (Southern BioTech #1070-05). Antibodies/isotype controls for surface staining, S2 and leucine-zipper tagged (Lz)CD95L were described before (Algeciras-Schimnich et al., 2003). Reagents used: propidium iodide (Sigma #P4864), puromycin (Sigma #P9620), G418 (Affymetrix #11379), zVAD-fmk (Sigma-Aldrich #V116, used at 20 μM), and doxycycline (Sigma #9891).

Cell lines. The ovarian cancer cell line HeyA8, the neuroblastoma cell line NB7, and the breast cancer cell line MCF-7 were grown in RPMI 1640 medium (Cellgro #10-040-CM), 10% heat-inactivated FBS (Sigma-Aldrich), 1% L-glutamine (Mediatech Inc), and 1% penicillin/streptomycin (Mediatech Inc). The human embryonic kidney cell line 293T was cultured in DMEM (Cellgro #10-013-CM), 10% heat-inactivated FBS, 1% L-Glutamine, and 1% penicillin/streptomycin.

HCT116 parental, Drosha$^{-/-}$, and Dicer$^{-/-}$ cells were generated by Narry Kim (Kim et al., 2016). HCT116 parental (cat#HC19023), a Drosha$^{-/-}$ clone (clone #40, cat#HC19020) and two Dicer$^{-/-}$ clones (clone #43, cat#HC19023 and clone #45, cat#HC19024) were purchased from Korean Collection for Type Cultures (KCTC). All HCT116 cells were cultured in McCoy's medium (ATCC, cat#30-2007), 10% heat-inactivated FBS, 1% L-Glutamine, and 1% penicillin/ streptomycin.

NB7 cells overexpressing wild type CD95L and mutant CD95L cDNAs were generated by seeding cells at 50,000 to 100,000 cells per well in a 6-well plate and infecting cells with lentivirus generated in 293T cells from the pLenti-CD95L, pLenti-CD95L1MUT, pLenti-CD95L3MUT, pLenti-CD95L^{MUT}, and pLenti-CD95L^{MUT}NP vectors in the presence of 8 μg/ml polybrene. Selection was done with 3 μg/ml puromycin 48 hours after infection. HCT116 and HCT116 Drosha$^{-/-}$ cells overexpressing CD95L^{MUT}NP were generated by seeding cells at 100,000 cells per well in a 24-well plate and infecting cells with lentivirus generated in 293T cells from the pLenti-CD95L^{MUT}NP vector in the presence of 8 μg/ml polybrene. Selection was done with 3 μg/ml puromycin 48 hours after infection. Both HeyA8 cells and HCT116 cells overexpressing CD95L were plated in 96-well plate for incuCyte analysis one day after selection in the presence of puromycin. MCF-7 cells overexpressing CD95 cDNAs were generated by seeding cells at 50,000 per well in a 6-well plate followed by infection with retrovirus generated in phoenix ampho 293 cells from the pLNCX2-CD95 or pLNCX2-CD95R6MUT vectors in the presence of 8 μg/ml polybrene. Selection was done with 200 μg/ml G418 48 hours after infection for 2 weeks. The HeyA8 cells used in *Figure 2D* carried a lentiviral Venus-siL3 sensor vector (Murmann et al.) and were infected with NucLight Red lentivirus (Essen Bioscience #4476) with 8 μg/ml polybrene and selected with 3 μg/ml puromycin and sorted for high Venus expression 48 hours later. HeyA8 ΔshR6 clone #2 sensor cells used in *Figure 2A* to *C* were infected with lentiviruses generated from the Venus-CD95L (full length) sensor vector to over-express the Venus-CD95L chimeric transcript. Cells were sorted for Venus expression 48 hours later.

Plasmids and constructs. The venus-CD95L ORF and venus-CD95 ORF (full length) sensor vectors were created by sub-cloning the Venus-CD95L or the Venus-CD95 inserts (synthesized by IDT with flanking XbaI RE site on the 5' end and EcoRI RE site at the 3' end in the pIDTblue vector), which are composed of the Venus ORF followed by either the CD95L ORF (accession number NM_000639.2) or the CD95 ORF (accession number BC012479.1) as artificial 3'UTR (both lacking the A in the start codon), respectively, into the modified CD510B vector using XbaI and EcoRI. Ligation was done with T4 DNA ligase.

The pLenti-CD95L was synthesized by sub-cloning an insert containing the CD95L ORF (synthesized by IDT as minigene with flanking 5' NheI RE site and 3' XhoI RE sites in pIDTblue vector) into the pLenti-GIII-CMV-RFP-2A-Puro vector (ABM Inc). The insert and the backbone were digested with NheI (NEB #R0131) and XhoI (NEB #R0146) restriction enzymes. Subsequent ligation with T4 DNA ligase created the pLenti-CD95L vector. The pLenti-CD95L1MUT and pLenti-CD95L3MUT vectors were created by subcloning a CD95L cDNA insert with 8 silent mutations at either the shL1 site (*GCATCATCTTTGGAGAAGCAA -> GCCTCGTCCCTAGAAAAACAG*) or at the shL3 site (*ACTGGGCTGTACTTTGTATAT -> ACCGGATTATATTTCGTGTAC*), respectively, into the pLenti-GIII-CMV-RFP-2A-Puro vector.

The pLenti-CD95L^{MUT} vector was created by subcloning a CD95L cDNA insert with 2 nucleotide substitutions in codon 218 (*TAT -> CGT)* resulting in replacement of tyrosine for arginine, which has been described to inhibit binding to CD95 (Schneider et al., 1997). The pLenti-CD95L^{MUT}NP vector insert contained both the Y218R mutation and a single nucleotide substitution at the second codon (*CAG -> TAG*), resulting in a premature stop codon right after the start codon.

The pLNCX2-CD95R6MUT vector was synthesized by replacing a 403bp fragment of the CD95 ORF insert from the pLNCX2-CD95 vector with a corresponding 403bp fragment that had 8 silent mutation substitutions at the shR6 site (5'-*GTGTCGCTGTAAACCAAACTT* -> 5'-*ATGTCGCTGCAAGCCCAATTT*-3') using BstXI (NEB #R0113) and BamHI (NEB #R3136) restriction enzymes (mutant insert was synthesized in a pIDTblue vector with 5' end BstXI site and 3' end BamHI RE site).

Dox-inducible vectors expressing shRNAs were constructed by subcloning an annealed double-stranded DNA insert containing the sequence encoding the shRNA hairpin (sense strand: 5'-
TGGCTTTATATATCTCCCTATCAGTGATAGAGATCGNNNNNNNNNNNNNNNNNNNNNCTC GAG
nnnnnnnnnnnnnnnnnnnnnTTTTTGTACCGAGCTCGGATCCACTAGTCCAGTGTGGGCATGCT GCGTTGACATTGATT-3') into the pTIP-shR6 vector (Hadji et al., 2014). BsaBI (NEB #R0537) and SphI-HF (NEB #R3182) were used to digest both the pTIP-shR6 vector (to excise the shR6 insert) and the insert followed by ligation with T4 DNA ligase. The template oligos were purchased from IDT. The poly-N represents the two 21bp sequences that transcribe for the sense (*N*) and antisense (*n*) shRNA.

CRISPR deletions. We identified two gRNAs that target upstream and downstream of the site to be deleted. These gRNAs were expected to result in the deletion of a DNA piece just large enough to remove the target site. The CRISPR gRNA gene blocks were from IDT and consisted of the scaffold 5'-
TGTACAAAAAAGCAGGCTTTAAAGGAACCAATTCAGTCGACTGGATCCGGTACCAAGGTC GGGCAGGAAGAGGGCCTATTTCCCATGATTCCTTCATATTTGCATATACGATACAAGGCTG TTAGAGAGATAATTAGAATTAATTTGACTGTAAACACAAAGATATTAGTACAAAATACGTGAC GTAGAAAGTAATAATTTCTTGGGTAGTTTGCAGTTTTAAAATTATGTTTTAAAATGGACTATC

ATATGCTTACCGTAACTTGAAAGTATTTCGATTTCTTGGCTTTATATATCTTGTGGAAAGG ACGAAACACCGNNNNNNNNNNNNNNNNNNNGTTTTAGAGCTAGAAATAGCAAGTTAAAAT AAGGCTAGTCCGTTATCAACTTGAAAAAGTGGCACCGAGTCGGTGCTTTTTTTCTAGACCC AGCTTTCTTGTACAAAGTTGGCATTA-3' (Mali et al., 2013); The poly-*NNNNNNNNNNNNNNNNNNN* re-presents the 19bp target sequence. The two 19bp target sequences for excision of the shL3 site (Δ41 deletion) were 5'-*CCTTGTGATCAATGAAACT*-3' (gRNA #1) and 5'-*GTTGTTGCAAGATTGACCC*-3' (gRNA #2). The two target sequences for the Δ227 deletion of the shR6 site were 5'-*GCACTTGGTATTCTGGGTC*-3' and 5'-*TGTTTGCTCATTTAAACAC*-3'. The two target sequences for Δ64 deletion of the siL3 site were 5'-*TAAAACCGTTTGCTGGGGC*-3' and 5'-*TATCCCCAGATCTACTGGG*-3'. The two target sequences for the deletion of the entire CD95 gene were 5'-*GTCAGGGTTCGTTGCACAAA*-3' and 5'-*TGCTTCTTGGATCCCTTAGA*-3'. Target sequences were identified using the CRISPR gRNA algorithm found at http://crispr.mit.edu/; only gRNAs with scores over 50 were used. These 8 gene blocks were sub-cloned into the pSC-B-amp/kan plasmid using the StrataClone Blunt PCR Cloning kit (Agilent Technologies #240207).

The target sites of siL3, shL3, and shR6 were homozygously deleted from target cells by co-transfecting Cas9 plasmid with each corresponding pair of pSC-B-gRNA plasmids. Briefly, 400,000 cells were seeded per well on a 6-well plate the day prior to transfection. Each well was transfected with 940 ng of Cas9-GFP plasmid (pMJ920) (Jinek et al., 2013) and 450 ng of each pSC-B-gRNA plasmid using Lipofectamine 2000 (ThermoFisher Scientific #11668027). Media was replaced next day. One to two days later, cells were sorted for the top 50% population with the highest green fluorescence. Those cells were cultured for an additional week to let them recover. The cells were then sorted by FACS (BD FACSAria SORP system) directly into 96-well plates containing a 1:1 ratio of fresh media:conditioned media for single cell cloning. Approximately two to three weeks later, single cell clones were expanded and subjected to genotyping. PCR using both a primer pair that flanked the region to be deleted and another pair containing one flanking primer and one internal primer was used to screen clones for homozygous deletion. For detection of the Δ41 deletion of the shL3 site, the flanking external primers were 5'-*TCTGGAATGGGAAGACACCT*-3' (Fr primer) and 5'-*CCTCCATCATCACCAGATCC*-3' (Rev primer), and the internal Rev primer was 5'-*ATATACAAAGTACAGCCCAGT*-3'. For detection of the Δ227 deletion of the shR6 site, the flanking external primers were 5'-*GGTGTCATGCTGTGACTGTTG*-3' (Fr primer) and 5'-*TTTAGCTTAAGTGGCCAGCAA*-3' (Rev primer), and the internal Rev primer was 5'-*AAGTTGGTTTACATCTGCAC*-3'. For detection of the Δ64 deletion of the siL3 site, the flanking external primers were 5'-*CTTGAGCAGTCAGCAACAGG*-3' (Fr primer) and 5'-*CAGAGGTTGGACAGGGAAGA*-3' (Rev primer), and the internal Rev primer was 5'-*ATATGGGTAATTGAAGGGCTG*-3'. For detection of the CD95 gene deletion, the flanking external primers were 5'-*TGTTTAATATAGCTGGGGCTATGC*-3' (Fr primer) and 5'-*TGGGACTCATGGGTTAAATAGAAT*-3' (Rev primer), and the internal reverse primer was 5'-*GACCAGTCTTCTCATTTCAGAGGT*-3'. After screening the clones, Sanger sequencing was performed to confirm that the proper deletion had occurred. Three clones were pooled for each si/shRNA target site deletion with the exception of HeyA8 ΔshR6 for which only clone #11 showed homozygous deletion of the shR6 site; clones #1 and 2 were not complete shR6 deletion mutants, but frame-shift mutations did occur in each allele (as in clone #11) making them CD95 knockout clones as depicted in *Figure S3B*.

Knockdown with pLKO lentiviruses. Cells were infected with the following pLKO.2 MISSION Lentiviral Transduction Particles (Sigma): pLKO.2-puro non-targeting (scramble)

shRNA particles (#SHC002V), 8 non-overlapping shRNAs against human CD95L mRNA (accession number #NM_000639), TRCN0000058998 (shL1: GCATCATCTTTGGAGAAGCAA), TRCN0000058999 (shL2: CCCATTTAACAGGCAAGTCCA), TRCN0000059000 (shL3: ACTGGGCTGTACTTTGTATAT), TRCN0000059001 (shL4: GCAGTGTTCAATCTTACCAGT), TRCN0000059002 (shL5: CTGTGTCTCCTTGTGATGTTT), TRCN0000372231 (shL6: TGAGCTCTCTCTGGTCAATTT), TRCN0000372232 (shL2': TAGCTCCTCAACTC ACCTAAT), and TRCN0000372175 (shL5': GACTAGAGGCTTGCATAATAA), and 9 non-overlapping shRNAs against human CD95 mRNA (accession number NM_000043), TRCN0000218492 (shR2: CTATCATCCTCAAGGACATTA), TRCN00000 38695 (shR5: GTTGCTAGATTATCGTCCAAA), TRCN0000038696 (shR6: GTGCAGA TGTAAACCAAACTT), TRCN0000038697 (shR7: CCTGAAACAGTGGCAATAAAT), TRCN0000038698 (shR8: GCAAAGAGGAAGGATCCAGAT), TRCN0000265627 (shR27': TTTTACTGGGTACATTTTATC), TRCN0000255406 (shR6': CCCTTGTGTTT GGAATTATAA), TRCN0000255407 (shR7': TTAAATTATAATGTTTGACTA), and TRCN0000255408 (shR8': ATATCTTTGAAAGTTTGTATT). Infection was carried out according to the manufacturer's protocol. In brief, 0.5 to 1 x 10^5 cells seeded the day before in a 6-well plate were infected with each lentivirus at an M.O.I of 3 in the presence of 8 µg/ml polybrene overnight. Media change was done the next day, followed by selection with 3 µg/ml puromycin 24 hours later. Selection was done for at least 48 hours until puromycin killed the non-infected control cells. For infection of NB7 cells over-expressing pLenti-CD95L with pLKO lentiviral particles, cells were seeded at 5,000 per well on a 24-well plate and infected with an M.O.I. of 20 to ensure complete infection. For infection of MCF-7 cells over-expressing pLNCX2-CD95 with pLKO lentiviruses, cells were seeded at 7,000 per well on a 24-well plate and infected at an M.O.I. of three. 3 µg/ml puromycin was added 48 hours after infection. For infection of HCT116, Drosha$^{-/-}$, and Dicer$^{-/-}$ cells, cells were seeded at 100,000 per well in a 24-well plate and infected at an M.O.I of three. 3 µg/ml puromycin was added 48 hours after infection.

Knockdown with pTIP-shRNA viruses. Cells were plated at 50,000 to 100,000 cells per well in a 6-well plate. Cells were infected with lentivirus generated in 293T cells from the desired pTIP-shRNA vector in the presence of 8 µg/ml polybrene. Media was replaced 24 hours later. Selection was done 48 hours after infection with 3 µg/ml puromycin. Induction of shRNA expression was achieved by adding 100 ng/ml doxycycline (Dox) to the media.

Transfection with short oligonucleotides. siRNAs were either purchased from Dharmacon (*Figures 3E-G* and *S5B* and *C*, and *S7B*) or synthesized by IDT (*Figures 1I, 2,* and *S1*) as sense and antisense RNA (or DNA for *Figure 2B*) oligos and annealed. The sense RNA oligonucleotides had 3' 2 deoxy-T overhangs. The antisense RNA oligos were phosphorylated at the 5' end and had 3' 2 deoxy-A overhangs. siRNAs targeting CD95L (and controls) were as follows: siRNA (Scr, sense: UGGUUUACAUGUUGUGUGA), siL1 (sense: UACCAGUGCUGAUCAUUUA), siL2 (sense: CAACGUAUCUGAGCUCUCU), siL3 (sense: GCCCUUCAAUUACCCAUAU), siL4 (sense: GGAAAGUGGCCCAUUUAAC), and siL3MUT (sense: GGACUUCAACUAGACAUCU). The siL3 DNA oligos (sense: GCCCTTCAATTACCCATAT) and Scr DNA oligos (sense: TGGTTTACATGTTGTGTGA) were used for the experiment in *Figure 2B*. Blunt siL3 and Scr RNA oligos without the deoxynucleotide overhangs as well as siL2 and siL3 RNA oligos with Cy5-labelled 5' or 3' ends

were used in the experiment in *Figure 2C*. DsiRNA used in *Figure S1* were Dsi13.X (sense RNA oligo: CAGGACUGAG AAGAAGUAAAACCdGdT, antisense RNA oligo: ACGGUUUUACUUCUUCUCAGUCCUGUA), DsiL3 (sense RNA oligo: CAGCCCUUCAAUUACCCAUAUCCdCdC, antisense RNA oligo: GGGGAUAUGGGUAAUUGAAGGGCUGCU), Dsi-13.2 (sense RNA oligo: AUCUU ACCAGUGCUGAUCAUUUAdTdA, antisense RNA oligo: UAUAAAUGAUCAGCACUGGUAAGAUUG), Dsi-13.3 (sense RNA oligo: AAAGUAUACUUCCGGGGUCAAUCdTdT, antisense RNA oligo: AAGAUUGACCCCGGAAGUAUACUUUGG), Dsi-13.9 (sense RNA oligo: CUUCCGGGGUCAAUCUUGCAACAdAdC, antisense RNA oligo: GUUGUUGC AAGAUUGACCCCGGAAGUA), and a non-targeting DsiRNA control Dsi-NC1 (Sense:5'-CGUUAAUCGCGUAUAAUACGCGUdAdT, antisense:5'-AUACGCGUAUUAUACGCGAUUAACGAC, IDT #51-01-14-03). Predesigned siRNA SmartPools targeting the 11 downregulated genes were obtained from Dharmacon and used in *Figure 3C* and *Figure S5B*. Each siRNA SmartPool consisted of 4 siRNAs with On-Target*plus* modification. The following SmartPools were used: L-014208-02 (NUCKS1); L-012212-00 (CAPZA1); L-018339-00 (CCT3); L-013615-00 (FSTL1); L-011548-00 (FUBP1); L-017242-00 (GNB1); L-014597-01 (NAA50); L-020893-01 (PRELID3B); L-019719-02 (SNRPE); L-003941-00 (TFRC); L-006630-00 (HIST1H1C). On-Target*plus* non-targeting control pool (D-001810-10) was used as negative control. HeyA8 cells were seeded at 750 cells per well on a 96-well plate one day before transfection. Cells were transfected using 0.1 µl of Lipofectamine RNAiMAX reagent (ThermoFisher Scientific #13778030) per well. HCT116 cells were seeded at 4000 cells per well on a 96-well plate one day before transfection. 0.2 µl of Lipofectamine RNAiMAX was used for transfection. Media was changed the day after transfection.

Soluble CD95L protein rescue experiments. NB7 cells were seeded at 500 cells per well in a 96-well plate. Next day, cells were infected with the scrambled pLKO lentiviruses or pLKO-shL1 lentiviruses at an M.O.I. of 50 (to achieve 100% transduction efficiency under conditions omitting the puromycin selection step) in the presence of 8 µg/ml polybrene and 100 ng/ml of S2 CD95L for 16 hrs. Media was replaced the next day with media containing varying concentrations of recombinant S2 CD95L (50 ng/ml and 100 ng/ml). Cell confluence was measured over time in the IncuCyte Zoom.

Real-time PCR. Total RNA was extracted and purified using QIAZOL Lysis reagent (QIAGEN) and the miRNeasy kit (QIAGEN). 200 ng of total RNA was used to generate cDNA using the High-Capacity cDNA reverse Transcription kit (Applied Biosystems #4368814). cDNA was quantified using Taqman Gene expression master mix (ThermoFisher Scientific #4369016) with specific primers from ThermoFisher Scientific for GAPDH (Hs00266705_g1), human CD95 (custom probe, Fr primer: *GGCTAACCCCACTCTATGAATCAAT*, Rev primer: *GGCCTGCCTGTTCAGTAACT*, Probe: *CCTTTTGCTGAAATATC*), human CD95L (Hs00181226_g1 and Hs00181225_m1), the shL3 target site in CD95L (custom probe, Fr primer: *GGTGGCCTTGTGATCAATGAAA*, Rev primer: *GCAAGATTGACCCCGGAAG TATA*, Probe: *CTGGGCTGTACTTTGTATATT*), and downstream of the shL3 site (custom probe, Fr primer: *CCCCAGGATCTGGTGATGATG*, Rev primer: *ACTGCCCCCAGGTAGCT*, Probe: *CCCACATCTGCCCAGTAGT*).

To perform arrayed real-time PCR (*Figure S4*), total RNA was extracted and used to make cDNA as described for standard real-time PCR. For Taqman Low Density Array (TLDA) profiling, custom-designed 384-well TLDA cards (Applied Biosystems #43422489) were used

and processed according to the manufacturer's instructions. Briefly, 50 µl cDNA from each sample (200 ng total input RNA) was combined with 50 µl TaqMan Universal PCR Master Mix (Applied Biosystems) and hence a total volume of 100 µl of each sample was loaded into each of the 8 sample loading ports on the TLDA cards that were preloaded with assays from Thermofisher Scientific for human GAPDH control (Hs99999905_m1) and for detection of ATP13A3 (Hs00225950_m1), CAPZA1 (Hs00855355_g1), CCT3 (Hs00195623_m1), FSTL1 (Hs00907496_m1), FUPB1 (Hs00900762_m1), GNB1 (Hs00929799_m1), HISTH1C (Hs00271185_s1), NAA50 (Hs00363889_m1), NUCKS1 (Hs01068059_g1), PRELID3B (Hs00429845_m1), SNRPE (Hs01635040_s1), and TFRC (Hs00951083_m1) after the cards reached room temperature. The PCR reactions were performed using Quantstudio 7 (ThermoFisher Scientific). Since each of the port loads each sample in duplicates on the TLDA card and because two biological replicates of each sample were loaded onto two separate ports, quadruplicate Ct values were obtained for each sample. Statistical analysis was performed using Student's t test. To prepare RNAs from CD95L overexpressing cells HeyA8 ΔshR6 clone #11 cells were plated at 75,000 cells per well in six-well plates and were infected with lentivirus generated in 293T cells from the pLenti-CD95L vector in the presence of 8 µg/ml polybrene. Selection was done with 3 µg/ml puromycin 48 hours after infection. Cells were plated at 600,000 per 15 mm dish (Greiner CELLSTAR, cat#P7237, Sigma) after one day of puromycin selection. Total RNA was harvested at 50 hours after plating for RNAseq analysis

Western blot analysis. Protein extracts were collected by lysing cells with RIPA lysis buffer (1% SDS, 1% Triton X-100, 1% deoxycholic acid). Protein concentration was quantified using the DC Protein Assay kit (Bio-Rad). 30 µg of protein were resolved on 12% SDS-PAGE gels and transferred to nitrocellulose membranes (Protran, Whatman) overnight at 25 mA. Membranes were incubated with blocking buffer (5% non-fat milk in 0.1% TBS/Tween-20) for 1 hour at room temperature. Membranes were then incubated with the primary antibody diluted in blocking buffer over night at 4°C. Membranes were washed 3 times with 0.1% TBS/Tween-20. Secondary antibodies were diluted in blocking buffer and applied to membranes for 1 hour at room temperature. After 3 more additional washes, detection was performed using the ECL reagent (Amersham Pharmacia Biotech) and visualized with the chemiluminescence imager G:BOX Chemi XT4 (Synoptics).

CD95 surface staining. A pellet of about 300,000 cells was resuspended in 2% BSA/PBS on ice. Cells were resuspended with either anti-APO-1 primary antibody or the IgG3 isotype control diluted to 10 µg/ml in 2% BSA/PBS. Cells were incubated on ice at 4°C for 30 minutes, washed with 2% BSA/PBS, and anti-IgG3-RPE was added diluted in 2% BSA/PBS. After an incubation for 30 minutes at 4°C, percent red cells were determined by flow cytometry (Beckman Coulter).

Cell death quantification (DNA fragmentation) and ROS production. A cell pellet (500,000 cells) was resuspended in 0.1% sodium citrate, pH 7.4, 0.05% Triton X-100, and 50µg/ml propidium iodide. After resuspension, cells were incubated 2 to 4 hours in the dark at 4°C. The percent of subG1 nuclei (fragmented DNA) was determined by flow cytometry. For pLKO shRNA infection experiments, subG1 quantification was performed eight days after infection. For siRNA and DsiRNA transfection experiments, subG1 quantification was performed four days after transfection. ROS production was quantified as previously described (Hadji et al., 2014).

Cell growth and fluorescence over time. After treatment/infection, cells were seeded at 700 to 1,500 per well in a 96-well plate in triplicate. Images were captured at indicated time points using an IncuCyte ZOOM live cell imaging system (Essen BioScience) with a 10x objective lens. Percent confluence, red object count, and the green object integrated intensity were calculated using the IncuCyte ZOOM software (version 2015A).

RNA-Seq analysis. HeyA8 ΔshR6 clone #11 was infected with pLKO-shScr or pLKO-shR6. A pool of three 293T ΔshL3 clones was infected with either pTIP-shScr or pTIP-shL3. After selection with puromycin, the pTIP-infected 293T cells were plated with Dox in duplicate at 500,000 cells per T175 flask. The pLKO-infected HeyA8 cells were plated at 500,000 cells per flask. Total RNA was harvested 50 hours and 100 hours after plating. RNA libraries were generated and sequenced (Genomics Core facility at the University of Chicago). The quality and quantity of the RNA samples was checked using an Agilent bio-analyzer. Paired end RNA-SEQ libraries were generated using Illumina TruSEQ TotalRNA kits using the Illumina provided protocol (including a RiboZero rRNA removal step). Small RNA-SEQ libraries were generated using Illumina small RNA SEQ kits using the Illumina provided protocol. Two small RNA-SEQ sub-libraries were generated: one containing library fragments 140-150 bp in size and one containing library fragments 150-200 bp in size (both including the sequencing adaptor of about 130bp). All three libraries (one RNA-SEQ and two small RNA-SEQ) were sequenced on an Illumina HiSEQ4000 using Illumina provided reagents and protocols. The raw counts for RNAs were calculated by HTSeq. The sequenced reads were mapped to hg38 human genome using Tophat and bowtie2. Differential gene expression was analyzed by R Bioconductor DESeq2 package using shrinkage estimation for dispersions and fold changes to improve stability and interpretability of estimates. P values and adj P values were calculated using the DESeq2 package. Counts and sequences of small RNAs were extracted from raw fastq file by UNIX shell scripts and then grouped and summarized by SQL language in database tables. To extract small RNAs (shRNA sequences) adaptor sequences were remove using Trim Galore software.

In order to identify differentially abundant RNAs using a method unbiased by genome annotation, we also analyzed the raw 100 bp reads for differential abundance. First, the second end in each paired end read was reverse complemented, so that both reads were on the same strand. Reads were then sorted and counted using the core UNIX utilities sort and uniq. Reads with fewer than 128 counts across all 16 samples were discarded. A table with all of the remaining reads was then compiled, summing counts from each sequence file corresponding to the same sample. This table contained a little over 100,000 reads. The R package edgeR (http://bioinformatics.oxfordjournals.org/content/26/1/139) was used to identify differentially abundant reads, and then these reads were mapped to the human genome using blat (http://genome.cshlp.org/content/12/4/656.abstract) to determine chromosomal location whenever possible. Homer (http://homer.salk.edu/homer/) was used to annotate chromosomal locations with overlapping genomic elements (such as genes). Raw read counts in each sequence file were normalized by the total number of unique reads in the file.

To identify the most significant changes in expression of RNAs both methods of RNAs Seq analysis (alignment and read based) were used to reach high stringency. All samples were prepared in duplicate and for each RNA the average of the two duplicate was used for further analysis. In the alignment based analysis only RNAs were considered that had a base mean of >2000 reads and were significantly deregulated between the groups (adjusted p-value <0.05). Only RNAs were scored as deregulated when they were more than 1.5 fold changed in the shL3 expressing cells at both time points and in the shR6 expressing cells at either time points (each compared to shScr expressing cells) (*Table S1*). This was done because we found that the pLKO

driven expression of shR6 was a lot lower than the pTIP driven expression of shL3 (see the quantification of the two shRNAs in *Figure S7A*) and likely as a result of the cell responses in the shR6 expressing cells were reduced. In the read based analysis only normalized read numbers of >10 across the samples in each treatment were considered. Only RNA reads were further considered that had a variation between duplicates of less than 2 fold. Only RNAs reads were considered that showed >1.5 change between treatment groups in both cell lines and both time points (*Table S1*). Using the chromosomal localization of each read the gene of origin was determined. Finally, All RNAs were counted that showed deregulation in the same direction with both methods. This resulted in the identification of 11 RNAs that were down and 1 that was upregulated in cells exposed to the shRNAs shL3 and shR6. To determine the number of seed matches in the 3'UTR of downregulated genes the 3'UTRs of the 11 mRNAs were extracted from the Homo sapiens gene (GRCh38.p7) dataset of the Ensembl 86 database using the Ensembl Biomart data mining tool. For each gene only the longest deposited 3'UTR was considered. Seed matches were counted in all 3'UTRs using in-house Perl scripts.

GSEA used in *Figure 3E* and *5C* was performed using the GSEA v2.2.4 software from the Broad Institute (www.http://software.broadinstitute.org/gsea); 1000 permutations were used The Sabatini gene lists (*Table 2*) were set as custom gene sets to determine enrichment of survival genes versus the nonsurvival control genes in downregulated genes from the RNA seq data; GSEA was also performed on all the gene ontology groups (MSigDB c5.all.v6.0). Adjusted p-values below 0.05 were considered significantly enriched. The GO enrichment analysis shown in *Figure 5E* was performed using the software available on www.Metascape.org using default running parameters.

AGO pull down

Between 10 and 25 x 10^6 HCT116 wt or Drosha$^{-/-}$ cells stably expressing either pLenti or pLenti-CD95L^{MUT}NP were lysed in NP40 lysis buffer (20 mM Tris, pH 7.5, 150 mM NaCl, 2 mM EDTA, 1% (v/v) NP40, supplemented with phosphatase inhibitors) on ice for 15 minutes. The lysate was sonicated 3 times for 30 s at 60% amplitude (Sonics, VCX130) and cleared by centrifugation at 12,000*g* for 20 minutes. AGO1-4 were pulled down by using 500 mg of Flag-GST-T6B peptide (Hauptmann et al., 2015) and with 60 ml anti-Flag M2 magnetic beads (Sigma-Aldrich) for 2 hrs at 4°C. The pull-down was washed 3 times in NP40 lysis buffer. During the last wash, 10% of beads were removed and incubated at 95°C for 5 minutes in 2x SDS-PAGE sample buffer. Samples were run on a 4-12% SDS-PAGE and transferred to nitrocellulose membrane. The pull-down efficiency was determined by immunoblotting against AGO1 and AGO2 (Abcam 98056 and 32381). To the remaining beads 500 µl TRIzol reagent were added and the RNA extracted according to the manufacturer's instructions. The RNA pellet was diluted in 20 µl of water. The sample was split and half of the sample was dephosphorylated with 0.5 U/µl of CIP alkaline phosphatase at 37°C for 15 min and subsequently radiolabeled with 0.5 µCi γ-^{32}P-ATP and 1 U/µl of T4 PNK kinase for 20 min at 37°C. The AGO1-4 interacting RNAs were visualized on a 15% urea-PAGE. The remaining RNA was taken through a small RNA library preparation as previously descried (Hafner et al., 2012). Briefly, RNA was ligated with 3' adenylated adapters and separated on a 15% denaturing urea-PAGE. The RNA corresponding to insert size of 19-35 nt was eluted from the gel, ethanol precipitated followed by 5' adapter ligation. The samples were separated on a 12% Urea-PAGE and extracted from the gel. Reverse transcription was performed using Superscript III reverse transcriptase and the cDNA amplified by PCR. The cDNA was sequenced on Illumina HiSeq 3000. Adapter sequences: Adapter 1 – NNTGACTGTGGAATTCTCGGGTGCCAAGG; Adapter 2 – NNACACTCTGGAATTCTCGGGTGCCAAGG, Adapter 3 –

NNACAGAGTGGAATTCTCGGGTGCCAAGG, Adapter 4 – NNGCGATATGGAATTCTCGGGTGCCAAGG, Adapter 47 – NNTCTGTGTGGAATTCTCGGGTGCCAAGG, Adapter 48 – NNCAGCATTGGAATTCTCGGGTGCCAAGG, Adapter 49 – NNATAGTATGGAATTCTCGGGTGCCAAGG, Adapter 50 – NNTCATAGTGGAATTCTCGGGTGCCAAGG. RT primer sequence: GCCTTGGCACCCGAGAATTCCA; PCR primer sequences: CAAGCAGAAGACGGCATACGAGATCGTGATGTGACTGGAGTTCCTTGGCACCCGAG AATTCCA. To identify CD95L derived small RNAs all reads (4 conditions in duplicate) after removal of the adaptor sequences were BLASTED against the CD95L ORF (derived from NM_000639.1). Only reads were considered with an evalue of less than 0.05 and 100% identity across the entire length of the read.

Conversion of shL3 and shR6 to siRNAs. From the RNA seq analysis with HeyA8 ΔshR6 infected with pLKO-shR6 and 293T ΔshL3 clones infected pTIP-shL3, we analyzed the mature double-stranded RNAs derived from pLKO-shR6 and pTIP-shL3 and found that the most abundant RNA forms were both shifted by one nucleotide. Based on these most abundant species observed after cellular processing, we converted shL3 and shR6 sequences to siRNAs. The genomic target sequence in shL3 (21nt) is 5'-ACUGGGCUGUACUUUGUAUAU-3'. For the shL3=>siL3 sense strand, one G was added before the A on the 5' end while the last U on the 3' end was deleted, and second and third to the last ribonucleotides on the 3' end (UA) were replaced with deoxyribonucleotides for stabilization. For shL3=>siL3 antisense strand, the last three nucleotides on the 5' end (AUA) were deleted and one U and two dTs (UdTdT) were added after the last U on the 3'end. The shL3=>siL3 sense strand is 5'-GACUGGGCUGUACUUUGUAdTdA-3' and antisense strand is 5'-/5Phos/UACAAAGUACAGCCCAGUUdTdT-3'. The shR6=>siRNA was designed in similar fashion except that two Gs instead of one G were added to the 5' end of the sense strand while UUdTdT instead of UdTdT was added to the 3' end of the antisense strand. The genomic target sequence in shR6 (21nt) is 5'-GUGCAGAUGUAAACCAAACUU-3'. The shR6=>siR6 sense strand is 5'-GGGUGCAGAUGUAAACCAAACUU-3' and antisense strand is 5'-/5Phos/UUUGGUUUACAUCUGCACUUdTdT-3'. Both shL3=>siL3 and ShR6=>siR6 siRNA duplexes were purchased from Dharmacon.

Construction of pTIP-shRNA libraries. The pTIP-shRNA libraries were constructed by subcloning libraries of 143bp PCR inserts of the form 5'-*XXXXXXXXXXXXXXXXXXXXXXXXXXATAGAGATCGNNNNNNNNN NNNNNNNNNNNNCTCGAGNNNNNNNNNNNNNNNNNNNNNNTTTTTGTACCGAGCTCGGAT CCACTAGTCCAGTGTGGGCATGCTGCGTTGACATTGATT*-3' into the pTIP-shR6 vector after excising the shR6 insert. The poly-N region represents the 21-mer sense and antisense shRNA hairpin. The intervening CTCGAG is the loop region of the shRNA. The 5 libraries targeting Venus, CD95L ORF, CD95L 3'UTR, CD95 ORF, or CD95 3'UTR were composed of every possible 21-mer shRNA (i.e. each nearest neighbor shRNA was shifted by 1 nucleotide). These libraries were synthesized together on a chip as 143 bp single-stranded DNA oligos (CustomArray Inc, Custom 12K oligo pool). Each shRNA pool had its own unique 5' end represented by the poly-*X* region. This allowed selective amplification of a particular pool using 1 of 5 unique Fr primers (CD95L ORF: 5'-*TGGCTTTATATATCTCCCTATCAGTG*-3', CD95L 3' UTR: 5'-*GGTCGTCCT ATCTATTATTATTCACG*-3', CD95 ORF: 5'-*TCTTGTGTCCAGACCAATTTATTTCG*-3', CD95 3'UTR: 5'-

CTCATTGACTATCGTTTTAGCTACTG-3', Venus: 5'-*TATCATCTTTCATGATGACTTTCCGG*-3') and the common reverse primer 5'-*AATCAATGTCAACGCAGCAT*-3'. Phusion High Fidelity Polymerase was used to amplify each library pool; standard PCR conditions were used with an annealing temperature of 61°C and 15 cycles. PCR reactions were purified using PCR Cleanup kit (QIAGEN). The pTIP-shR6 vector and each of the amplified libraries were digested with SphI-HF and BsaBI. Digested PCR products were run on either a 2% Agarose gel or a 20% polyacrylamide (29:1) gel made with 0.5 x TBE buffer. PCR products were extracted using either Gel Extraction kit (QIAGEN) for extraction from Agarose gels or via electro-elution using D-Tube Dialyzer Mini columns (Novagen #71504). Purified PCR inserts were then ligated to the linearized pTIP vector with T4 DNA ligase for 24 hours at 16°C. The ligation mixtures were transformed via electroporation in MegaX DH10B T1 cells (Invitrogen #C6400) and plated on 24 cm ampicillin dishes. At least 10 colonies per pool were picked and sequenced to verify successful library construction. After verification, all colonies per library were pooled together and plasmid DNA extracted using the MaxiPrep kit (QIAGEN). The 5 pTIP-shRNA library DNA preps were used to produce virus in 293T cells.

Lethality screen with pTIP-shRNA libraries. NB7 cells were seeded at 1.5 x 10^6 per 145 cm^2 dish. Two dishes were infected with each of the 5 libraries with a transduction efficiency of about 10 to 20%. Media was replaced next day. Infected cells were selected with 1.5 µg/ml puromycin. Cells infected with the Venus, CD95L ORF, and CD95L 3'UTR-targeting libraries were pooled in a 1:1:1 ratio to make the CD95L cell pool. Likewise, cells infected with the Venus, CD95 ORF, and CD95 3'UTR-targeting libraries were pooled to make the CD95 receptor cell pool. The CD95 and the CD95L cell pools were plated separately each in 2 sets of duplicates seeded at 600,000 cells per 145cm^2 dish. One set received 100 ng/ml Dox, and the other one was left untreated (total of 4 dishes per combined pool; 2 received no treatment and 2 received Dox). Cells infected with the different libraries were also plated individually in triplicate with or without Dox on a 96-well plate to assess the overall toxicity of each pool. DNA was collected from each 145cm^2 dish 9 days after Dox addition.

The shRNA barcodes were amplified from the harvested DNA template using NEB Phusion Polymerase with 4 different pairs of primers (referred to as N, N+1, N+2, and N+3) in separate reactions per DNA sample. The N pair consisted of the primers used to amplify the CD95L ORF library (Fr: 5'-*TGGCTTTATATATCTCCCTATCAGTG*-3' and Rev: 5'-*AATCAATGTCAACGCAGCAT*-3'). The N+1 primers had a single nucleotide extension at each 5' end of the N primers corresponding to the pTIP vector sequence (Fr: 5'-*TTGGCTTTATATATCTCCCTATCAGTG*-3' and Rev: 5'-*TAATCAATGTCAACGCAGCAT*-3'). The N+2 primers had 2 nucleotide extensions (Fr: 5'-*CTTGGCTTTATATATCTCCCTATCAGTG*-3' and Rev: 5'-*ATAATCAATGTCAACGCAGCAT*-3'), and the N+3 primers had 3 nucleotide extensions (Fr: 5'-*TCTTGGCTTTATATATCTCCCTATCAGTG*-3' and Rev: 5'-*AATAATCAATGTCAACGCAGCAT*-3'). The barcodes from the pTIP-shRNA library plasmid preparations were also amplified using Phusion Polymerase with the N, N+1, N+2, and N+3 primer pairs. The shRNA barcode PCR products were purified from a 2% Agarose gel and submitted for 100 bp paired-end deep sequencing (Genomics Core facility at the University of Chicago). DNA was quantitated using the Qubit. The 4 separate PCR products amplified using N, N+1, N+2, and N+3 were combined in equimolar amounts for each sample. Libraries were generated using the Illumina TruSeq PCR-free kit using the Illumina provided protocol. The libraries were sequenced using the HiSEQ4000 with Illumina provided reagents and protocols. Raw sequence counts for DNAs were calculated

by HTSeq. shRNA sequences in the PCR pieces of genomic DNA were identified by searching all reads for the sense sequence of the mature shRNA plus the loop sequence CTCGAG. To avoid a division by zero problem during the subsequent analyses all counts of zero in the raw data were replaced with 1. A few sequences with a total read number <10across all plasmids reads were not further considered. In the CD95L pool this was only one shRNA (out of 2362 shRNAs) (L792') and in the CD95 20 shRNAs (out of 3004 shRNAs) were not represented (R88, R295, R493, R494, R496, R497, R498, R499, R213', R215', R216', R217', R220', R221', R222', R223', R225', R226', R258', R946', R1197', R423'). While most shRNAs in both pools had a unique sequence two sequences occurred 6 times (L605', L607', L609', L611', L613', L615', and L604', L606', L608', L610', L612', L614'). In these cases read counts were divided by 6. Two shRNAs could not be evaluated: 1) shR6 in the CD95 pool. It had a significant background due to the fact that the pTIP-shR6 was used as a starting point to clone all other shRNAs. 2) shL3 was found to be a minor but significant contaminant during the infection of some of the samples. For each condition two technical duplicates and two biological duplicates were available. To normalize reads in order to determine the change in relative representation of shRNAs between conditions, the counts of each shRNA in a subpool (all replicates and all conditions) was divided by the total number of shRNAs in each subpool (%). First, the mean of the technical replicates (R1 and R2) was taken. To analyze the biological replicates and to determine the changes between conditions, two analyses were performed: 1) The change in shRNA representation between the cloned plasmid library and cells infected with the library and then cultured for 9 days without Dox (infection -Dox). Fold downregulation was calculated for each subpool as [(plasmid %/-Dox1 %+plasmid %/-Dox2 %)/2]. 2) The difference in shRNA composition between the infected cells cultured with (infection +Dox) and without Dox. Fold downregulation was calculated for each subpool as [(-Dox1 %/+Dox1 %)+(-Dox1 %/+Dox2 %)+(-Dox2 %/+Dox1 %)+(-Dox2 %/+Dox2 %)/4]. Only shRNAs were considered that were at least 5 fold underrepresented in either of the two analyses (data in *Table S3*).

The toxicity index (TI). The TI is defined by the sum of the counts of a 6mer or 8mer seed match in the 3'UTRs of critical survival genes divided by the seed match counts in the 3'UTRs of nonsurvival genes. We used the 1882 survival genes recently described in a CRISPR/Cas9 lethality screen by Wang et al. (Wang et al., 2015). The survival genes were defined by having a CRIPSR score of <-0.1 and an adjusted p-value of <0.05. We chose as a control group to these top essential genes the bottom essential genes using inverse criteria (CRISPR score of >0.1 and adjusted p-value of <0.05) and are referring to them as the "nonsurvival genes". Both counts were normalized for the numbers of genes in each gene set. 3'UTRs were retrieved as described above. For the survival genes 1846 and for the nonsurvival genes 416 3'UTRs were found. For each gene only seed matches in the longest 3'UTR were counted. The TI was calculated for each of the 4096 possible 6mer combinations and each of the 65536 possible 8mer combinations (*Table S4*). These numbers were then assigned to the results of the shRNA screen (*Table S5*). An alternative TI was calculated based on the top 850 most highly expressed survival genes (all expressed >1000 average reads) and select 850 expression matched genes not described to be critical for cancer cell survival.

Sylamer analysis. Sylamer is a tool to test for the presence of RNAi-type regulation effects from a list of differentially expressed genes, independently from small RNA measurements (van Dongen et al., 2008) (http://www.ebi.ac.uk/research/enright/software/sylamer). For short stretches of RNA (in this case length 6, 7, and 8 in length corresponding to the lengths of the determinants of seed region binding in RNAi-type binding events), Sylamer tests for all possible

motifs of this length whether the motif occurrences are shifted in sequences associated with the list under consideration, typically 3'UTRs when analyzing RNAi-type binding events. A shift or enrichment of such a motif towards the down-regulated end of the gene list is consistent with upregulation of a small RNA that has the motif as the seed region. Sylamer tests in small increments along the list of genes, using a hypergeometric test on the counts of a given word, comparing the leading part of the gene list to the universe of all genes in the list. For full details refer to (van Dongen et al., 2008). Enriched motifs stand out from the back-ground of all motifs tested, as visible in the Sylamer plot. The plot consist of many different lines, each line representing the outcomes of a series of tests for a single word, performed along regularly spaced intervals (increments of 200 genes) of the gene list. Each test yields the log-transformed P-value arising from a hypergeometric test as indicated above. If the word is enriched in the leading interval the log-transformed value has its value plotted on the positive y-axis (sign changed), if the word is depleted the log-transformed value is plotted on the negative y-axis. 3' UTRs were used from Ensembl, version 76. As required by Sylamer, they were cleaned of low-complexity sequences and repetitive fragments using respectively Dust (Morgulis et al., 2006) with default parameters and the RSAT interface (Medina-Rivera et al., 2015) to the Vmatch program, also run with default parameters. Sylamer (version 12-342) was run with the markov correction parameter set to 4.

Statistical analyses. Continuous data were summarized as means and standard deviations and dichotomous data as proportions. Continuous data were compared using t-tests for two independent groups and one-way ANOVA for 3 or more groups. For evaluation of continuous outcomes over time, two-way ANOVA was used with one factor for the treatment conditions of primary interest and a second factor for time treated as a categorical variable to allow for non-linearity. Comparisons of single proportions to hypothesized null values were evaluated using binomial tests. Statistical tests of two independent proportions were used to compare dichotomous observations across groups. To test if higher TI is enriched in shRNAs that were highly downregulated, p-values were calculated based on permutated datasets using Mann-Whitney U tests. The ranking of TI was randomly shuffled 10,000 times and the W statistic from our dataset was compared to the distribution of the W statistic of the permuted datasets. Test of enrichment was based on the filtered data of at least 5-fold difference, which we define as a biologically meaningful. Fisher Exact Test was performed to assess enrichment of downregulated genes amongst genes with si/shRNA seed matches. All statistical analyses were conducted in Stata 14 or R 3.3.1.

Data availability. The accession numbers for the RNA-Seq and expression data reported in this paper are GSE87817 and GSE96620.

Acknowledgements
We are grateful to Lindsay Stolzenburg and Ann Harris for helping to set up the CRISPR/Cas9 gene editing method, to Denise Scholtens for biostatistics support, and to Matthew Schipma for biocomputational support. M.H. and A.A.S were supported by the Intramural Research Program of NIAMS. A.A.S. acknowledges support by the Swedish Research Council postdoctoral fellowship. This work was funded by training grants T32CA070085 (to M.P.) and T32CA009560 (to W.P.) R50CA211271 (to J.C.Z.), and R35CA197450 (to M.E.P.).

Author contributions
W.P. planned the study and performed experiments. M.P. established the multiplex qPCR method and performed experiments, Q.Q.G., A.H., A.S.Q., A.S., A.H.K., and A.E.M. performed experiments, S.D. performed the SYMALER analysis, E.B. and J.S.Z. provided biocomputational and K.A.K. biostatistics support, A.A.S. performed the AGO2 pull down experiment, M.H. provided assistance and discussions on the mechanism of RNAi and the RISC, and M.E.P. directed the study and wrote the manuscript.

Additional files
Supplementary Information accompanies this paper at

Figure legends

Figure 1. CD95 and CD95L derived si/shRNAs kill cells in the absence of the targeted site in CD95 or CD95L. (**A**) Schematic of the genomic locations and sequences of the gRNAs used to excise the siL3 (Δ64bp) and shL3 (Δ41bp) target sites from CD95L. PAM site is underlined. Green indicates a gRNA targeting the sense strand. Blue indicates a gRNA targeting the antisense strand. (**B**) Schematic showing the genomic locations and sequences of the gRNAs used to excise the shR6 (Δ227bp) target site. (**C**) PCR with flanking (*top panels*) and internal (*bottom panels*) primers used to confirm the Δ41 deletion in the shL3 site in 293T clones. Cells transfected with Cas9 only (Cas9) are wild-type, clone #3 is heterozygous, and clones #1 and #5 carry homozygous deletions. (**D**) Quantitative PCR for endogenous CD95L with a primer downstream of the Δ41 shL3 deletion and another primer internal to the deleted region. nd, not detectable. (**E**) PCR with flanking (*top row*) and internal (*bottom row*) primers used to confirm the presence of the shL3 Δ41 (*top panel*), siL3 Δ64 (*middle panel*), and shR6 Δ227 (*bottom panel*) deletions in HeyA8 clones. Mix, HeyA8 cells after transfection with Cas9 and gRNAs but before single cell cloning. (**F**) Quantitative PCR for CD95 in HeyA8 cells transfected with Cas9 plasmid (Cas9) alone, or the HeyA8 ΔshR6 clone #11. RNA was extracted 5 days after infection with pLKO-shScr, pLKO-shR6, pLKO-shR2, or pLKO-shR6' (targeting the 3'UTR). (**G**) Percent cell confluence over time of 293T cells (*left*) and a pool of three 293T clones with a homozygous deletion of the shL3 target site (*right*) infected with pTIP-shScr or pTIP-shL3 and treatment with or without Dox. (**H**) *Left:* Percent confluence over time of HeyA8 cells infected with pLKO-shScr, pLKO-shR6, or pLKO-shL3. *Centre:* Percent confluence over time of a HeyA8 clone with a homozygous deletion of the shR6 target site infected with either pLKO-shScr or pLKO-shR6. *Right:* Percent confluence over time of a pool of three HeyA8 clones with a homozygous deletion of the shL3 site infected with either pLKO-shScr or pLKO-shL3. (**I**) Percent confluence over time of a pool of three HeyA8 clones harboring a homozygous deletion of the siRNA L3 (siL3) target site after transfection with different concentrations of siScr or siL3.

Figure 2. Toxicity of CD95L derived siRNAs involves canonical RNAi activity. (**A**) Percent cell confluence (*left*) and total green object integrated intensity (*right*) over time of a HeyA8 CD95 knockout clone (ΔR6 cl#2) expressing the Venus-CD95L sensor after transfection with 25 nM of single-stranded sense, single-stranded antisense, or double-stranded (ds) siScr or siL3 siRNAs. The CD95L sensor is schematically shown and comprises the Venus ORF fused to the CD95L ORF lacking the A of the ATG start codon (X). (**B**) Percent cell confluence (*left*) and total green object integrated intensity (*right*) over time of the HeyA8 CD95L sensor cell used in *Figure 2A* after transfection with 5 nM siScr or siL3 double-stranded RNA (dsRNA) or double-stranded DNA (dsDNA). (**C**) Summary of experiments to test whether siL3 and siL2 siRNAs modified as indicated (*left*) were active (check mark) or not (X) in reducing green fluorescence or cell growth (both >70% reduction at end point) when transfected at 25 nM siRNAs (except for blunt end oligonucleotides which were used at 5 nM and compared to 5 nM of siL3) into HeyA8 CD95L sensor cells used in *Figure 2A*. Endpoints were 164 hours for blunt end siRNA transfection, 180 hrs for modified siL3 and 144 hrs for modified siL2 siRNA transfections. (**D**) Red object count over time of HeyA8 cells (expressing NucRed) after transfection with different ratios of siL3 and mutant siL3 (siL3MUT). (**E**) Percent cell confluence over time of HCT116 parental (*left*) or Dicer$^{-/-}$ (clone #43, another Dicer$^{-/-}$ clone, #45, gave a similar result, data not shown), or Drosha$^{-/-}$ (*right*) cells after infection with either shScr, shL3 or shR6. Inserts show expression levels of Drosha/Dicer and AGO2 levels in the tested cells. (**F**) Western blot analysis of HCT116 wt, Dicer$^{-/-}$ or Drosha$^{-/-}$ cells 5 days after infection with either pLKO-shScr or pLKO-

shR6. (**G**) Percent cell confluence over time of HCT116 wt, Dicer$^{-/-}$ and Drosha$^{-/-}$ cells after transfection with 25 nM siScr or siL3. (**H**) Percent reduction in Venus expression (green) and in cell number (red object count (red)) over time of HeyA8 cells expressing the Venus-CD95L sensor and red nuclei after transfection with 5 nM of different chimeric siRNAs generated by substituting nucleotides in the toxic siL3 with the scrambled siRNA sequence beginning at either the seed match end (top) or the opposite end (bottom) of siL3 after 188 hours. The schematic in the middle shows the sequence of siL3 and the Scr siRNA (both sense and antisense strands). The 6mer seed sequence region of siL3 (positions 2 to 7) is highlighted in light blue. Nucleotides shared by siScr and siL3 are shown in grey font.

Figure 3. Toxic shRNAs derived from CD95 and CD95L cause downregulation of critical survival genes. (**A**) Schematic of RNA-Seq work flow for total RNA sample prepared both before (50 hrs) and during (100 hrs) induction of DISE after expressing either shR6 or shL3 from different vector systems (i.e. pLKO-shR6 and pTIP-shL3) in different cells (HeyA8 shR6 Δ227 cells and 293T shL3 Δ41 cells). (**B**) One mRNA was up and 11 mRNAs were downregulated in the cells treated with toxic shL3 and shR6 as shown in *Figure 3A*. mRNAs shown in red were found to be essential cancer survival genes in two CRISPR lethality screens. The number of essential genes was enriched from 6.6% of the tested genes (Blomen et al., 2015; Wang et al., 2015) to 54.5% in our study ($p=3 \times 10^{-6}$ according to binomial distribution). The number of shL3 and shR6 6mer seed sequences in the 3'UTRs is shown for each gene in the green and yellow ovals, respectively. (**C**) The level of growth inhibition observed in HeyA8 cells transfected with siRNA SmartPools (25 nM) individually targeting the listed survival genes. The seven genes are shown targeting of which significantly reduced cell growth compared to cells transfected with a siScr pool at 140 hrs (samples done in quadruplicate) with an ANOVA $p<0.05$. (**D**) Gene set enrichment analysis for a group of 1846 survival genes (*top 4 panels*) and 416 nonsurvival genes (*bottom 4 panels*) identified in a genome-wide CRISPR lethality screen (Wang et al., 2015) after introducing Dox-inducible shL3 in 293T ΔshL3 cells (*left-most panels*), shR6 in HeyA8 ΔshR6 cells (*center-left panels*), shL1 in parental 293T cells (*center-right panels*), and siL3 in HeyA8 cells (*right-most panels*). Scrambled sequences served as controls. p-values indicate the significance of enrichment. (**E**) Schematics showing all RNAs at least 1.5 fold downregulated (adj p-value <0.05) in cells treated as in *Figure 3A*. Of the histones only the ones underlined contain a 3'UTR.

Figure 4. DISE inducing si- and shRNAs target critical survival genes through RNAi. (**A**) Sylamer plots for the list of genes in the shL3 experiment (top) and the shR6 experiment (bottom) ordered from down-regulated to up-regulated. The most highly enriched sequence is shown which in each case is the 8mer seed match of the introduced shRNA. The red line corresponds to a p-value threshold of 0.05 after Bonferroni correction for the number of words tested (65536). Bonferroni-adjusted p-values are shown. The unadjusted p-values are 1.58E-24 and 1.35E-26, respectively. The black line corresponds to the represents the sequences carrying the let-7 8mer seed match. (**B**) Location of the 6mer seed matches of either shL3 or shR6 in the 3'UTRs of the 11 genes (shown at scale) identified in the screen described in *Figure 3A*. Red font indicates a critical survival gene. (**C**) A series of six 2x2 contingency tables comparing whether or not a critical survival gene is downregulated after treatment with the indicated siRNA or shRNA to whether or not its 3'UTR contains at least 1 seed match for the introduced sh/siRNA. p-values were calculated using Fisher's Exact Test to determine any significant relationship between gene downregulation and presence of seed matches in 3'UTR.

Figure 5. Identifying all toxic shRNAs derived from CD95L and CD95. (**A**) Schematic showing the cloned shRNAs covering the ORF of Venus and the ORFs and 3'UTRs of CD95L and CD95. The 3'UTR is displayed as a dashed line because it was not included in the full-length Venus-CD95L/CD95 sensors. (**B**) Work-flow of pTIP-shRNA library synthesis, shRNA screen and data analysis. (**C**) Ranked fold reduction of shRNAs spanning Venus and CD95L (ORF and 3'UTR) (*left 3 panels*) and Venus and CD95 (ORF and 3'UTR) (*right 3 panels*). The ranked lists were separated into the shRNAs derived from Venus (top), the ORFs (center) and the 3'UTRs (bottom). The p-value of enrichment for each ranked set of shRNAs is given. Only the parts of the ranked lists are shown with the downregulated shRNAs. For all 6 panels, the top section of each panel (boxed in blue) contains the data on shRNAs downregulated after infection of cells and cultured for 9 days without Dox when compared to the composition of the shRNA plasmid library and the bottom half (boxed in orange) contains the data on shRNAs downregulated after culture with Dox for 9 days when compared to the culture without Dox. P-values were calculated using Mann Whitney U tests with a one-sided alternative that the rank was lower. (**D**) The location of all shRNAs significantly downregulated at least 5 fold along the sequences of Venus, CD95L ORF, CD95L 3'UTR (left panel) and Venus, CD95 ORF, and CD95 3'UTR (right panel). The top half of each sub panel (blue ticks) shows the shRNAs downregulated after infection and the bottom half (orange ticks) contains the data on shRNAs downregulated after culture with Dox for 9 days. Significance of enrichment in the different subpanels is shown. p-values were calculated according to statistical tests of two proportions. Each data set was compared to the corresponding Venus distribution. Green line: sequence that corresponds to the intracellular domain of CD95L. (**E**) Fold downregulation versus ranked Toxicity Index for shRNAs of the Venus/CD95L pool (*left three panels*) and the Venus/CD95 pool (*right three panels*). Orange and blue tick marks indicate the same as in *Figure 4D*. To test if higher TI is enriched in shRNAs that were highly downregulated, p-values were calculated based on permutated datasets using Mann-Whitney U tests. The ranking of TI was randomly shuffled 10,000 times and the W statistic from our dataset was compared to the distribution of the W statistic of the permuted datasets.

Figure 6. The CD95L RNA is toxic to cancer cells. (**A**) *Left*: the different CD95L mutants used. *Right:* Percent cell confluence over time of HeyA8 parental cells in the absence (*left panel*) or in the presence of zVAD-fmk (*center panel*), or $CD95^{-/-}$ cells (*right panel*; clone #11, see *Figure S3*; similar results were obtained with clones 1 and 2 (data not shown)) after infection with lentiviral CD95L, $CD95L^{MUT}$, or $CD95L^{MUT}$NP. (**B**) *Left*: Western blot analysis of HeyA8 cells overexpressing different CD95L mutant RNAs. Cells expressing $CD95L^{MUT}$ or CD95L were pretreated with zVAD. Note, the small amount of truncated CD95L in cells infected with CD95L MUT-NP does not have CD95 binding activity. *Right*: qPCR analysis for CD95L of the same samples. (**C**, **D**) Quantification of cell death (**C**) and ROS production (**D**) in cells expressing either pLenti (C) or pLenti-CD95L (L) at different time points.* $p<0.05$, ** $p<0.001$, *** $p<0.0001$. (**E**) Gene set enrichment analysis for the 1846 survival genes (*top panel*) and the 416 nonsurvival genes (*bottom panel*) of mRNAs downregulated in CD95L expressing HeyA8 $CD95^{-/-}$ cells compared to parental HeyA8 cells. p-values indicate the significance of enrichment. (**F**) The genes downregulated in all cells after introduction of the four si/shRNAs derived from either CD95 or CD95L (see *Figure 3D*). Histones underlined contain a 3'UTR. (**G**) Metascape analysis of 5 RNA Seq data sets analyzed. The boxed GO term clusters were highly enriched in all 5 data sets.

Figure 7. Toxic small RNAs are generated in cells expressing CD95L mRNA and loaded into the RISC. (**A**) Percent cell confluence over time of HCT116 parental (*left*) or Drosha$^{-/-}$ (*right*) cells after infection with CD95^{MUT}NP. (**B**) Phase contrast images of Drosha$^{-/-}$ cells 9 hours after infection with either empty vector or CD95L^{MUT}NP. (**C**) *Top*: autoradiograph on pulled down RNAs pulled down with the AGO binding peptide. *Bottom*: Western blot analysis of pulled AGO proteins. (**D**) Pie charts showing the relative ratio of small RNAs pulled down with the AGO proteins in wt and Drosha$^{-/-}$ cells. Depicted are all the amounts of all small RNAs that contributed at least 0.01% to the total RNA content. Only in the Drosha$^{-/-}$ cells was a significant amount of CD95L derived AGO bound reads found. They represented the 75th most abundant small RNA species (arrow). The average number of total sequenced reads (of two duplicates) are shown for each condition. (**E**) *Top*: Number of reads (normalized per million) of the top five most abundant small RNAs in the RISC of either HCT116 wt-pLenti or -pLenti-CD95L cells. *Bottom*: Number of reads (per million) of the top five genes with small RNAs most abundant in the RISC of either HCT116 Drosha$^{-/-}$ pLenti, or -pLenti-CD95L cells and of CD95L derived. Note: miR-21 is not included as it is already shown in the top row. Bottom right panel: Abundance of AGO bound CD95L derived small RNAs. Shown in all panels is the abundance of RNAs in the four samples. v, pLenti; L, pLenti-CD95L expressing cells. (**F**) Length distribution of AGO bound RNAs across the four samples. The length of the most prevalent species is given for the two Drosha$^{-/-}$ samples. (**G**) Alignment of the detected AGO associated CD95L derived reads with the ORF of CD95L. Bottom panel: The average of all downregulated shRNAs (>5 fold) in the toxicity screen in *Figure 5D* between the shRNAs downregulated in cells after infection and after Dox treatment.

References

Algeciras-Schimnich, A., Pietras, E.M., Barnhart, B.C., Legembre, P., Vijayan, S., Holbeck, S.L., and Peter, M.E. (2003). Two CD95 tumor classes with different sensitivities to antitumor drugs. Proc Natl Acad Sci U S A *100*, 11445-11450.

Barnhart, B.C., Legembre, P., Pietras, E., Bubici, C., Franzoso, G., and Peter, M.E. (2004). CD95 ligand induces motility and invasiveness of apoptosis-resistant tumor cells. EMBO J *23*, 3175-3185.

Birmingham, A., Anderson, E.M., Reynolds, A., Ilsley-Tyree, D., Leake, D., Fedorov, Y., Baskerville, S., Maksimova, E., Robinson, K., Karpilow, J.*, et al.* (2006). 3' UTR seed matches, but not overall identity, are associated with RNAi off-targets. Nat Methods *3*, 199-204.

Blomen, V.A., Majek, P., Jae, L.T., Bigenzahn, J.W., Nieuwenhuis, J., Staring, J., Sacco, R., van Diemen, F.R., Olk, N., Stukalov, A.*, et al.* (2015). Gene essentiality and synthetic lethality in haploid human cells. Science *350*, 1092-1096.

Bramsen, J.B., Laursen, M.B., Nielsen, A.F., Hansen, T.B., Bus, C., Langkjaer, N., Babu, B.R., Hojland, T., Abramov, M., Van Aerschot, A.*, et al.* (2009). A large-scale chemical modification screen identifies design rules to generate siRNAs with high activity, high stability and low toxicity. Nucleic Acids Res *37*, 2867-2881.

Ceppi, P., Hadji, A., Kohlhapp, F., Pattanayak, A., Hau, A., Xia, L., Liu, H., Murmann, A.E., and Peter, M.E. (2014). CD95 and CD95L promote and protect cancer stem cells. Nature Commun *5*, 5238.

Chen, L., Park, S.M., Tumanov, A.V., Hau, A., Sawada, K., Feig, C., Turner, J.R., Fu, Y.X., Romero, I.L., Lengyel, E.*, et al.* (2010). CD95 promotes tumour growth. Nature *465*, 492-496.

Drachsler, M., Kleber, S., Mateos, A., Volk, K., Mohr, N., Chen, S., Cirovic, B., Tuttenberg, J., Gieffers, C., Sykora, J.*, et al.* (2016). CD95 maintains stem cell-like and non-classical EMT programs in primary human glioblastoma cells. Cell Death Dis *7*, e2209.

ElOjeimy, S., McKillop, J.C., El-Zawahry, A.M., Holman, D.H., Liu, X., Schwartz, D.A., Day, T.A., Dong, J.Y., and Norris, J.S. (2006). FasL gene therapy: a new therapeutic modality for head and neck cancer. Cancer Gene Ther *13*, 739-745.

Fedorov, Y., Anderson, E.M., Birmingham, A., Reynolds, A., Karpilow, J., Robinson, K., Leake, D., Marshall, W.S., and Khvorova, A. (2006). Off-target effects by siRNA can induce toxic phenotype. RNA *12*, 1188-1196.

Friesen, C., Fulda, S., and Debatin, K.M. (1999). Cytotoxic drugs and the CD95 pathway. Leukemia *13*, 1854-1858.

Grimm, D., Streetz, K.L., Jopling, C.L., Storm, T.A., Pandey, K., Davis, C.R., Marion, P., Salazar, F., and Kay, M.A. (2006). Fatality in mice due to oversaturation of cellular microRNA/short hairpin RNA pathways. Nature *441*, 537-541.

Gu, S., Jin, L., Zhang, Y., Huang, Y., Zhang, F., Valdmanis, P.N., and Kay, M.A. (2012). The loop position of shRNAs and pre-miRNAs is critical for the accuracy of dicer processing in vivo. Cell *151*, 900-911.

Guo, H., Ingolia, N.T., Weissman, J.S., and Bartel, D.P. (2010). Mammalian microRNAs predominantly act to decrease target mRNA levels. Nature *466*, 835-840.

Ha, M., and Kim, V.N. (2014). Regulation of microRNA biogenesis. Nat Rev Mol Cell Biol *15*, 509-524.

Hadji, A., Ceppi, P., Murmann, A.E., Brockway, S., Pattanayak, A., Bhinder, B., Hau, A., De Chant, S., Parimi, V., Kolesza, P.*, et al.* (2014). Death induced by CD95 or CD95 ligand elimination. Cell Reports *10*, 208-222.
Hafner, M., Renwick, N., Farazi, T.A., Mihailovic, A., Pena, J.T., and Tuschl, T. (2012). Barcoded cDNA library preparation for small RNA profiling by next-generation sequencing. Methods *58*, 164-170.
Hamilton, A.J., and Baulcombe, D.C. (1999). A species of small antisense RNA in posttranscriptional gene silencing in plants. Science *286*, 950-952.
Hart, T., Brown, K.R., Sircoulomb, F., Rottapel, R., and Moffat, J. (2014). Measuring error rates in genomic perturbation screens: gold standards for human functional genomics. Mol Syst Biol *10*, 733.
Hart, T., Chandrashekhar, M., Aregger, M., Steinhart, Z., Brown, K.R., MacLeod, G., Mis, M., Zimmermann, M., Fradet-Turcotte, A., Sun, S.*, et al.* (2015). High-Resolution CRISPR Screens Reveal Fitness Genes and Genotype-Specific Cancer Liabilities. Cell *163*, 1515-1526.
Hauptmann, J., Schraivogel, D., Bruckmann, A., Manickavel, S., Jakob, L., Eichner, N., Pfaff, J., Urban, M., Sprunck, S., Hafner, M.*, et al.* (2015). Biochemical isolation of Argonaute protein complexes by Ago-APP. Proc Natl Acad Sci U S A *112*, 11841-11845.
Hyer, M.L., Voelkel-Johnson, C., Rubinchik, S., Dong, J., and Norris, J.S. (2000). Intracellular Fas ligand expression causes Fas-mediated apoptosis in human prostate cancer cells resistant to monoclonal antibody-induced apoptosis. Mol Ther *2*, 348-358.
Jackson, A.L., Burchard, J., Schelter, J., Chau, B.N., Cleary, M., Lim, L., and Linsley, P.S. (2006). Widespread siRNA "off-target" transcript silencing mediated by seed region sequence complementarity. RNA *12*, 1179-1187.
Jinek, M., East, A., Cheng, A., Lin, S., Ma, E., and Doudna, J. (2013). RNA-programmed genome editing in human cells. eLife *2*, e00471.
Khan, A.A., Betel, D., Miller, M.L., Sander, C., Leslie, C.S., and Marks, D.S. (2009). Transfection of small RNAs globally perturbs gene regulation by endogenous microRNAs. Nat Biotechnol *27*, 549-555.
Kim, D.H., Behlke, M.A., Rose, S.D., Chang, M.S., Choi, S., and Rossi, J.J. (2005). Synthetic dsRNA Dicer substrates enhance RNAi potency and efficacy. Nat Biotechnol *23*, 222-226.
Kim, Y.K., Kim, B., and Kim, V.N. (2016). Re-evaluation of the roles of DROSHA, Export in 5, and DICER in microRNA biogenesis. Proc Natl Acad Sci U S A *113*, E1881-1889.
Kleber, S., Sancho-Martinez, I., Wiestler, B., Beisel, A., Gieffers, C., Hill, O., Thiemann, M., Mueller, W., Sykora, J., Kuhn, A.*, et al.* (2008). Yes and PI3K Bind CD95 to Signal Invasion of Glioblastoma. Cancer Cell *13*, 235-248.
Krammer, P.H. (2000). CD95's deadly mission in the immune system. Nature *407*, 789-795.
Krol, J., Loedige, I., and Filipowicz, W. (2010). The widespread regulation of microRNA biogenesis, function and decay. Nat Rev Genet *11*, 597-610.
Lin, X., Ruan, X., Anderson, M.G., McDowell, J.A., Kroeger, P.E., Fesik, S.W., and Shen, Y. (2005). siRNA-mediated off-target gene silencing triggered by a 7 nt complementation. Nucleic Acids Res *33*, 4527-4535.
Lu, J., Getz, G., Miska, E.A., varez-Saavedra, E., Lamb, J., Peck, D., Sweet-Cordero, A., Ebert, B.L., Mak, R.H., Ferrando, A.A.*, et al.* (2005). MicroRNA expression profiles classify human cancers. Nature *435*, 834-838.
Mali, P., Yang, L., Esvelt, K.M., Aach, J., Guell, M., DiCarlo, J.E., Norville, J.E., and Church, G.M. (2013). RNA-guided human genome engineering via Cas9. Science *339*, 823-826.

Marques, J.T., and Williams, B.R. (2005). Activation of the mammalian immune system by siRNAs. Nat Biotechnol *23*, 1399-1405.

Medina-Rivera, A., Defrance, M., Sand, O., Herrmann, C., Castro-Mondragon, J.A., Delerce, J., Jaeger, S., Blanchet, C., Vincens, P., Caron, C.*, et al.* (2015). RSAT 2015: Regulatory Sequence Analysis Tools. Nucleic Acids Res *43*, W50-56.

Morgens, D.W., Deans, R.M., Li, A., and Bassik, M.C. (2016). Systematic comparison of CRISPR/Cas9 and RNAi screens for essential genes. Nat Biotechnol *34*, 634-636.

Morgulis, A., Gertz, E.M., Schaffer, A.A., and Agarwala, R. (2006). A fast and symmetric DUST implementation to mask low-complexity DNA sequences. J Comput Biol *13*, 1028-1040.

Murmann, A.E., McMahon, K.M., Halluck-Kangas, A., Ravindran, N., Patel, M., Law, C., Brockway, S., Wei, J.J., Thaxton, C.S., and Peter, M.E. Induction of DISE in ovarian cancer cells in vivo. Oncotarget, Accepted.

Patel, M., and Peter, M.E. Identification of DISE-inducing shRNAs by monitoring cellular responses. Cell Cycle, Accepted.

Peter, M.E., Budd, R.C., Desbarats, J., Hedrick, S.M., Hueber, A.O., Newell, M.K., Owen, L.B., Pope, R.M., Tschopp, J., Wajant, H.*, et al.* (2007). The CD95 receptor: apoptosis revisited. Cell *129*, 447-450.

Petri, S., and Meister, G. (2013). siRNA design principles and off-target effects. Methods Mol Biol *986*, 59-71.

Pham, D.H., Moretti, P.A., Goodall, G.J., and Pitson, S.M. (2008). Attenuation of leakiness in doxycycline-inducible expression via incorporation of 3' AU-rich mRNA destabilizing elements. Biotechniques *45*, 155-156.

Pratt, A.J., and MacRae, I.J. (2009). The RNA-induced silencing complex: a versatile gene-silencing machine. J Biol Chem *284*, 17897-17901.

Qadir, A.S., Ceppi, P., Brockway, S., Law, C., Mu, L., Khodarev, N.N., Kim, J., Zhao, J.C., Putzbach, W., Murmann, A.E.*, et al.* (2017). CD95/Fas Increases Stemness in Cancer Cells by Inducing a STAT1-Dependent Type I Interferon Response. Cell Rep *18*, 2373-2386.

Robbins, M.A., Li, M., Leung, I., Li, H., Boyer, D.V., Song, Y., Behlke, M.A., and Rossi, J.J. (2006). Stable expression of shRNAs in human CD34+ progenitor cells can avoid induction of interferon responses to siRNAs in vitro. Nat Biotechnol *24*, 566-571.

Schneider, P., Bodmer, J.L., Holler, N., Mattmann, C., Scuderi, P., Terskikh, A., Peitsch, M.C., and Tschopp, J. (1997). Characterization of Fas (Apo-1, CD95)-Fas ligand interaction. J Biol Chem *272*, 18827-18833.

Schoggins, J.W., Wilson, S.J., Panis, M., Murphy, M.Y., Jones, C.T., Bieniasz, P., and Rice, C.M. (2011). A diverse range of gene products are effectors of the type I interferon antiviral response. Nature *472*, 481-485.

Siomi, H., and Siomi, M.C. (2009). On the road to reading the RNA-interference code. Nature *457*, 396-404.

Sudarshan, S., Holman, D.H., Hyer, M.L., Voelkel-Johnson, C., Dong, J.Y., and Norris, J.S. (2005). In vitro efficacy of Fas ligand gene therapy for the treatment of bladder cancer. Cancer Gene Ther *12*, 12-18.

Sun, H., Liu, Y., Bu, D., Liu, X., Norris, J.S., and Xiao, S. (2012). Efficient growth suppression and apoptosis in human laryngeal carcinoma cell line HEP-2 induced by an adeno-associated virus expressing human FAS ligand. Head & neck *34*, 1628-1633.

Teitz, T., Wei, T., Valentine, M.B., Vanin, E.F., Grenet, J., Valentine, V.A., Behm, F.G., Look, A.T., Lahti, J.M., and Kidd, V.J. (2000). Caspase 8 is deleted or silenced preferentially in childhood neuroblastomas with amplification of MYCN. Nat Med *6*, 529-535.

Ting, A.H., Suzuki, H., Cope, L., Schuebel, K.E., Lee, B.H., Toyota, M., Imai, K., Shinomura, Y., Tokino, T., and Baylin, S.B. (2008). A requirement for DICER to maintain full promoter CpG island hypermethylation in human cancer cells. Cancer Res *68*, 2570-2575.

van Dongen, S., Abreu-Goodger, C., and Enright, A.J. (2008). Detecting microRNA binding and siRNA off-target effects from expression data. Nat Methods *5*, 1023-1025.

Wang, T., Birsoy, K., Hughes, N.W., Krupczak, K.M., Post, Y., Wei, J.J., Lander, E.S., and Sabatini, D.M. (2015). Identification and characterization of essential genes in the human genome. Science *350*, 1096-1101.

Watanabe, C., Cuellar, T.L., and Haley, B. (2016). Quantitative evaluation of first, second, and third generation hairpin systems reveals the limit of mammalian vector-based RNAi. RNA Biol *13*, 25-33.

Zamore, P.D., Tuschl, T., Sharp, P.A., and Bartel, D.P. (2000). RNAi: double-stranded RNA directs the ATP-dependent cleavage of mRNA at 21 to 23 nucleotide intervals. Cell *101*, 25-33.

Figure 1

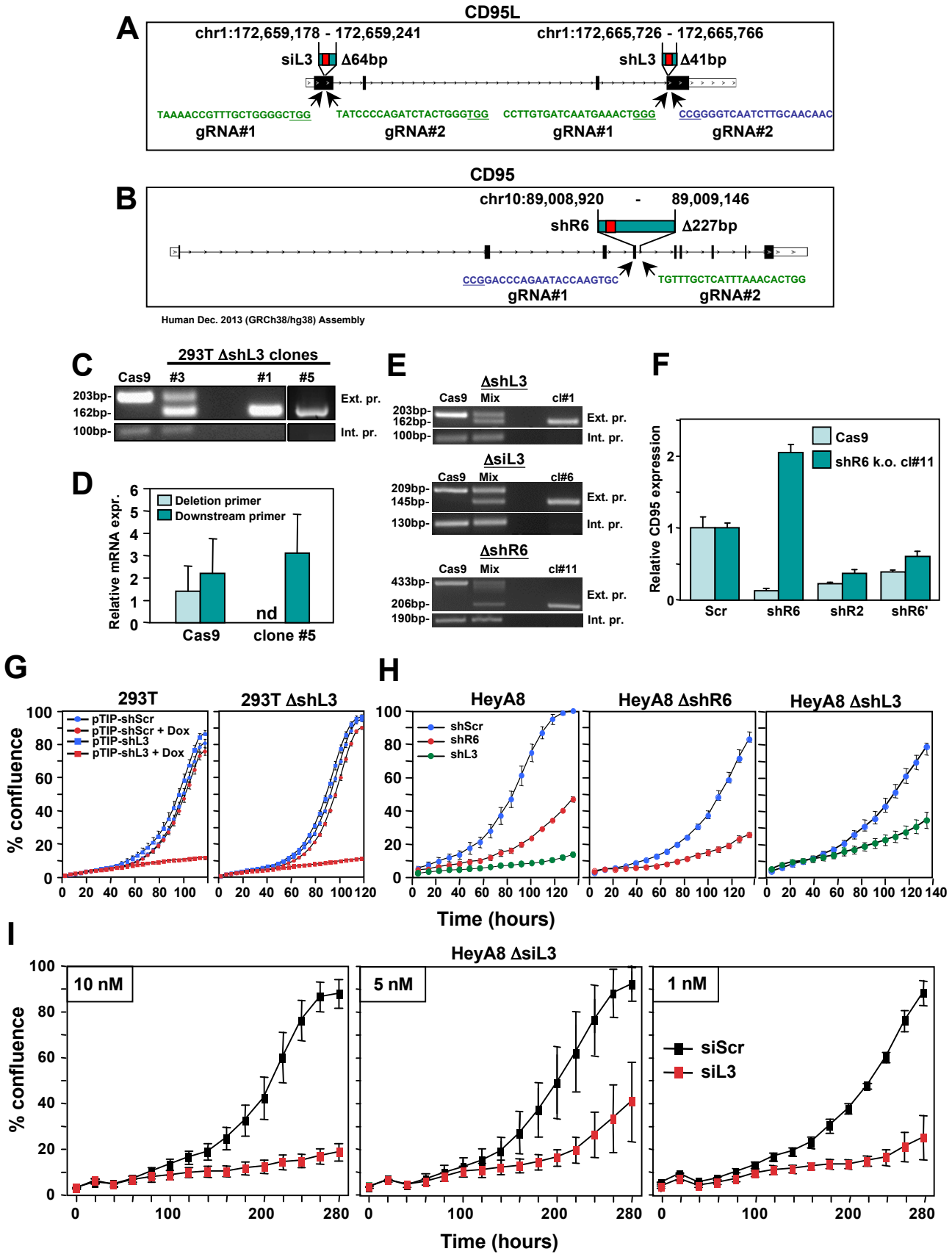
A
CD95L
chr1:172,659,178 - 172,659,241
chr1:172,665,726 - 172,665,766
siL3
Δ64bp
shL3
Δ41bp
TAAAACCGTTTGCTGGGGCTGG
TATCCCCAGATCTACTGGGTGG
CCTTGTGATCAATGAAACTGGG
CCGGGGTCAATCTTGCAACAAC
gRNA#1
gRNA#2
gRNA#1
gRNA#2
B
CD95
chr10:89,008,920 - 89,009,146
shR6
Δ227bp
CCGGACCCAGAATACCAAGTGC
TGTTTGCTCATTTAAACACTGG
gRNA#1
gRNA#2
Human Dec. 2013 (GRCh38/hg38) Assembly
C
293T ΔshL3 clones
Cas9
#3
#1
#5
203bp-
162bp-
100bp-
Ext. pr.
Int. pr.
D
Relative mRNA expr.
Deletion primer
Downstream primer
nd
Cas9
clone #5
E
ΔshL3
Cas9
Mix
cl#1
203bp-
162bp-
100bp-
Ext. pr.
Int. pr.
ΔsiL3
Cas9
Mix
cl#6
209bp-
145bp-
130bp-
Ext. pr.
Int. pr.
ΔshR6
Cas9
Mix
cl#11
433bp-
206bp-
190bp-
Ext. pr.
Int. pr.
F
Relative CD95 expression
Cas9
shR6 k.o. cl#11
Scr
shR6
shR2
shR6'
G
293T
293T ΔshL3
% confluence
pTIP-shScr
pTIP-shScr + Dox
pTIP-shL3
pTIP-shL3 + Dox
H
HeyA8
HeyA8 ΔshR6
HeyA8 ΔshL3
shScr
shR6
shL3
Time (hours)
I
HeyA8 ΔsiL3
10 nM
5 nM
1 nM
% confluence
siScr
siL3
Time (hours)

Figure 2

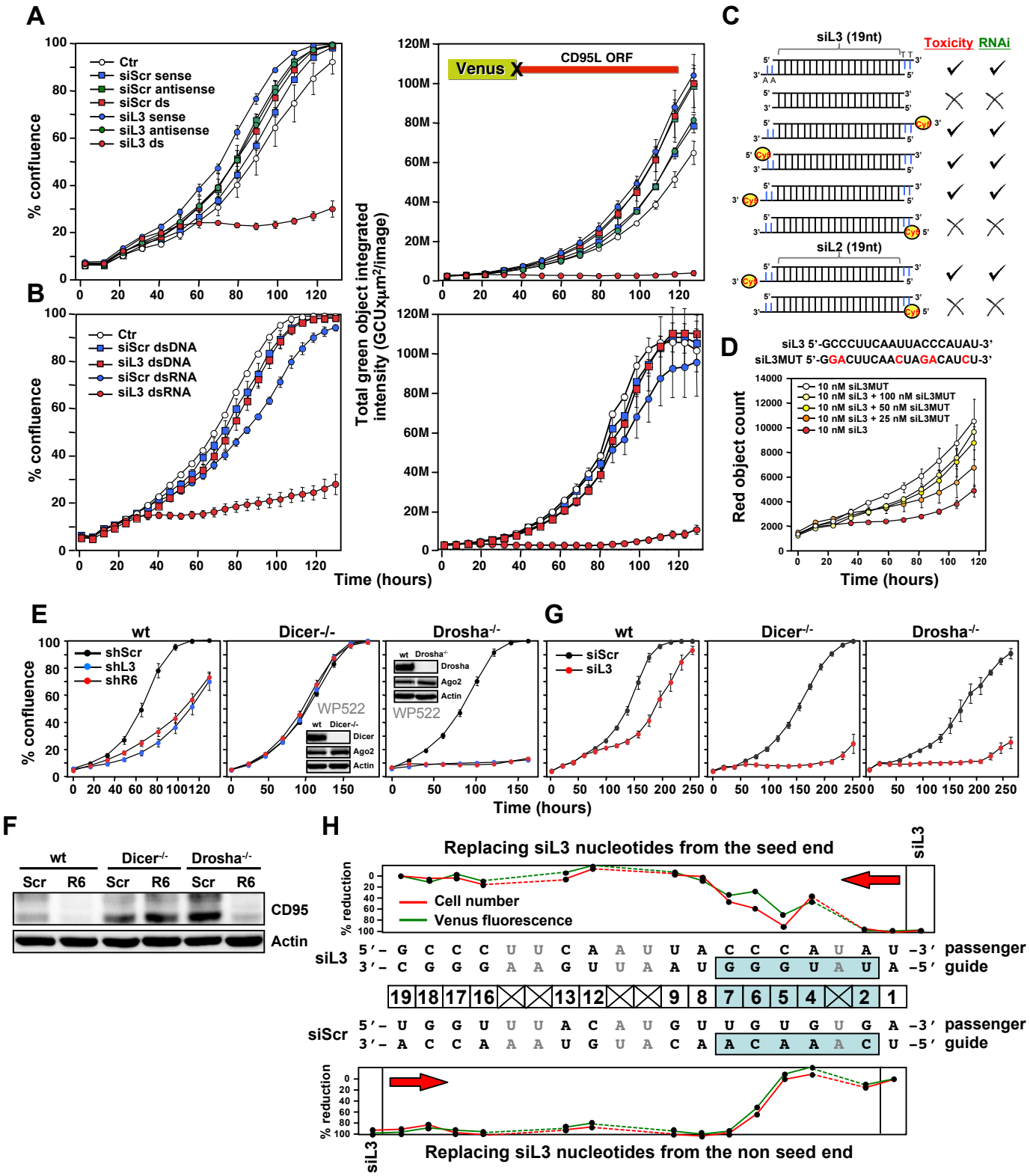
A
% confluence
Ctr
siScr sense
siScr antisense
siScr ds
siL3 sense
siL3 antisense
siL3 ds
Venus
CD95L ORF
Total green object integrated intensity (GCUxμm²/image)
B
siScr dsDNA
siL3 dsDNA
siScr dsRNA
siL3 dsRNA
Time (hours)
C
siL3 (19nt)
Toxicity
RNAi
siL2 (19nt)
D
siL3 5'-GCCCUUCAAUUACCCAUAU-3'
siL3MUT 5'-GGACUUCAACUAGACAUCU-3'
10 nM siL3MUT
10 nM siL3 + 100 nM siL3MUT
10 nM siL3 + 50 nM siL3MUT
10 nM siL3 + 25 nM siL3MUT
10 nM siL3
Red object count
Time (hours)
E
wt
Dicer-/-
Drosha-/-
shScr
shL3
shR6
WP522
Drosha
Ago2
Actin
Dicer
G
siScr
siL3
F
Scr
R6
CD95
Actin
H
Replacing siL3 nucleotides from the seed end
siL3
% reduction
Cell number
Venus fluorescence
siL3 5'- G C C C U U C A A U U A C C C A U A U -3' passenger
3'- C G G G A A G U U A A U G G G U A U A -5' guide
19 18 17 16 13 12 9 8 7 6 5 4 2 1
siScr 5'- U G G U U U A C A U G U U G U G U G A -3' passenger
3'- A C C A A A U G U A C A A C A A A C U -5' guide
Replacing siL3 nucleotides from the non seed end

Figure 3

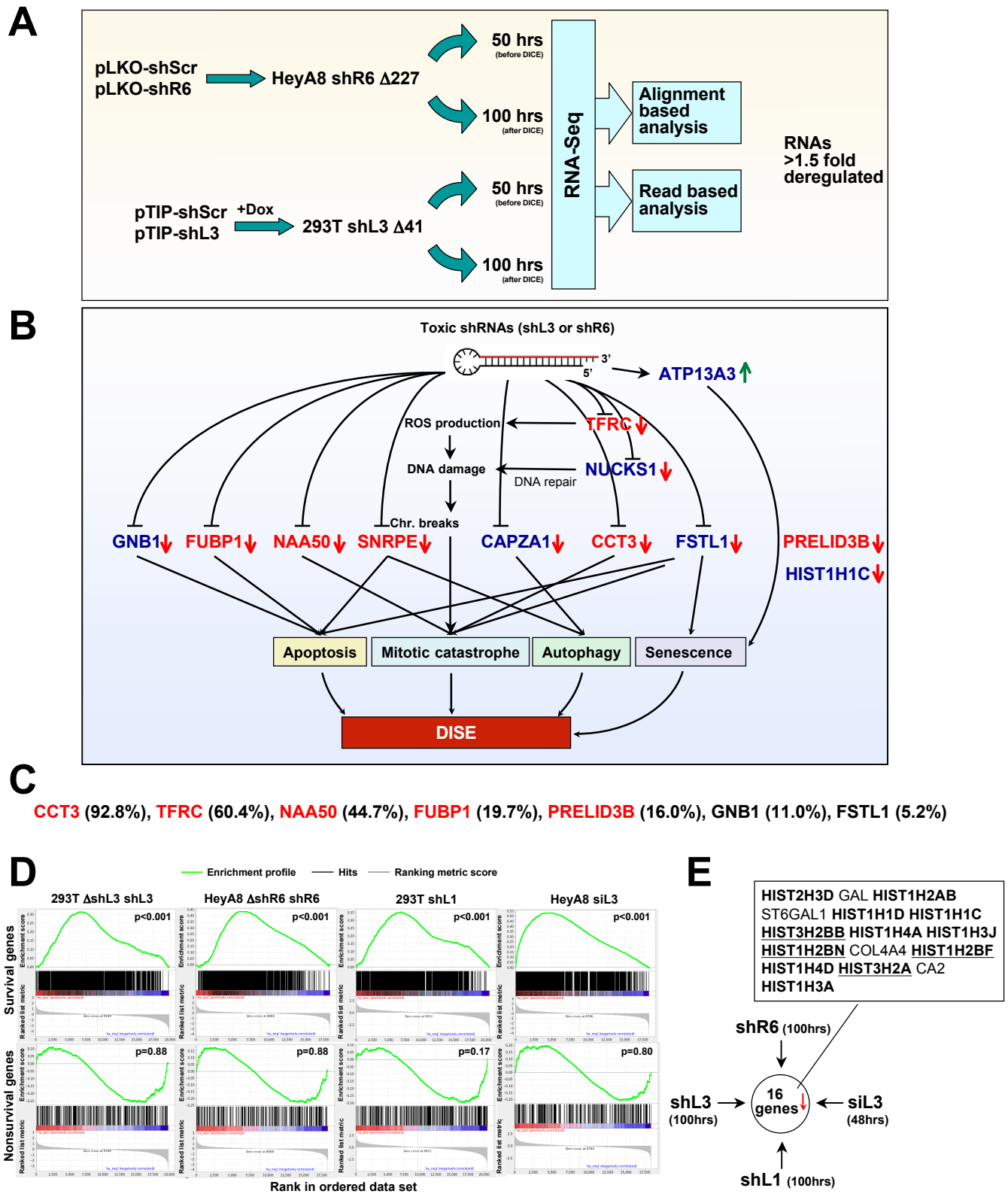
A
pLKO-shScr
pLKO-shR6
HeyA8 shR6 Δ227
pTIP-shScr
pTIP-shL3
+Dox
293T shL3 Δ41
50 hrs (before DICE)
100 hrs (after DICE)
50 hrs (before DICE)
100 hrs (after DICE)
RNA-Seq
Alignment based analysis
Read based analysis
RNAs >1.5 fold deregulated
B
Toxic shRNAs (shL3 or shR6)
3'
5'
ATP13A3
ROS production
TFRC
DNA damage
NUCKS1
DNA repair
Chr. breaks
GNB1
FUBP1
NAA50
SNRPE
CAPZA1
CCT3
FSTL1
PRELID3B
HIST1H1C
Apoptosis
Mitotic catastrophe
Autophagy
Senescence
DISE
C
CCT3 (92.8%), TFRC (60.4%), NAA50 (44.7%), FUBP1 (19.7%), PRELID3B (16.0%), GNB1 (11.0%), FSTL1 (5.2%)
D
Enrichment profile
Hits
Ranking metric score
293T ΔshL3 shL3
HeyA8 ΔshR6 shR6
293T shL1
HeyA8 siL3
Survival genes
Nonsurvival genes
p<0.001
p<0.001
p<0.001
p<0.001
p=0.88
p=0.88
p=0.17
p=0.80
Rank in ordered data set
E
HIST2H3D GAL HIST1H2AB
ST6GAL1 HIST1H1D HIST1H1C
HIST3H2BB HIST1H4A HIST1H3J
HIST1H2BN COL4A4 HIST1H2BF
HIST1H4D HIST3H2A CA2
HIST1H3A
shR6 (100hrs)
shL3 (100hrs)
16 genes
siL3 (48hrs)
shL1 (100hrs)

Figure 4

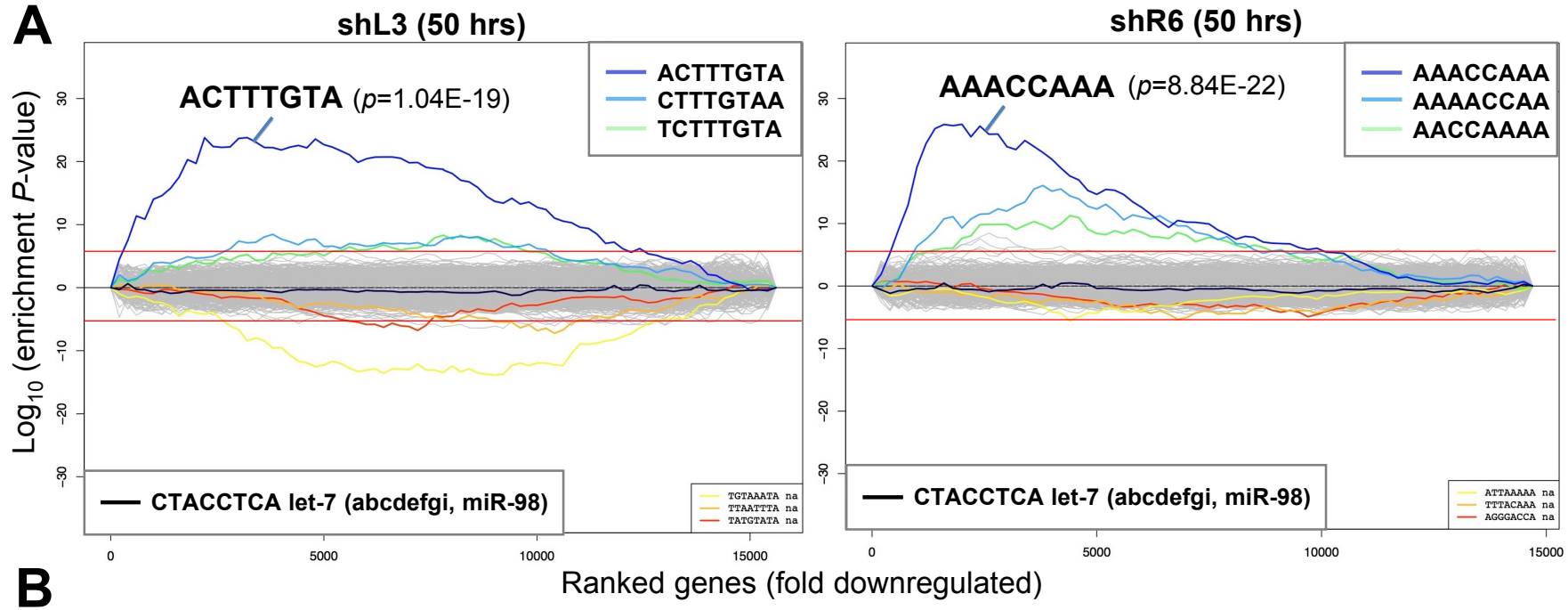

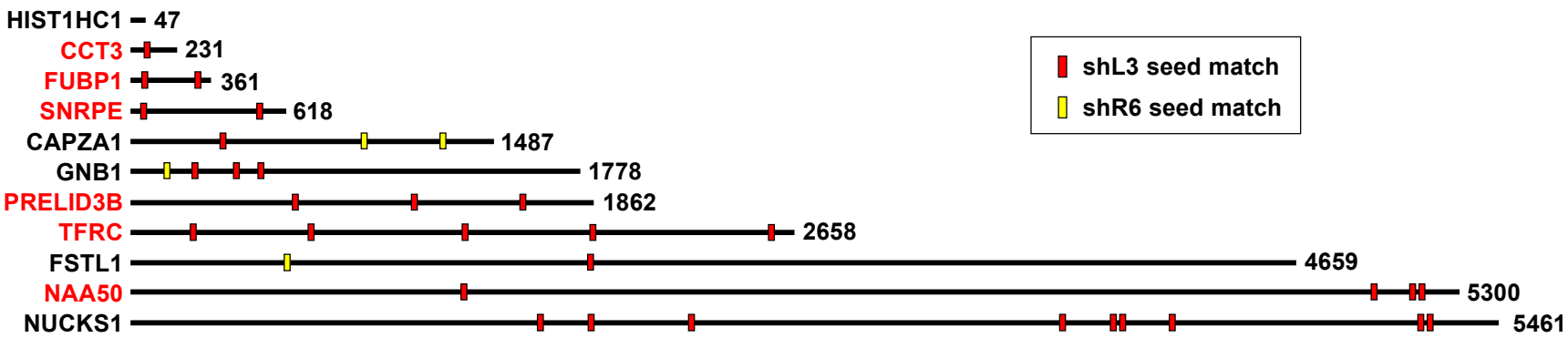

C

Downregulated

		shL3 (50hrs) No	shL3 (50hrs) Yes	shL3 (100hrs) No	shL3 (100hrs) Yes	shR6 (50hrs) No	shR6 (50hrs) Yes	shR6 (100hrs) No	shR6 (100hrs) Yes	shL1 (100hrs) No	shL1 (100hrs) Yes	siL3 (48hrs) No	siL3 (48hrs) Yes
Seed match present	No	825	2	783	48	1113	13	1108	16	600	189	1205	238
	Yes	904	55	850	109	612	40	619	31	746	259	244	93
	P-value	2.83E-13		2.58E-05		6.65E-09		4.31E-05		0.38		5.74E-06	

Figure 5

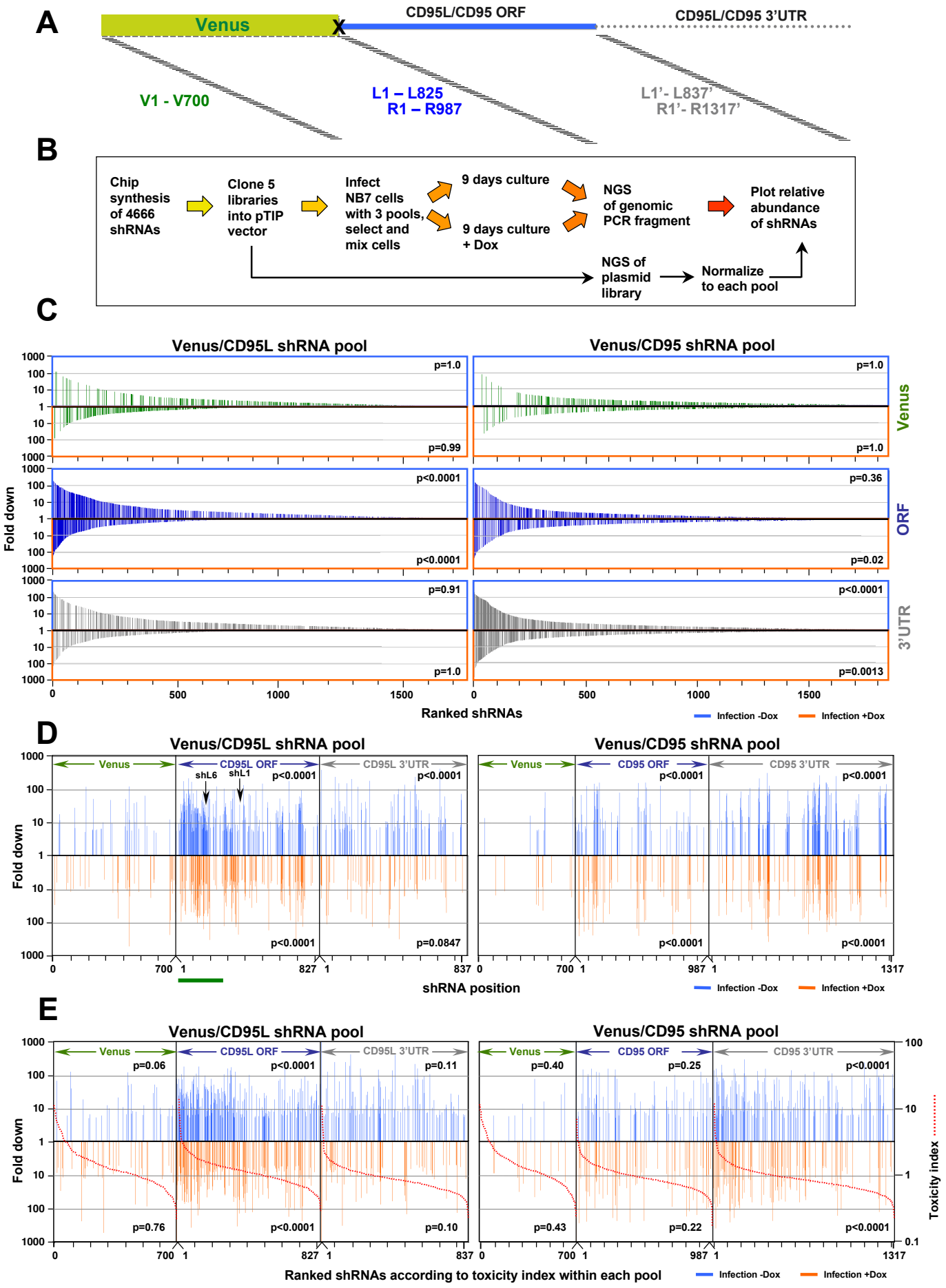
A
Venus
CD95L/CD95 ORF
CD95L/CD95 3'UTR
V1 - V700
L1 – L825
R1 – R987
L1'- L837'
R1'- R1317'
B
Chip synthesis of 4666 shRNAs
Clone 5 libraries into pTIP vector
Infect NB7 cells with 3 pools, select and mix cells
9 days culture
9 days culture + Dox
NGS of genomic PCR fragment
Plot relative abundance of shRNAs
NGS of plasmid library
Normalize to each pool
C
Venus/CD95L shRNA pool
Venus/CD95 shRNA pool
Fold down
Venus
ORF
3'UTR
Ranked shRNAs
Infection -Dox
Infection +Dox
D
Venus/CD95L shRNA pool
Venus/CD95 shRNA pool
CD95L ORF
CD95L 3'UTR
CD95 ORF
CD95 3'UTR
shL6
shL1
shRNA position
E
Venus/CD95L shRNA pool
Venus/CD95 shRNA pool
Toxicity index
Ranked shRNAs according to toxicity index within each pool

Figure 6

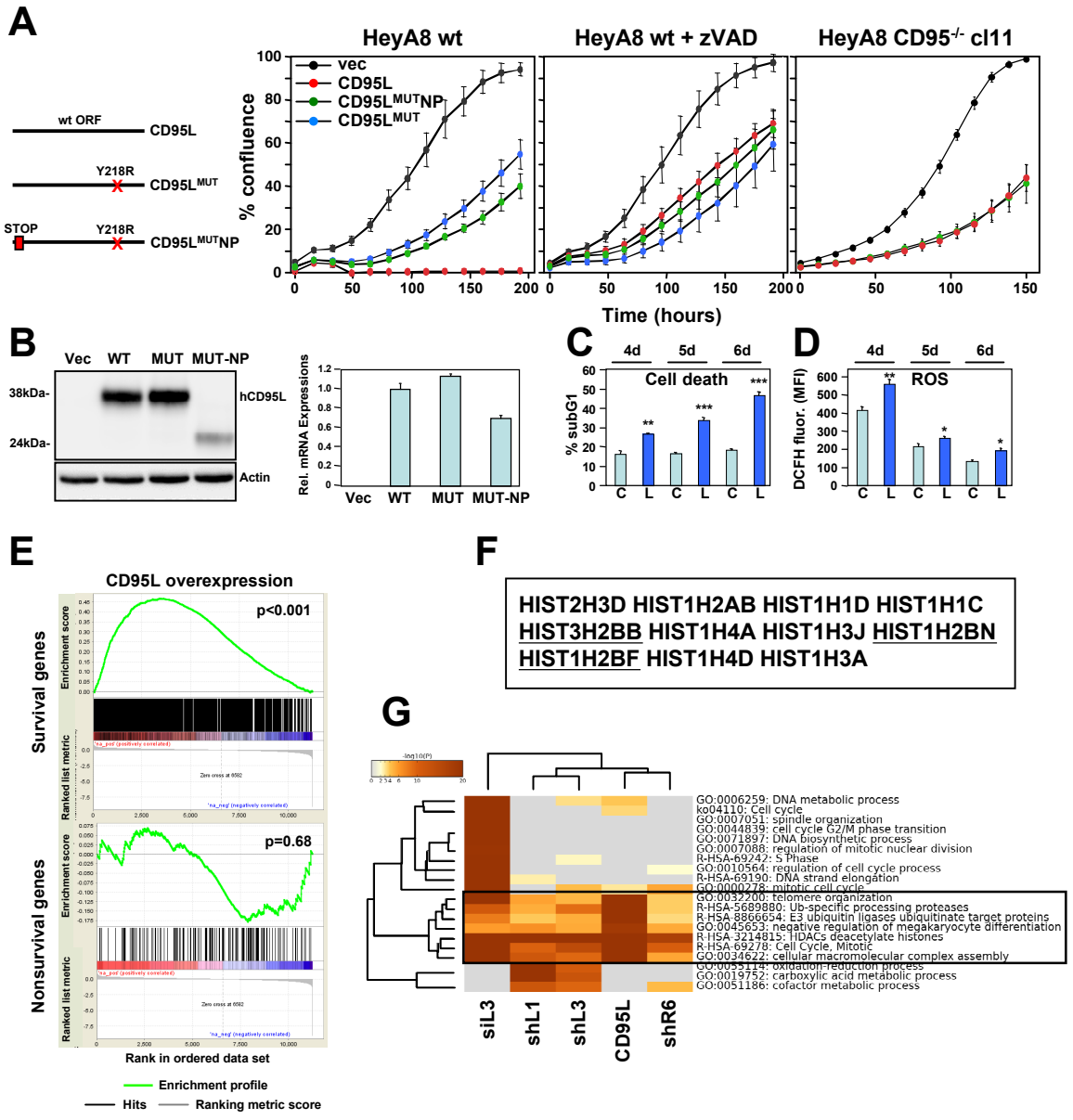
A
HeyA8 wt
HeyA8 wt + zVAD
HeyA8 CD95-/- cl11
wt ORF
CD95L
Y218R
CD95L MUT
STOP
Y218R
CD95L MUT NP
vec
CD95L
CD95L MUT NP
CD95L MUT
% confluence
Time (hours)
B
Vec WT MUT MUT-NP
38kDa-
24kDa-
hCD95L
Actin
Rel. mRNA Expressions
Vec WT MUT MUT-NP
C
4d 5d 6d
Cell death
% subG1
C L C L C L
D
4d 5d 6d
ROS
DCFH fluor. (MFI)
C L C L C L
E
CD95L overexpression
Survival genes
Nonsurvival genes
p<0.001
p=0.68
Enrichment score
Ranked list metric
Rank in ordered data set
Enrichment profile
Hits
Ranking metric score
F
HIST2H3D HIST1H2AB HIST1H1D HIST1H1C
HIST3H2BB HIST1H4A HIST1H3J HIST1H2BN
HIST1H2BF HIST1H4D HIST1H3A
G
-log10(P)
GO:0006259: DNA metabolic process
ko04110: Cell cycle
GO:0007051: spindle organization
GO:0044839: cell cycle G2/M phase transition
GO:0071897: DNA biosynthetic process
GO:0007088: regulation of mitotic nuclear division
R-HSA-69242: S Phase
GO:0010564: regulation of cell cycle process
R-HSA-69190: DNA strand elongation
GO:0000278: mitotic cell cycle
GO:0032200: telomere organization
R-HSA-5689880: Ub-specific processing proteases
R-HSA-8866654: E3 ubiquitin ligases ubiquitinate target proteins
GO:0045653: negative regulation of megakaryocyte differentiation
R-HSA-3214815: HDACs deacetylate histones
R-HSA-69278: Cell Cycle, Mitotic
GO:0034622: cellular macromolecular complex assembly
GO:0055114: oxidation-reduction process
GO:0019752: carboxylic acid metabolic process
GO:0051186: cofactor metabolic process
siL3
shL1
shL3
CD95L
shR6

Figure 7

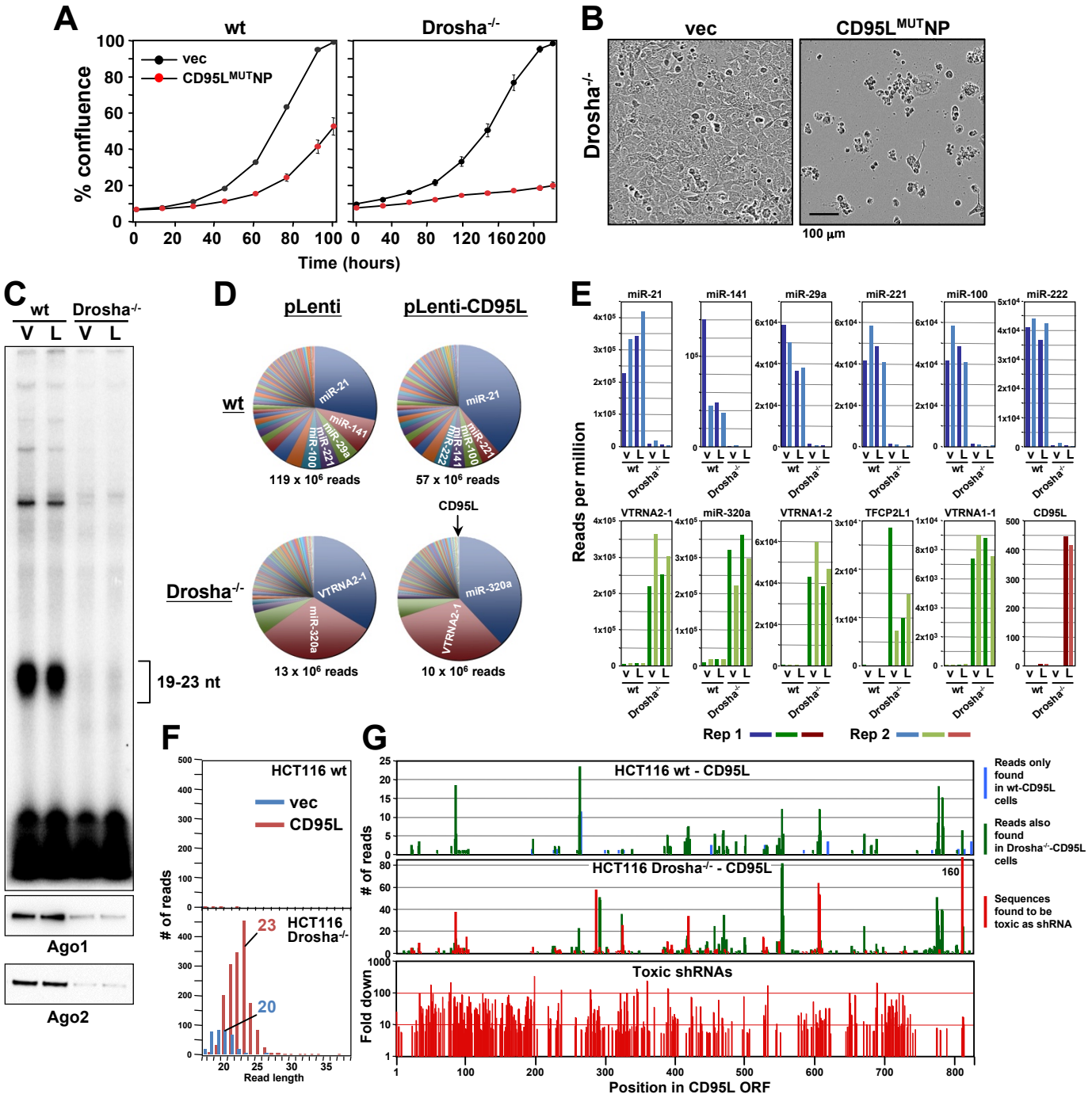
A
wt
Drosha-/-
vec
CD95LMUTNP
% confluence
Time (hours)
B
vec
CD95LMUTNP
Drosha-/-
100 µm
C
wt
Drosha-/-
V L V L
19-23 nt
Ago1
Ago2
D
pLenti
pLenti-CD95L
wt
miR-21
miR-141
miR-29a
miR-221
miR-100
miR-222
119 x 10^6 reads
57 x 10^6 reads
CD95L
Drosha-/-
VTRNA2-1
miR-320a
13 x 10^6 reads
10 x 10^6 reads
E
miR-21
miR-141
miR-29a
miR-221
miR-100
miR-222
VTRNA2-1
miR-320a
VTRNA1-2
TFCP2L1
VTRNA1-1
CD95L
Reads per million
Rep 1
Rep 2
F
HCT116 wt
vec
CD95L
HCT116 Drosha-/-
# of reads
Read length
23
20
G
HCT116 wt - CD95L
HCT116 Drosha-/- - CD95L
160
Toxic shRNAs
Fold down
Position in CD95L ORF
Reads only found in wt-CD95L cells
Reads also found in Drosha-/--CD95L cells
Sequences found to be toxic as shRNA

Supplementary figures

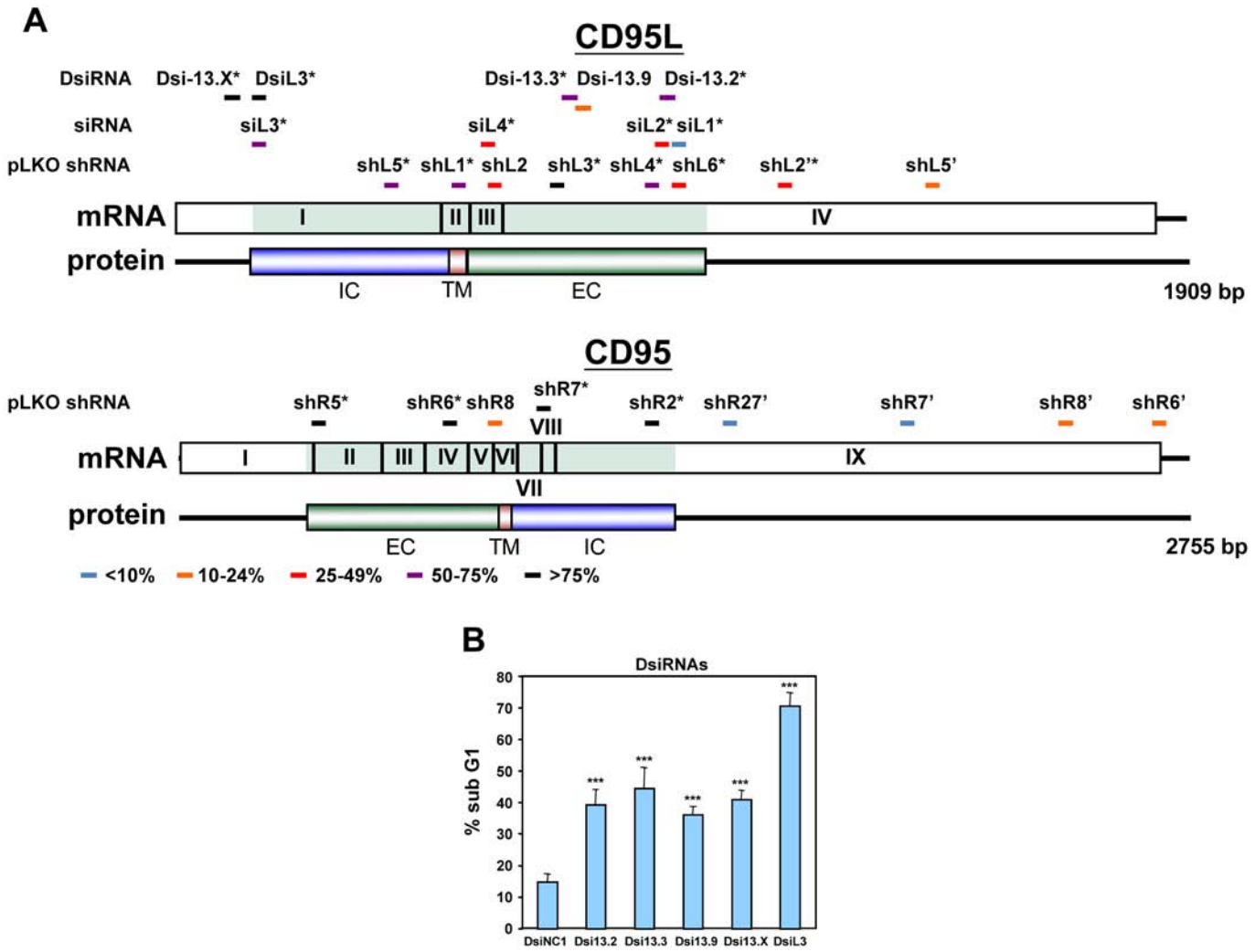

Figure S1. The majority of siRNAs and shRNAs targeting CD95L or CD95 are toxic. (**A**) Location of target sites, growth inhibitory activities and toxicity of all tested siRNAs, DsiRNAs, and pLKO-shRNAs targeting CD95L and CD95. Experiments were performed in HeyA8 cells at an MOI of 3 for pLKO-shRNA infection, transfected with 25 nM of siRNAs, or 5 nM of DsiRNAs, respectively. Color code indicates the level of growth reduction caused by each sh/siRNA. sh/siRNAs labeled with an asterisk induced significant cell death as monitored by nuclear PI staining. Both exon/intron structure and protein domains are shown for both CD95L and CD95. EC, extracellular domain; TM, transmembrane domain; IC, intracellular domain. (**B**) PI staining was used to quantify percent subG1 of HeyA8 cells 4 days after transfection with 5 nM of CD95L derived DsiRNAs. *** $p<0.0001$.

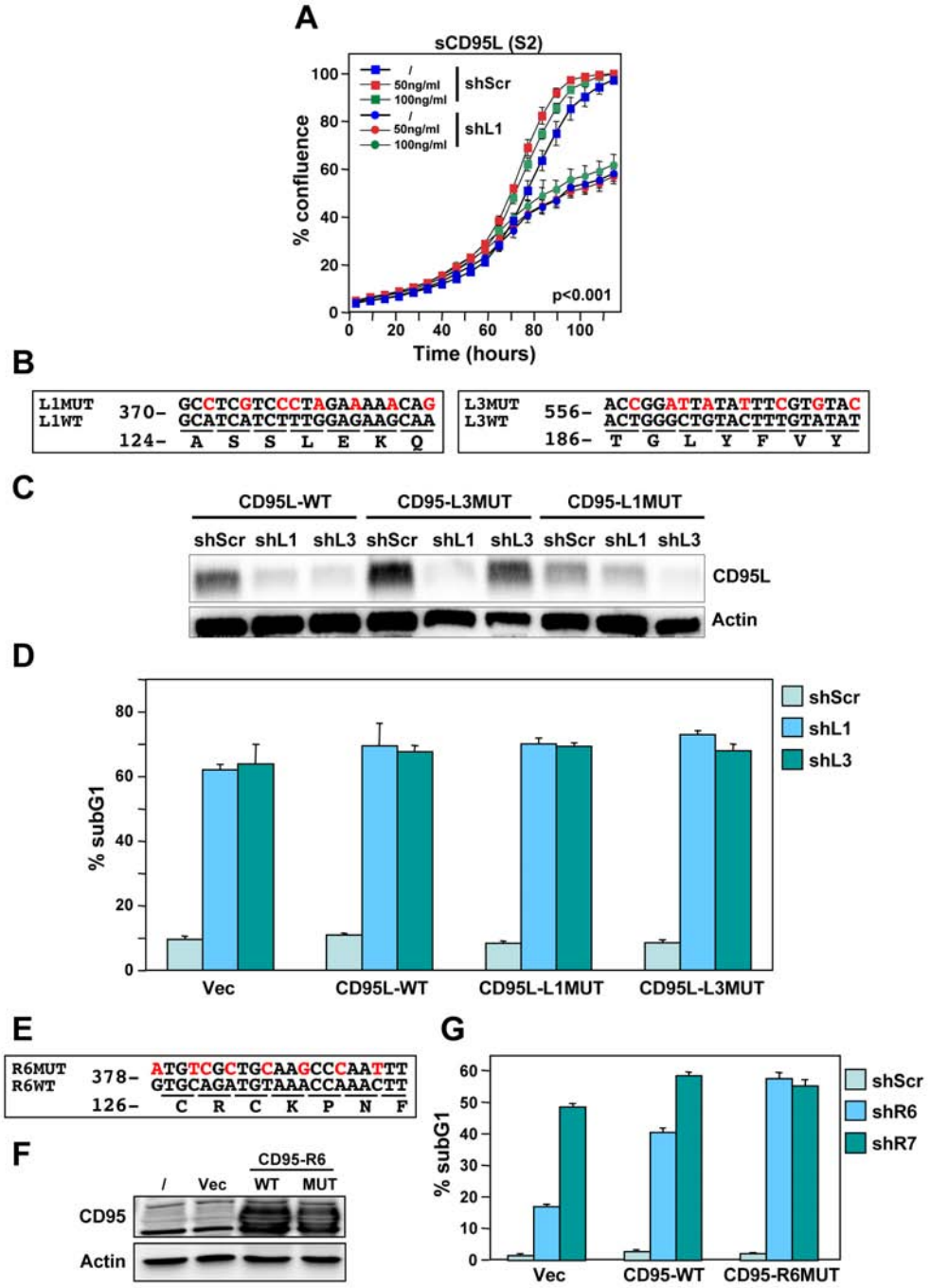

Figure S2. Exogenous CD95L or CD95 proteins do not protect cells from toxicity of CD95L/CD95 derived shRNAs. (**A**) Percent cell confluence over time of NB7 cells after infection with either pLKO-shScr or pLKO-shL1 and concurrent treatment with different concentrations of soluble CD95L protein (S2). Two-way ANOVA was performed for pairwise comparisons of % confluence over time between shScr expressing cells untreated or treated with 100 ng/ml S2. (**B**) Schematic of the eight silent mutations introduced to the shL1 and the shL3 target sites of CD95L. (**C**) Western blot analysis of CD95L and β-actin in NB7 cells over-expressing CD95L-WT, CD95-L1MUT, or CD95-L3MUT 5 days after infection with pLKO-shScr, pLKO-shL1, or pLKO-shL3. (**D**) Percent nuclear PI staining of NB7 cells expressing empty pLenti vector, CD95L-WT, CD95-L1MUT, or CD95-L3MUT 7 days after infection with either pLKO-shScr, pLKO-shL1, or pLKO-shL3. Values were calculated as mean ± S.D. (**E**) Schematic of the 8 silent mutations introduced at the shR6 site of CD95. (**F**) Western blot analysis of CD95 and β-actin in MCF-7 cells over-expressing CD95-WT or CD95-R6MUT. (**G**) Percent nuclear PI staining of MCF-7 cells expressing empty pLNCX2 vector, CD95-WT, or CD95-R6MUT 7 days after infection with pLKO-shScr, pLKO-shR6, or pLKO-shR7. Values were calculated as mean ± S.D.

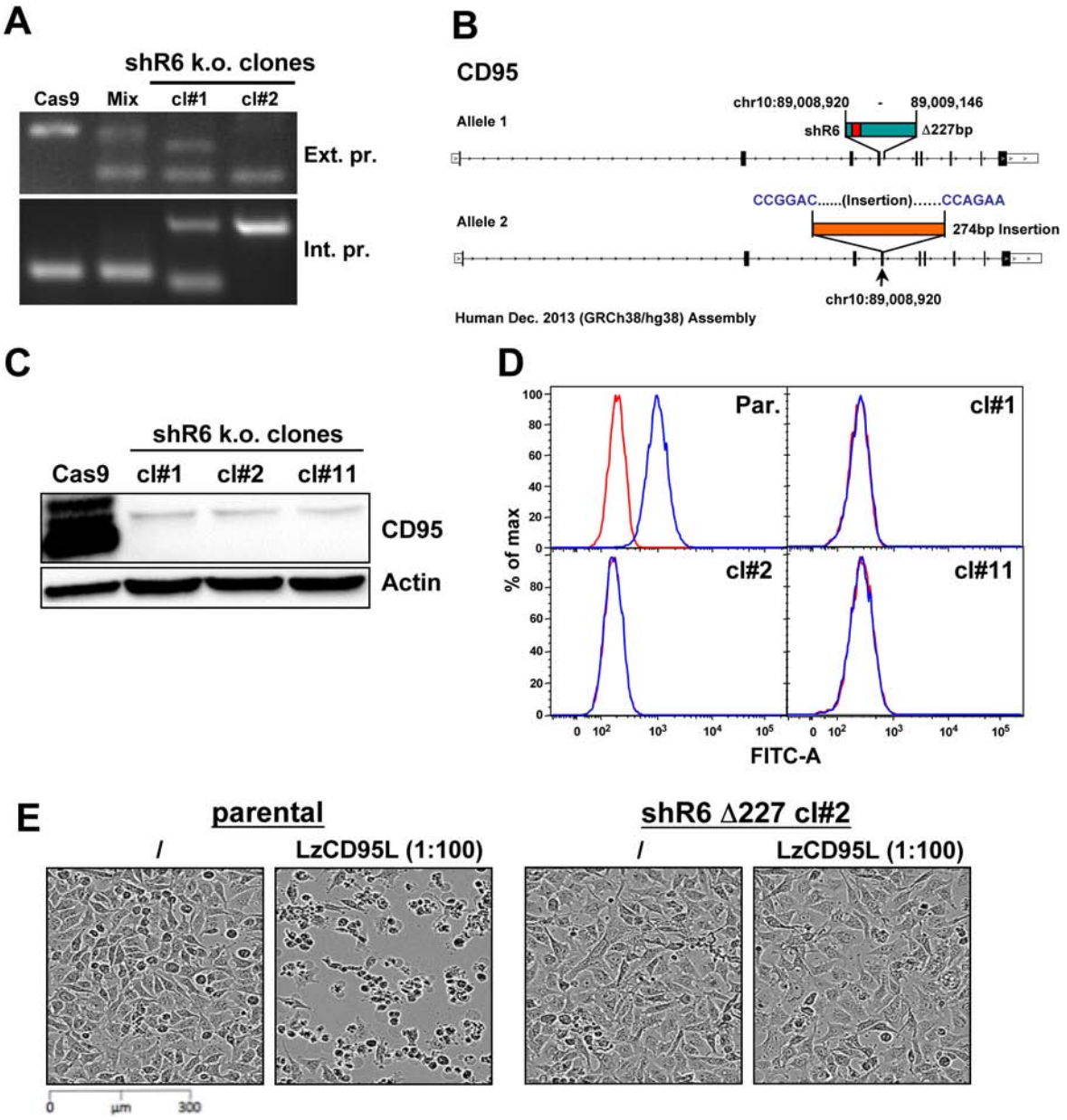

Figure S3. Knockout of CD95 in HeyA8 cells. (**A**) PCR showing a Δ227 shR6 deletion and insertions in HeyA8 clones #1 and #2. (**B**) Schematic of the Δ227 deletion in allele #1 and partial insertion of a pSC-B plasmid fragment in allele #2 in HeyA8 clone #2 based on Sanger sequencing of isolated bands from PCR shown in a. Note, cl#1 and #2 have the expected Δ227 shR6 deletion in one allele and an insertion in the other. cl#11 has a homozygous Δ227 shR6 deletion. The deleted region is shown in green containing the shR6 target site in red. pSC-B vector sequences are shown in blue letters. (**C**) Western blot for CD95 and β-actin in Cas9-control transfected HeyA8 cells and HeyA8 shR6 knockout clones #1, #2, and #11. (**D**) Surface staining for CD95 in parental HeyA8 cells and HeyA8 shR6 knockout clones #1, #2, and #11. (**E**) Images showing apoptosis induction with LzCD95L treatment (4.5 hrs) in parental HeyA8 cells but not in clone #2.

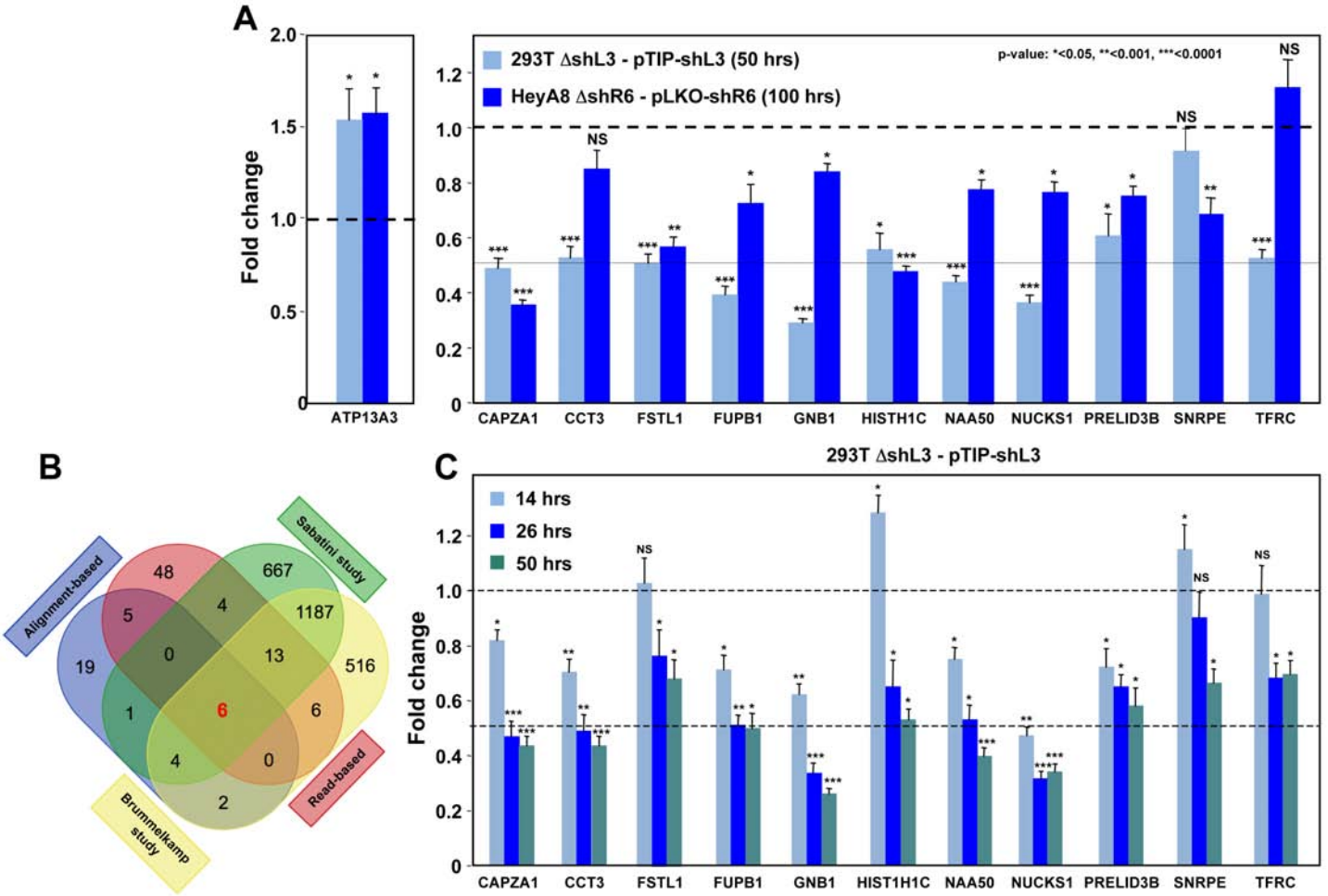

Figure S4. Down-regulation of critical survival genes after treatment with CD95 and CD95L-derived shRNAs and siRNAs. (**A**) Arrayed quantitative PCR of genes found to be down-regulated (or upregulated as with ATP13A3) in *Figure 3B* both in 293T ΔshL3-pTIP-shL3 cells 50 hrs post-Dox treatment and HeyA8 ΔshR6-pLKO-shR6 100 hrs post infection and puromycin selection. NS, not significant. (**B**) Venn diagram showing overlap of genes determined to be down-regulated with both read-based and alignment-based analyses of the RNA-Seq data depicted in *Figure 3A* with the critical survival genes found in the Sabatini and Brummelkamp studies (Blomen et al., 2015; Wang et al., 2015), all listed in ***Table S2***. The Venn diagram was generated using http://bioinformatics.psb.ugent.be/webtools/Venn. (**C**) Kinetic quantitative PCR of the down-regulated genes in the 293T ΔshL3 pTIP-shL3 cells. RNA was collected at 14 hrs, 26 hrs, and 50 hrs after treatment with Dox. NS, not significant, * $p<0.05$, ** $p<0.001$, *** $p<0.0001$.

The following describes the 11 genes that were significantly downregulated after introducing the toxic shRNAs shL3 or shR6 into cancer cells (see ***Figure 3B***) and some of their cancer relevant activities:

1) CAPZA1 (capping actin protein of muscle Z-line alpha subunit 1) is an actin capping protein. CAPZA1 knockdown has been reported to cause disassembly of autophagosomes (Mi et al., 2015) It is overexpressed in malignant melanoma (Sun et al., 2011).
2) CCT3 (chaperonin containing TCP1 subunit 3) is part of a chaperon complex that folds various proteins including actin and tubulin. CCT3 is required for proper mitotic progression (Zhang et al., 2016).
3) FSTL1 (follistatin-like 1) is a putative activin-binding protein. Knockdown of FSTL1 in lung cancer cells resulted in mitotic arrest followed by apoptosis promoted by the activation of caspase-3 and -9 (Bae et al., 2016). FSTL1 is downregulated during cellular senescence of human mesenchymal stem cells (Yoo, Choi, & Kim, 2013).
4) FUBP1 (far upstream element binding protein 1). A lack of FUBP1 causes a cell-autonomous defect in the maintenance of fetal and adult hematopoietic stem cells (HSCs). FUBP1-deficient adult HSCs exhibit significant transcriptional changes, including upregulation of the cell-cycle inhibitor p21 and the pro-

apoptotic Noxa molecule, suggesting they undergo apoptosis (Rabenhorst et al., 2015). In addition, FUBP1 binds to an upstream element of the c-myc promoter and regulates the c-myc mRNA level, thus regulating proliferation (Jang et al., 2009). Finally, FUBP1 is upregulated in many tumors and acts as an oncoprotein by stimulating proliferation and inhibiting apoptosis (Baumgarten et al., 2014).

5) GNB1 (G-protein beta submit 1) is tumor-promoting in breast cancer. Data suggest that GNB1 plays an important role in the mTOR-related anti-apoptosis pathway (Wazir, Jiang, Sharma, & Mokbel, 2013).
6) HIST1H1C. A specific role of this particular histone in cancer cell survival has not yet been described. (Knockdown causes cell cycle arrest in MCF-7 cells; (http://journals.plos.org/plosgenetics/article?id=10.1371%2Fjournal.pgen.1000227)).
7) NAA50 (N(alpha)-acetyltransferase 50, NatE catalytic subunit) is required for sister chromatid separation *in vivo* (Hou, Chu, Kong, Yokomori, & Zou, 2007).
8) NUCKS1 (nuclear casein kinase and cyclin dependent kinase substrate 1) is a chromatin-associated protein with a role in the DNA damage response. Knocking down NUCKS1 causes chromosomal breaks (Parplys et al., 2015).
9) PRELID3B (PRELI domain containing 3B) is an inner mitochondrial protein. Knocking down PRELID3B decreases cell viability (http://www.genecards.org/cgi-bin/carddisp.pl?gene=PRELID3B).
10) SNRPE (small nuclear ribonucleoprotein polypeptide E). siRNA-mediated depletion of SNRPE stimulated autophagy and led to a marked reduction of cell viability in breast, lung, and melanoma cancer cell lines, whereas it had little effect on the survival of the nonmalignant MCF-10A breast epithelial cells (Quidville et al., 2013).
11) TFRC (transferrin receptor). Blocking TFRC function with a neutralizing antibody inhibits cell proliferation and survival (Pham et al., 2014). Suppression of TFRC led to apoptosis of renal cells (Gui et al., 2013) and cell cycle arrest in esophageal squamous cell carcinoma cells (Chan et al., 2014).

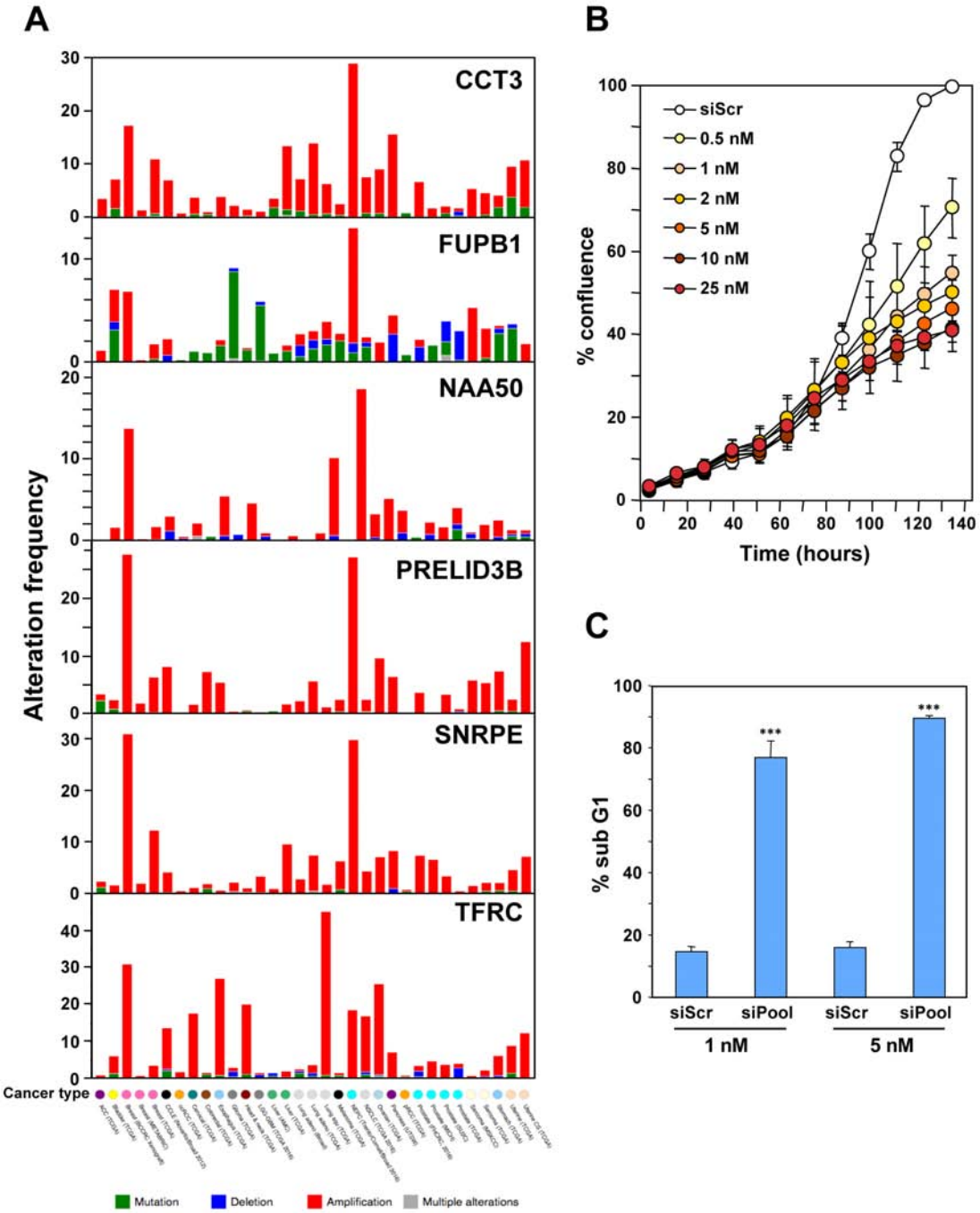

Figure S5. Characterization of the six genes downregulated in shL3 and shR6 treated cells and found to be critical survival genes in lethality screens. (**A**) The six downregulated survival genes were queried individually using default settings with all studies selected in the cBioPortal for Cancer Genomics hosted by Memorial Sloan Kettering Cancer Center (http://www.cbioportal.org/) (Cerami et al., 2012; Gao et al., 2013). Datasets with alterations in 5 out of the 6 essential genes reporting both copy number alterations and mutational data were included. To avoid reporting duplicate datasets, The Cancer Genome Atlas publications were excluded. After filtering, 33 datasets representing cancers from 23 different sites reported alterations in the downregulated survival genes. (**B**) Percent confluence over time of HeyA8 cells transfected with increasing concentrations of a pool of siRNAs (28 different siRNAs) targeting 7 different genes: CCT3, TFRC, NAA50, FUBP1, PRELID3B, GNB1 and FSTL1. Each siRNA SmartPool was comprised of 4 individual siRNAs. Values were calculated from samples done in quadruplicates shown as the mean ± S.E. (**C**) PI staining used to quantify percent subG1 for cells 4 days after transfection with 1 nM and 5 nM of combined siRNA pools targeting the 7 different survival genes as in *Figure S5B*. *** $p<0.0001$.

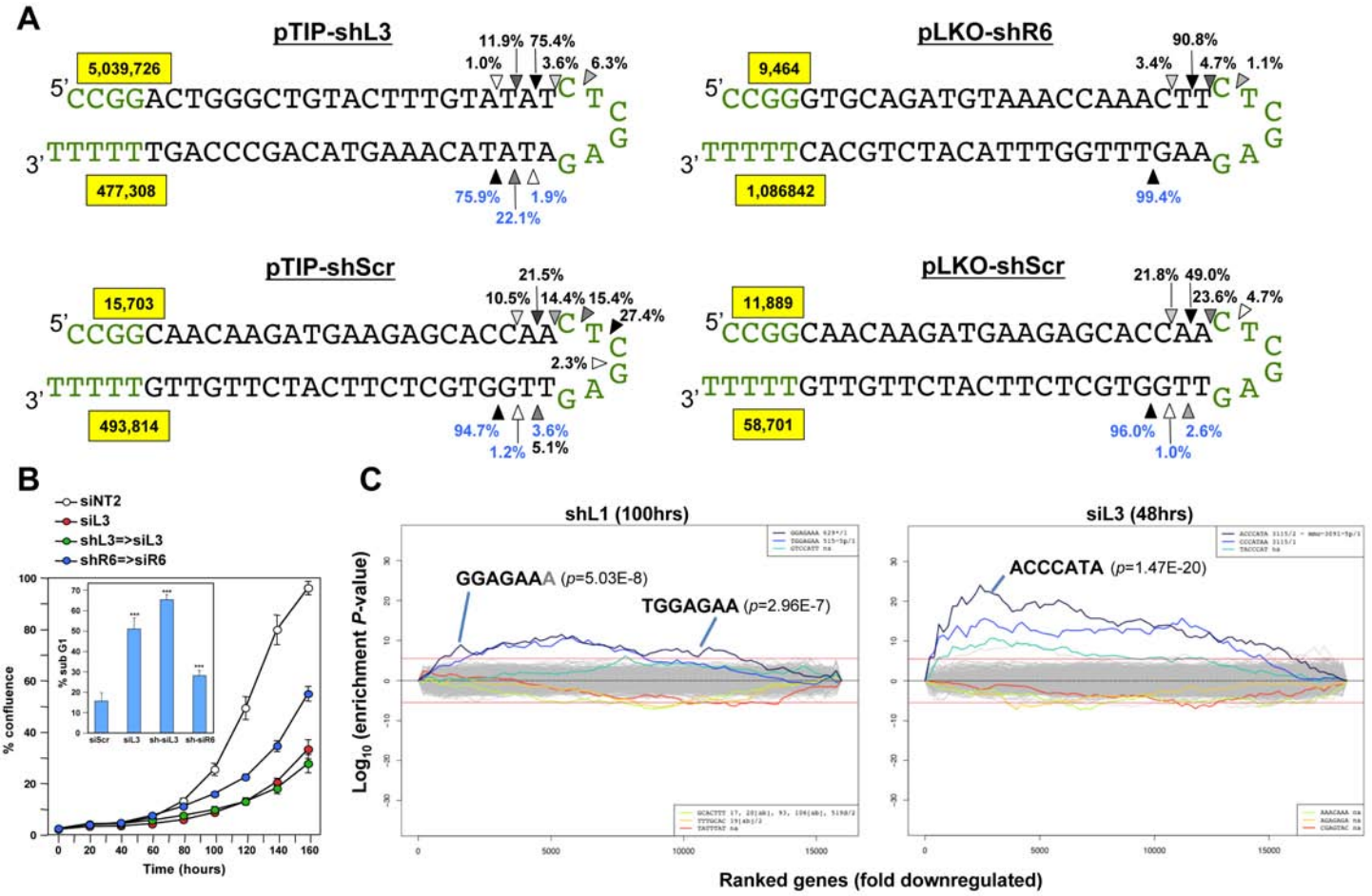

Figure S6. Quantification of the mature shRNA forms. (**A**) Graphical representation of the percentage of the different Dicer cut sites to produce the mature passenger (top) and guide (bottom) strands of 3 shRNAs expressed from two vectors. All analyses were performed with cells 50 hrs after either Dox addition (in pTIP expressing cells) or infection with the pLKO virus. Letters in green: vector sequences; black: passenger and guide strands of shRNAs; Arrow heads label the most highly cleaved residues; the darker the arrow head the more highly cleaved. Numbers in yellow box represent total number of reads detected for passenger and guide strands. (**B**) Percent cell confluence in HeyA8 cells after transfection with shL3=>siL3 (shL3 converted to an siRNA) or shR6=>siR6 (shR6 converted to an siRNA). Conversion was based on the most common mature double-stranded RNA form produced as indicated by the results in *Figure S6A*. Insert: percent DNA fragmentation in the same samples. *** p<0.0001. (**C**) Sylamer plots for the list of genes in the shL1 experiment (293T cells 100 hrs after infection with pLKO-shL1) (left) and the siL3 experiment (48 hrs after transfection of HeyA8 cells with siL3) (right) ordered from down-regulated to up-regulated. The most highly enriched sequences are shown which in each case is the 7mer seed match of the introduced shRNA. The red line corresponds to a p-value threshold of 0.05 after Bonferroni correction for the number of words tested. Bonferroni-adjusted p-values are shown.

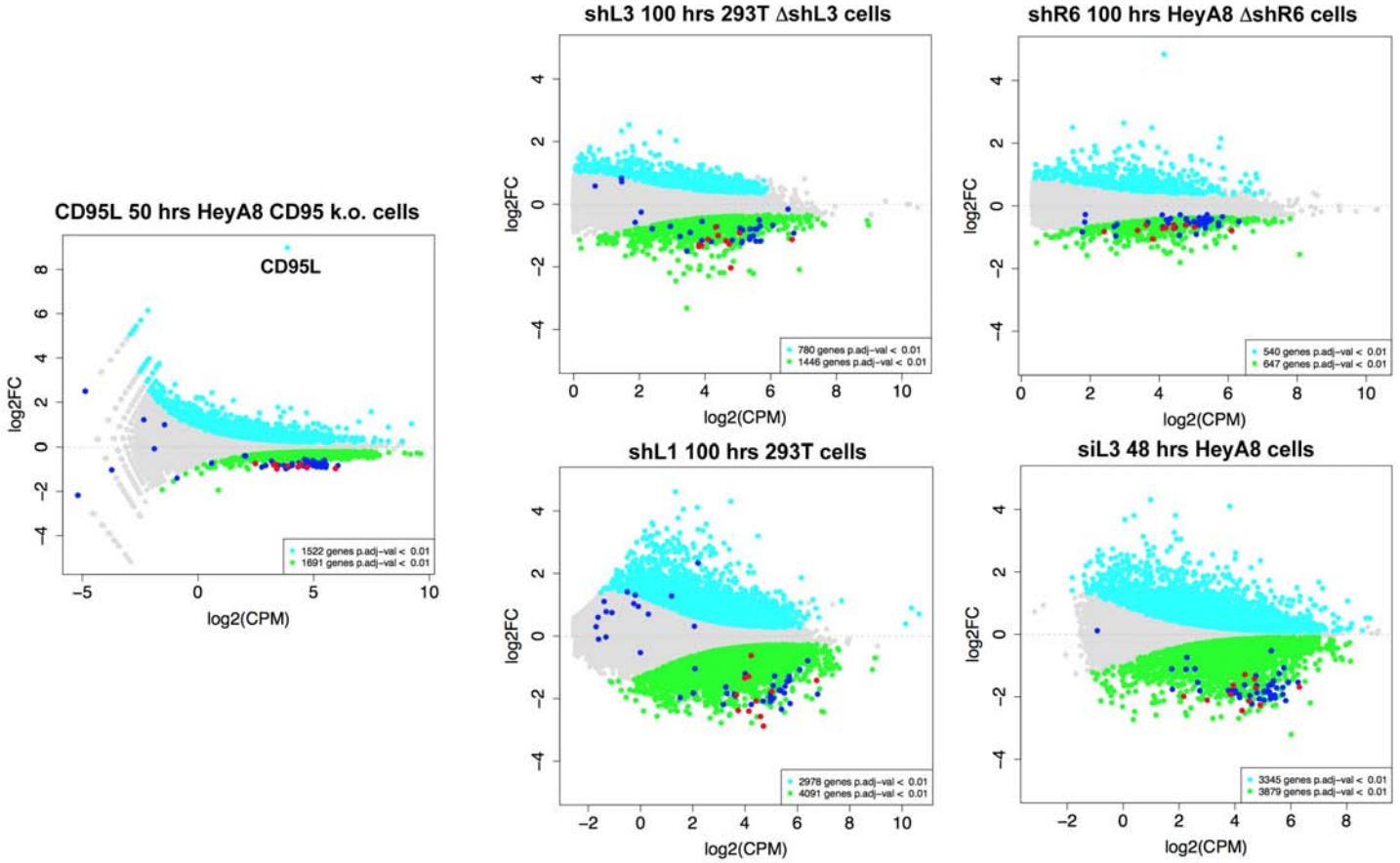

Figure S7. Histones are downregulated in all forms of DISE but are not the most highly expressed genes in cells. MA plots comparing the expression level (CPM) and fold change in the five RNA Seq data sets in his study. Shown are all RNAs that were >1.5 fold deregulated with an adjusted p-value of <0.01. Significantly downregulated RNAs are shown in green upregulated RNAs in cyan. All 73 histones are shown as dark blue dots and the 11 histones downregulated in all 5 data sets are shown as red dots.

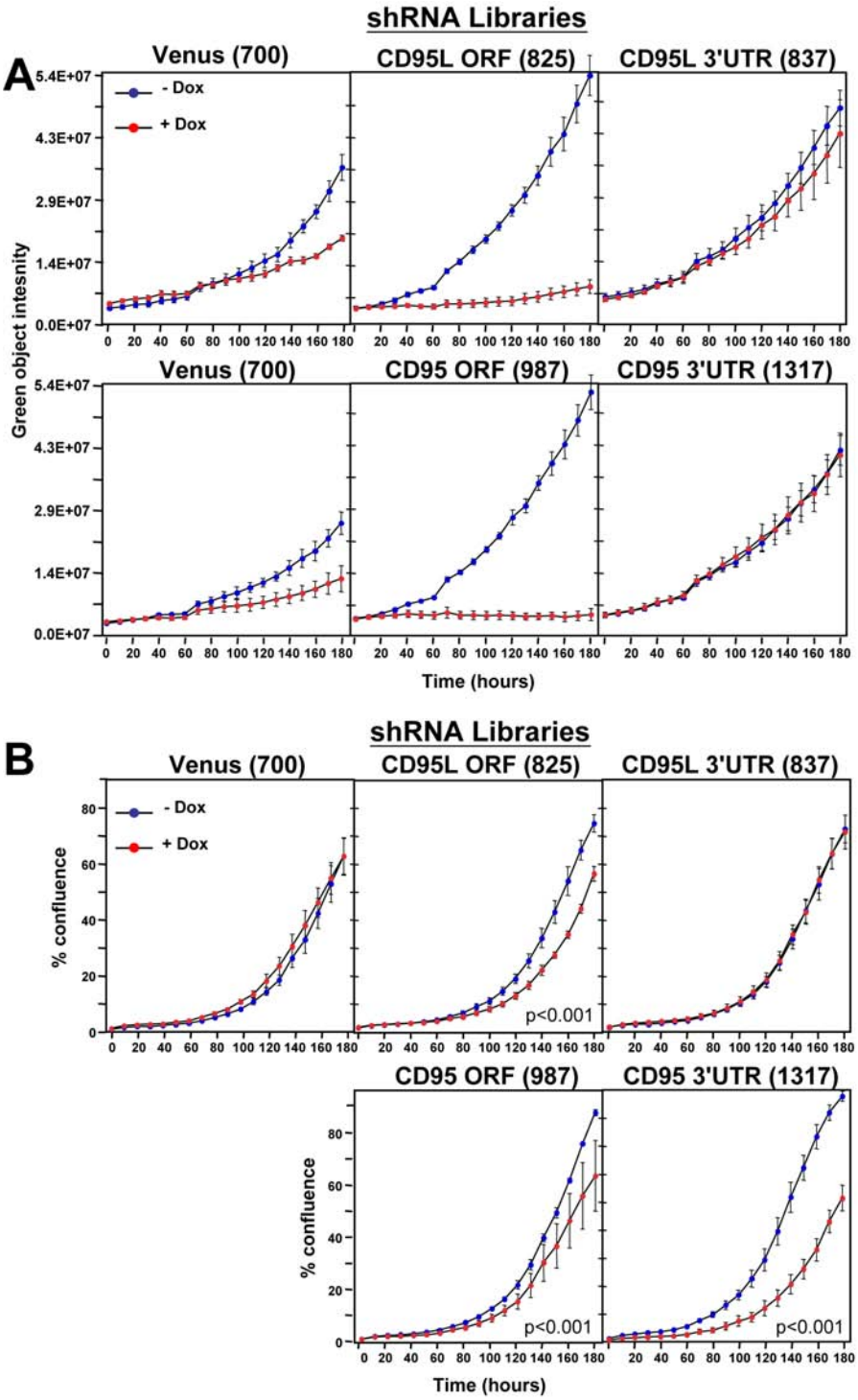

Figure S8. Toxicity and RNAi of individual shRNA pools. (**A**) *Top panels:* Green object intensity over time of NB7 Venus-CD95L sensor cells infected with the pTIP-Venus shRNA pool (*left panel*), pTIP-CD95L ORF shRNA pool (*center panel*), or pTIP-CD95L 3'UTR shRNA pool (*right panel*) with or without Dox treatment. *Bottom panels:* Green object intensity over time of NB7 Venus-CD95 sensor cells infected with the pTIP-Venus shRNA pool (*left panel*), pTIP-CD95 ORF shRNA pool (*center panel*), or pTIP-CD95 3'UTR shRNA pool (*right panel*) with or without Dox treatment. (**B**) Percent confluence over time of parental NB7 cells infected with the pTIP-Venus shRNA pool (*top left panel*), pTIP-CD95L ORF shRNA pool (*top center panel*), pTIP-CD95L 3'UTR shRNA pool (*top right panel*), pTIP-CD95 ORF-shRNA pool (*bottom center panel*), and pTIP-CD95 3'UTR shRNA pool (*bottom right panel*) with or without Dox treatment. P-values were calculated using two-way ANOVA with a factor for Dox treatment and a factor for time.

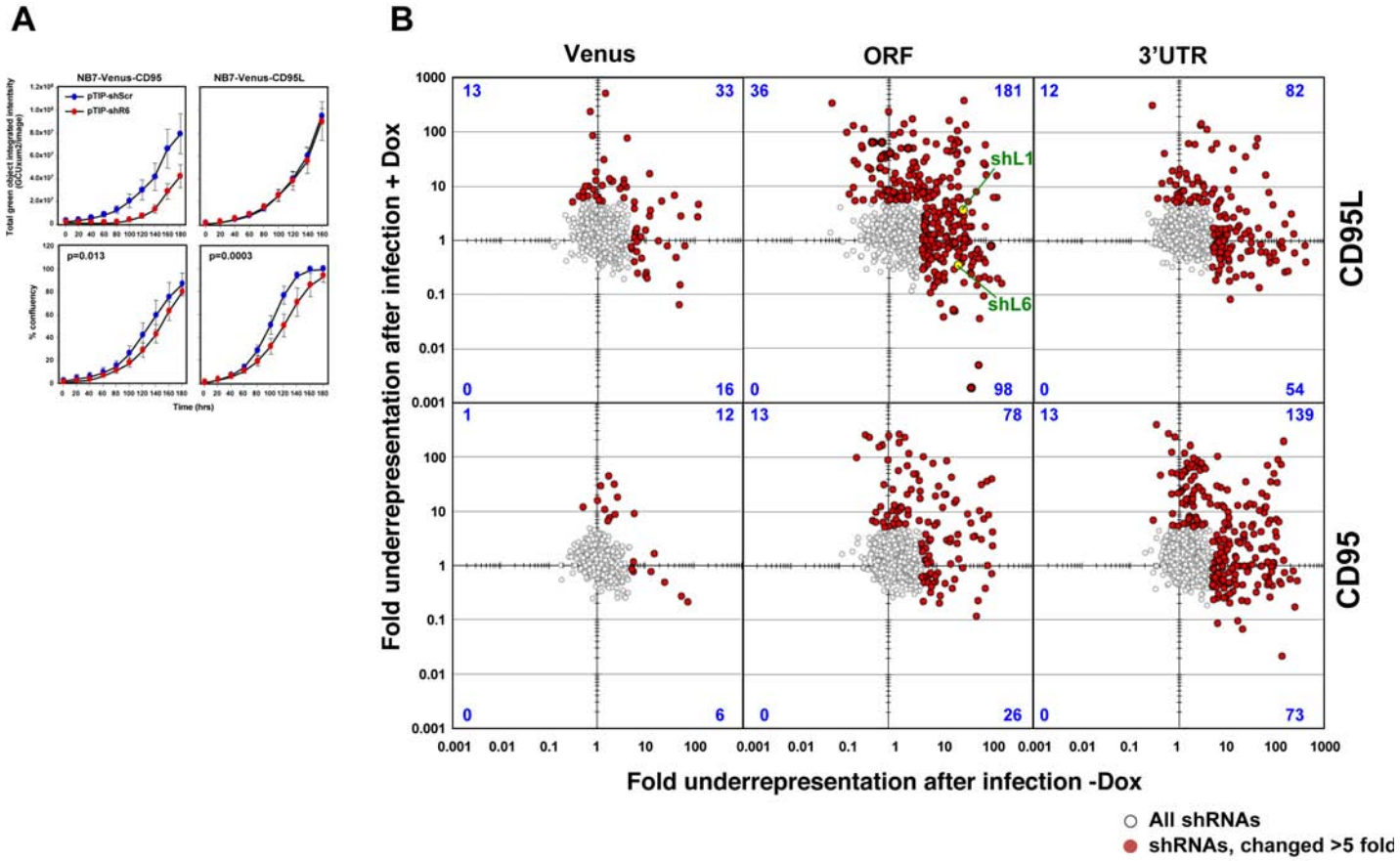

Figure S9. Fold change in shRNA representation after infection of NB7 cells and after treatment with Dox. (**A**) Change in green fluorescence (top panels) and percent cell confluence (bottom panels) over time of NB7 cells expressing either Venus-CD95 (left panels) or Venus-CD95L (right panels). Cells were infected with the Tet-inducible pTIP-shR6 virus, selected for two days with puromycin and then subjected to an analysis in the IncuCyte Zoom. No Dox was added. Two other inducible constructs (pTIP-shL1 and pTIP-shL3) were tested in the same way and no evidence of leakiness was observed (data not shown), supporting the finding in the shRNA screen that certain shRNA constructs display leakiness while others do not. (**B**) Scatterplot showing the fold change of shRNAs after infection of cells and culture for 9 days without Dox when compared to the composition of the shRNA plasmid library (X axis) and the fold change of shRNAs after culture with Dox for 9 days when compared to the culture without Dox (Y axis). The red dots are the shRNAs that were significantly downregulated at least 5 fold. The number of shRNAs labeled in red in each quartile is given in blue. Two of the shRNAs tested before are labeled in green.

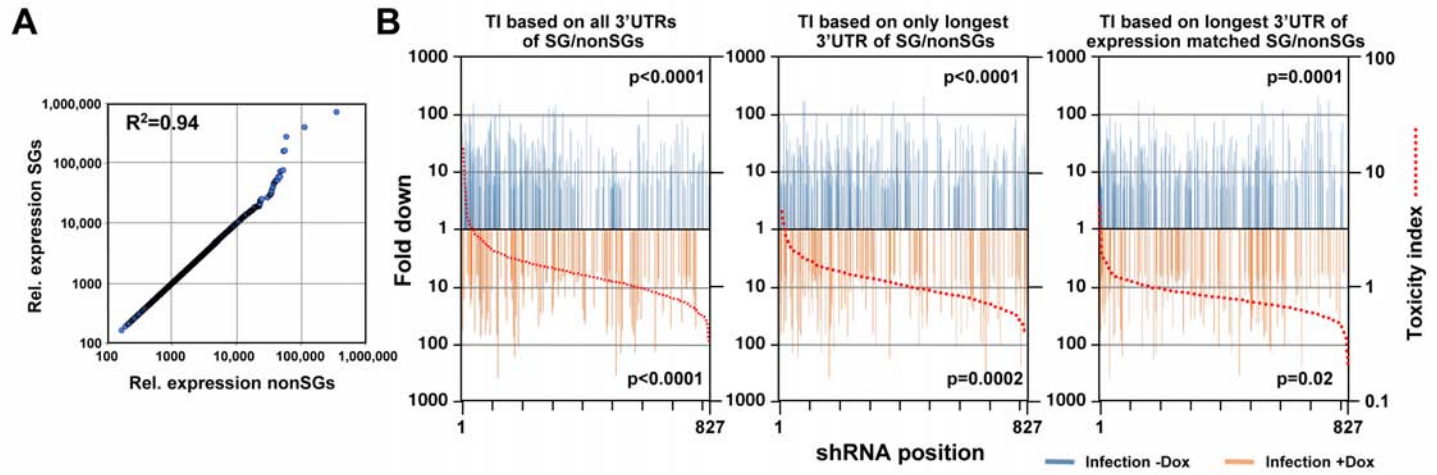

Figure S10. Does DISE preferentially target survival genes or all highly expressed genes? (**A**) Correlation between 1185 survival genes (genes identified as critical survival genes in two genome-wide lethality screens (Blomen et al., 2015; Wang et al., 2015) and expressed at least at 100 reads in all of the 16 control RNA Seq samples in this study) and 1185 expression matched nonsurvival genes (genes not identified as critical survival genes in two genome-wide lethality screens (Blomen et al., 2015; Wang et al., 2015) and expressed at least at 100 reads in all of the 16 control RNA Seq samples in this study). (**B**) Reanalysis of the CD95L ORF data in Figure 5E using two alternative ways to calculate the toxicity index (TI). *Left:* the analysis shown in Figure 5E with the data ranked using the original TI (using all known 3'UTRs for each gene group). *Center*: analysis with the data ranked using the original TI but based on only the longest 3'UTR for each gene. *Right*: analysis with the data ranked using the new TI based on expression matched SGs and nonSGs identified in A and using the longest 3'UTR for each gene. To test if higher TI is enriched in shRNAs that were highly downregulated, p-values were calculated based on permutated datasets using Mann-Whitney U tests.

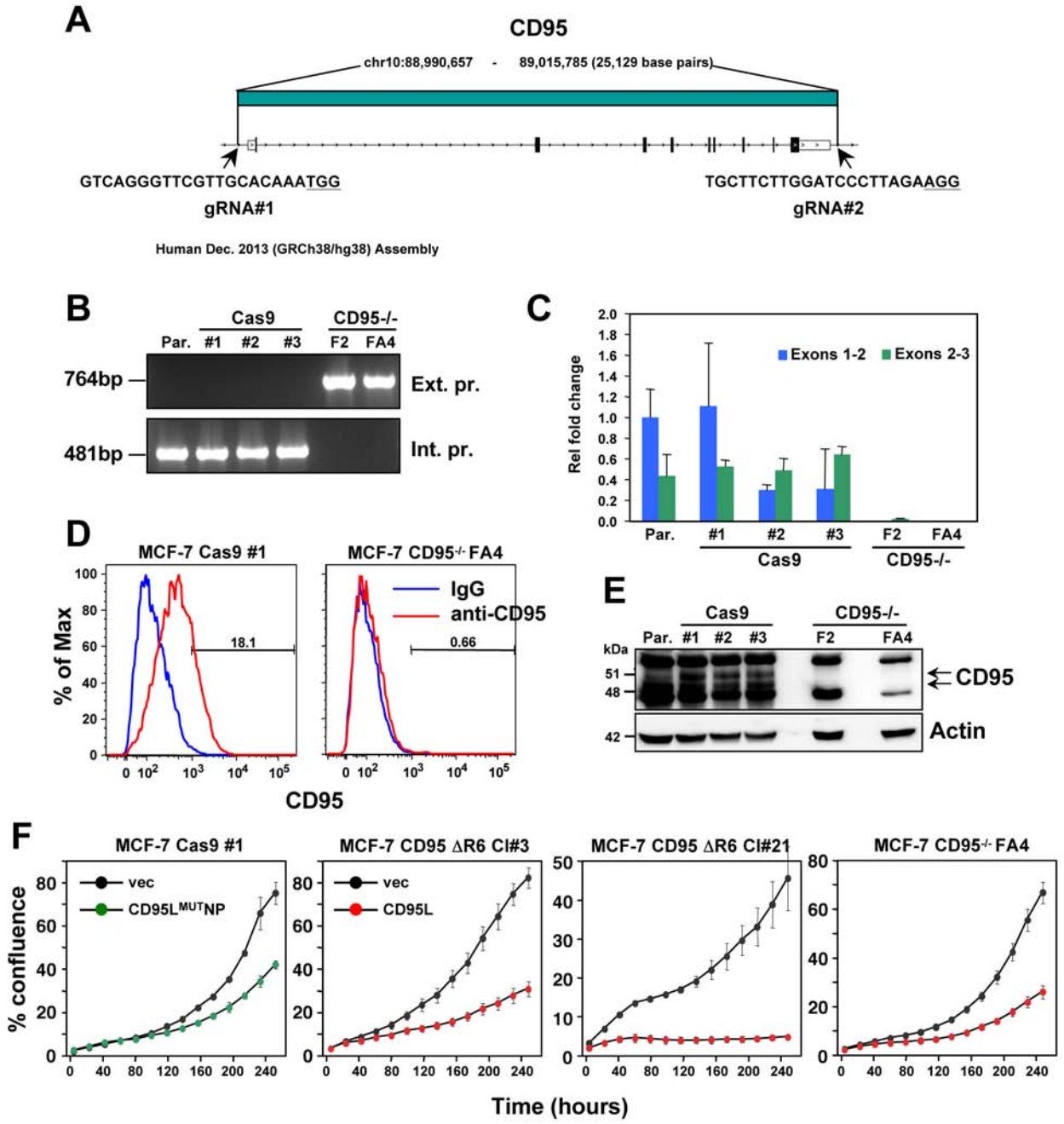

Figure S11. CD95L is toxic to MCF-7 cells lacking the entire CD95 gene. (**A**) Schematic of the genomic locations and sequences of the gRNAs used to excise the entire CD95 gene in MCF-7 cells. PAM site is underlined. (**B**) PCR with flanking (*top panels*) and internal (*bottom panels*) primers used to confirm the absence of the CD95 gene in MCF-7 clones. Parental (Par.) cells and three clones infected with Cas9 only (Cas9) and two complete k.o. clones (F2 and FA4) are shown. (**C**) qPCR analysis of the indicated clones using primers spanning either exon 1/2 or exon 2/3 of the CD95 gene. (**D**) Surface staining for CD95 of one wt and one k.o. clone. (**E**) Western blot analysis of all clones. (**F**) *Far left panel*: Confluency over time of MCF-7 Cas9 clone #1 infected with empty vector or with the RNA only version of CD95L (wt CD95L killed the cells within a few hours, not shown). *The three right panels*: MCF-7 CD95$^{-/-}$ FA4 or two MCF-7 clones in which we deleted the shR6 site resulting in an out-of-frame shift (generated as described in *Figure 1B* and *S3*) after infection with either vector or wt CD95L.

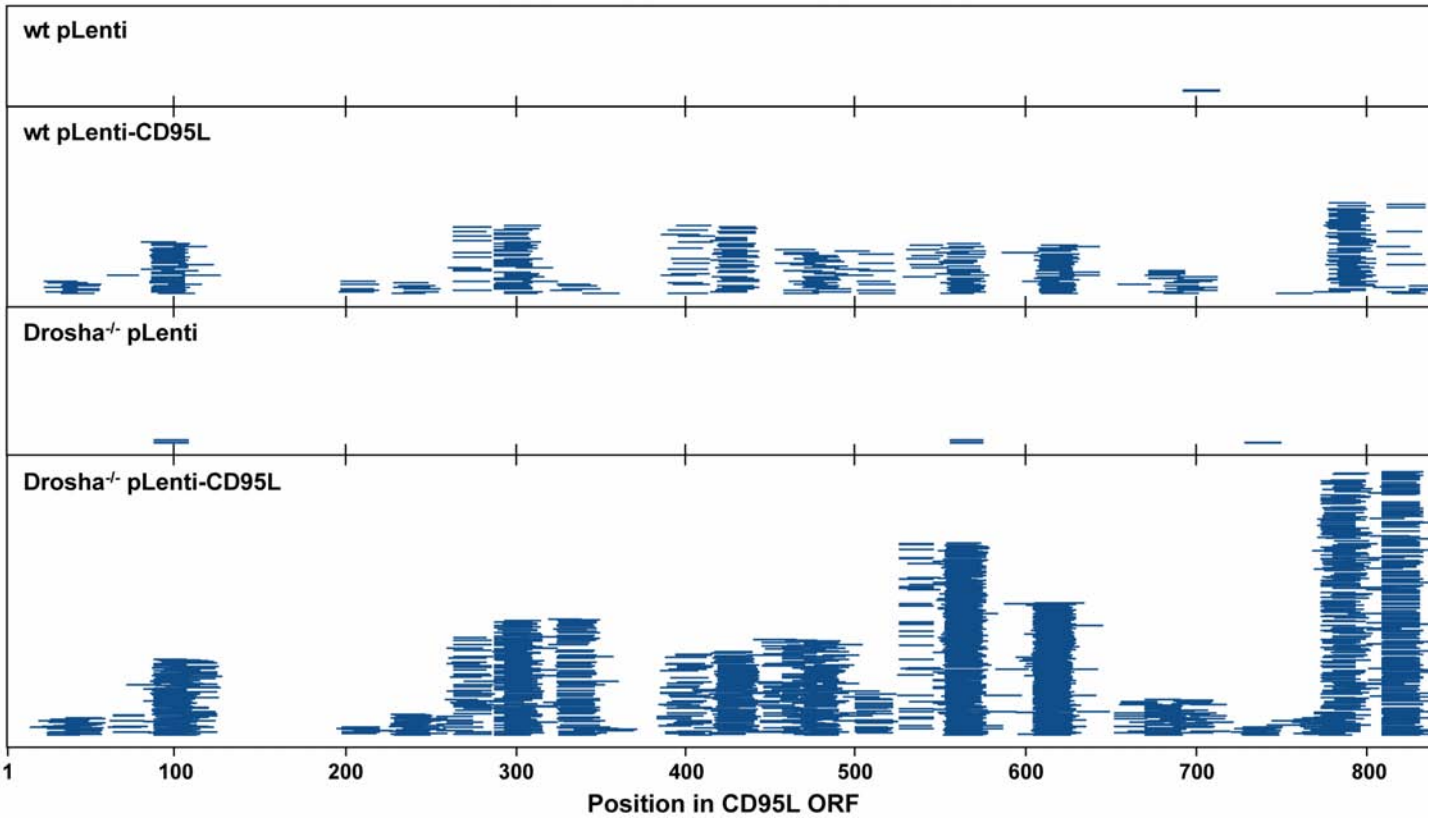

Figure S12. Alignment of CD95L derived AGO-bound RNAs with CD95L mRNA. All reads in all four conditions (see four panels, done in duplicates) were BLASTed against the ORF of CD95L. Reads are shown at scale aligned with the CD95L mRNA.

Supplementary Tables and movies:

Table S1: Results of the RNA-Seq analysis used to generate *Figure 3B*.

Table S2: Gene lists used in this work.

Table S3: shRNA screen data.

Table S4: The 6mer and 8mer toxicity index.

Table S5: Correlation between experimental shRNA toxicity and TI.

Movie S1: CD95 k.o. HeyA8 cells (clone 11) infected with pLenti control virus.

Movie S2: CD95 k.o. HeyA8 cells (clone 11) infected with pLenti-CD95Lvirus.

Movie S3: HeyA8 cells infected with pLKO-shScr.

Movie S4: HeyA8 cells infected with pLKO-shL3.

Supplementary references

Bae, K., Park, K. E., Han, J., Kim, J., Kim, K., & Yoon, K. A. (2016). Mitotic cell death caused by follistatin-like 1 inhibition is associated with up-regulated Bim by inactivated Erk1/2 in human lung cancer cells. *Oncotarget, 7*(14), 18076-18084. doi:10.18632/oncotarget.6729

Baumgarten, P., Harter, P. N., Tonjes, M., Capper, D., Blank, A. E., Sahm, F., . . . Mittelbronn, M. (2014). Loss of FUBP1 expression in gliomas predicts FUBP1 mutation and is associated with oligodendroglial differentiation, IDH1 mutation and 1p/19q loss of heterozygosity. *Neuropathol Appl Neurobiol, 40*(2), 205-216. doi:10.1111/nan.12088

Blomen, V. A., Majek, P., Jae, L. T., Bigenzahn, J. W., Nieuwenhuis, J., Staring, J., . . . Brummelkamp, T. R. (2015). Gene essentiality and synthetic lethality in haploid human cells. *Science, 350*(6264), 1092-1096. doi:10.1126/science.aac7557

Cerami, E., Gao, J., Dogrusoz, U., Gross, B. E., Sumer, S. O., Aksoy, B. A., . . . Schultz, N. (2012). The cBio cancer genomics portal: an open platform for exploring multidimensional cancer genomics data. *Cancer Discov, 2*(5), 401-404. doi:10.1158/2159-8290.CD-12-0095

Chan, K. T., Choi, M. Y., Lai, K. K., Tan, W., Tung, L. N., Lam, H. Y., . . . Law, S. (2014). Overexpression of transferrin receptor CD71 and its tumorigenic properties in esophageal squamous cell carcinoma. *Oncol Rep, 31*(3), 1296-1304. doi:10.3892/or.2014.2981

Gao, J., Aksoy, B. A., Dogrusoz, U., Dresdner, G., Gross, B., Sumer, S. O., . . . Schultz, N. (2013). Integrative analysis of complex cancer genomics and clinical profiles using the cBioPortal. *Science signaling, 6*(269), pl1. doi:10.1126/scisignal.2004088

Gui, S., Sang, X., Zheng, L., Ze, Y., Zhao, X., Sheng, L., . . . Tang, M. (2013). Intragastric exposure to titanium dioxide nanoparticles induced nephrotoxicity in mice, assessed by physiological and gene expression modifications. *Part Fibre Toxicol, 10*, 4. doi:10.1186/1743-8977-10-4

Hou, F., Chu, C. W., Kong, X., Yokomori, K., & Zou, H. (2007). The acetyltransferase activity of San stabilizes the mitotic cohesin at the centromeres in a shugoshin-independent manner. *J Cell Biol, 177*(4), 587-597. doi:10.1083/jcb.200701043

Jang, M., Park, B. C., Kang, S., Chi, S. W., Cho, S., Chung, S. J., . . . Park, S. G. (2009). Far upstream element-binding protein-1, a novel caspase substrate, acts as a cross-talker between apoptosis and the c-myc oncogene. *Oncogene, 28*(12), 1529-1536. doi:10.1038/onc.2009.11

Mi, N., Chen, Y., Wang, S., Chen, M., Zhao, M., Yang, G., . . . Yu, L. (2015). CapZ regulates autophagosomal membrane shaping by promoting actin assembly inside the isolation membrane. *Nat Cell Biol, 17*(9), 1112-1123. doi:10.1038/ncb3215

Parplys, A. C., Zhao, W., Sharma, N., Groesser, T., Liang, F., Maranon, D. G., . . . Wiese, C. (2015). NUCKS1 is a novel RAD51AP1 paralog important for homologous recombination and genome stability. *Nucleic Acids Res, 43*(20), 9817-9834. doi:10.1093/nar/gkv859

Pham, D. H., Powell, J. A., Gliddon, B. L., Moretti, P. A., Tsykin, A., Van der Hoek, M., . . . Pitson, S. M. (2014). Enhanced expression of transferrin receptor 1 contributes to oncogenic signalling by sphingosine kinase 1. *Oncogene, 33*(48), 5559-5568. doi:10.1038/onc.2013.502

Quidville, V., Alsafadi, S., Goubar, A., Commo, F., Scott, V., Pioche-Durieu, C., . . . Andre, F. (2013). Targeting the deregulated spliceosome core machinery in cancer cells triggers mTOR blockade and autophagy. *Cancer Res, 73*(7), 2247-2258. doi:10.1158/0008-5472.CAN-12-2501

Rabenhorst, U., Thalheimer, F. B., Gerlach, K., Kijonka, M., Bohm, S., Krause, D. S., . . . Zornig, M. (2015). Single-Stranded DNA-Binding Transcriptional Regulator FUBP1 Is Essential for Fetal and Adult Hematopoietic Stem Cell Self-Renewal. *Cell Rep, 11*(12), 1847-1855. doi:10.1016/j.celrep.2015.05.038

Sun, D., Zhou, M., Kowolik, C. M., Trisal, V., Huang, Q., Kernstine, K. H., . . . Shen, B. (2011). Differential expression patterns of capping protein, protein phosphatase 1, and casein kinase 1 may serve as diagnostic markers for malignant melanoma. *Melanoma Res, 21*(4), 335-343. doi:10.1097/CMR.0b013e328346b715

Wang, T., Birsoy, K., Hughes, N. W., Krupczak, K. M., Post, Y., Wei, J. J., . . . Sabatini, D. M. (2015). Identification and characterization of essential genes in the human genome. *Science, 350*(6264), 1096-1101. doi:10.1126/science.aac7041

Wazir, U., Jiang, W. G., Sharma, A. K., & Mokbel, K. (2013). Guanine nucleotide binding protein beta 1: a novel transduction protein with a possible role in human breast cancer. *Cancer Genomics Proteomics, 10*(2), 69-73.

Yoo, J. K., Choi, S. J., & Kim, J. K. (2013). Expression profiles of subtracted mRNAs during cellular senescence in human mesenchymal stem cells derived from bone marrow. *Exp Gerontol, 48*(5), 464-471. doi:10.1016/j.exger.2013.02.022

Zhang, Y., Wang, Y., Wei, Y., Wu, J., Zhang, P., Shen, S., . . . Yu, L. (2016). Molecular chaperone CCT3 supports proper mitotic progression and cell proliferation in hepatocellular carcinoma cells. *Cancer Lett, 372*(1), 101-109. doi:10.1016/j.canlet.2015.12.029